

Review of two-photon exchange in electron scattering*

J. Arrington,¹ P. G. Blunden,² W. Melnitchouk³

¹Physics Division, Argonne National Laboratory, Argonne, Illinois 60439, USA

²University of Manitoba, Winnipeg, Manitoba, Canada R3T 2N2

³Jefferson Lab, Newport News, Virginia 23606, USA

Abstract

We review the role of two-photon exchange (TPE) in electron–hadron scattering, focusing in particular on hadronic frameworks suitable for describing the low and moderate Q^2 region relevant to most experimental studies. We discuss the effects of TPE on the extraction of nucleon form factors and their role in the resolution of the proton electric to magnetic form factor ratio puzzle. The implications of TPE on various other observables, including neutron form factors, electroproduction of resonances and pions, and nuclear form factors, are summarized. Measurements seeking to directly identify TPE effects, such as through the angular dependence of polarization measurements, nonlinear ε contributions to the cross sections, and via e^+p to e^-p cross section ratios, are also outlined. In the weak sector, we describe the role of TPE and γZ interference in parity-violating electron scattering, and assess their impact on the extraction of the strange form factors of the nucleon and the weak charge of the proton.

arXiv:1105.0951v1 [nucl-th] 4 May 2011

*Dedicated to the memory of John A. Tjon.

Contents

1	Introduction	3
2	Elastic electron–nucleon scattering	4
2.1	<i>Kinematics</i>	4
2.2	<i>Born approximation</i>	5
2.3	<i>Form factors in the Born approximation</i>	6
3	Experimental observables and measurements	7
3.1	<i>Verification of the discrepancy</i>	7
3.2	<i>Early estimates of two-photon exchange corrections</i>	9
3.3	<i>Experimental signatures of two-photon exchange contributions</i>	11
3.3.1	Comparisons of positron–proton and electron–proton scattering	11
3.3.2	Improved measurements of the Rosenbluth–polarization discrepancy	12
3.3.3	Experimental limits on nonlinearities	13
3.4	<i>Conclusions from early experiments</i>	14
4	Two-photon exchange	16
4.1	<i>General properties of radiative corrections</i>	16
4.2	<i>Soft two-photon exchange effects</i>	18
4.3	<i>Hadron structure effects</i>	20
4.4	<i>Inelastic contributions</i>	22
4.4.1	Δ intermediate states	22
4.4.2	Nucleon resonances	24
4.5	<i>Electron–muon scattering</i>	26
4.6	<i>High Q^2 partonic models</i>	28
4.7	<i>Dispersion relations</i>	29
5	Impact of two-photon exchange on observables	32
5.1	<i>Cross sections and Rosenbluth separations</i>	32
5.2	<i>e^+p/e^-p ratios</i>	34
5.3	<i>Polarization measurements</i>	35
5.4	<i>Global form factor analysis</i>	37
5.4.1	Initial attempts to combine Rosenbluth and polarization data	38
5.4.2	Extraction of form factors including TPE contributions	39
5.4.3	Impact on the extracted charge radius of the proton	40
5.5	<i>Normal asymmetries</i>	41
6	Two-photon exchange in other reactions	43
6.1	<i>Neutron form factors</i>	43
6.2	<i>Electroproduction of resonances</i>	44
6.3	<i>Timelike form factors</i>	46
6.4	<i>Pion form factor</i>	46
6.5	<i>Electron–nucleus scattering</i>	49
6.5.1	TPE in deuteron form factors	49
6.5.2	^3He elastic form factors	49

7	Parity-violating electron scattering	50
7.1	<i>Parity-violating asymmetries</i>	51
7.2	<i>Two-boson exchange corrections</i>	52
7.2.1	Nucleon elastic contributions	54
7.2.2	Δ intermediate states	55
7.2.3	Effects on the strange form factors	57
7.3	γZ corrections to the proton weak charge	59
8	Conclusions and outlook	65

1 Introduction

The electromagnetic probe has been a primary experimental tool in the study of hadron physics for many decades. Electromagnetic interactions are extremely well understood, and the pointlike nature of electrons and muons make them ideal probes of the internal structure of hadrons. Lepton scattering experiments provide the cleanest information available on fundamental quantities such as hadron form factors and parton distributions. In addition, the relatively small value of the electromagnetic coupling means that measurements on nuclei probe the entire nuclear volume, without the significant attenuation of the beam over the length of the nucleus that yields a dominance of surface effects in some hadron beam measurements.

Because of the power of the electromagnetic probe, a great deal of our information on the structure of the nucleon comes from unpolarized measurements of the inclusive lepton-nucleon cross section. More recently, polarized beams have been used to provide additional information on the spin structure of the nucleon and to improve our knowledge of the nucleon form factors. As one of the most fundamental observables characterizing the composite nature of the nucleon, electromagnetic form factors have over the past few decades provided considerable insight into the nucleon internal structure, with the electric (G_E) and the magnetic (G_M) form factors encoding the (transverse) spatial distributions of the nucleon's charge and magnetization (for reviews see Refs. [1, 2, 3]). While these can in principle be extracted from the unpolarized cross sections, polarization measurements have played a critical role in studies of the nucleon form factors over the last decade.

These polarization measurements have led to a renaissance in studies of the structure of the proton and neutron, providing significantly improved measurements of their form factors over a wide range of momentum transfer Q^2 (which, loosely speaking, is inversely proportional to the resolution at which the structure is probed). However, while these measurements significantly improved the precision with which the form factors could be extracted, they also showed a significant discrepancy with extractions from the unpolarized cross sections in kinematic regions where both techniques provide precise measurements. Because these, and essentially all other electron scattering measurements, are analyzed in the one-photon exchange or Born approximation, this discrepancy led to a serious reexamination of the possible role played by the two-photon exchange (TPE) process. Early measurements and calculations suggested that the TPE corrections were small, although recent studies are providing ever more convincing evidence that these corrections can nonetheless be extremely important in specific observables.

In the 10 years since the form factor discrepancy was confirmed, a great deal of progress has been made in understanding TPE contributions. There have been several approaches used to calculate TPE contributions for a variety of reactions and observables, as well as a significant effort aimed at constraining these experimentally. At present there are calculations of TPE that are consistent with all existing experimental constraints, which can explain the form factor discrepancy, and which allow extraction of the proton form factors without yielding a significant theoretical uncertainty in the extraction. In addition, a set of experiments is underway which will allow for direct verification of these

calculations, and thus provide a final resolution to the issue. With extensive experimental checks of the TPE calculations, reliable estimates can be made for other reactions, and it will be possible to identify other cases where TPE effects may be large enough that they pose concerns for the interpretation of precision experiments.

It is therefore timely to review the recent experimental and theoretical efforts dedicated to studying TPE in electromagnetic processes, and more generally the impact of two-boson (γ or Z) exchange corrections which enter into weak processes induced by electromagnetic probes. In Sec. 2 we provide an overview of the relevant electron scattering formalism, including definitions of kinematics and scattering amplitudes. Section 3 discusses the initial evidence for TPE effects, as well as constraints from early measurements. The formalism and calculations of TPE corrections are presented in Sec. 4, and their impact on elastic scattering measurements examined in Sec. 5. Implications of TPE for observables in other electron–hadron scattering reactions are discussed in Sec. 6. Finally, in Sec. 7 we review the role of two-photon and γZ interference in parity-violating electron scattering and their impact on the extraction of the strange form factors of the nucleon and the weak charge of the proton. We end with conclusions and outlook for future studies of two-photon exchange in Sec. 8.

2 Elastic electron–nucleon scattering

In this section we define the general kinematics of elastic electron–nucleon scattering (Sec. 2.1), and present amplitudes and cross sections in the one-photon exchange or Born approximation (Sec. 2.2). The extraction of the electromagnetic form factors in the Born approximation using the Rosenbluth separation and polarization transfer methods is discussed in Sec. 2.3.

2.1 Kinematics

For the elastic scattering process $eN \rightarrow eN$ the four-momenta of the initial and final electrons are labeled by k and k' , with corresponding energies E and E' , and of the initial and final nucleons by p and p' , respectively. The four-momentum transfer from the electron to the nucleon is given by $q = p' - p = k - k'$, with $Q^2 \equiv -q^2 > 0$. Conventionally the scattering cross section is defined in terms of Q^2 and the electron scattering angle θ , or equivalently the dimensionless quantities

$$\tau = \frac{Q^2}{4M^2}, \quad \varepsilon = \frac{\nu^2 - \tau(1 + \tau)}{\nu^2 + \tau(1 + \tau)}, \quad (1)$$

where $\nu = k \cdot p/M^2 - \tau$. In the target rest frame the variable ε is related to the scattering angle θ by

$$\varepsilon = \left(1 + 2(1 + \tau) \tan^2 \frac{\theta}{2}\right)^{-1}, \quad (2)$$

and is identified with the relative flux of longitudinal virtual photons. In terms of τ and ε the incident electron energy is

$$E = M \left(\tau + \sqrt{\tau(1 + \tau)(1 + \varepsilon)/(1 - \varepsilon)} \right), \quad (3)$$

and the scattered electron energy is $E' = E - 2M\tau$.

One can also express the elastic cross section in terms of any two of the Mandelstam variables s (total electron–nucleon invariant mass squared), t , and u , where

$$s = (k + p)^2 = (p' + k')^2, \quad t = (k - k')^2 = q^2, \quad u = (p - k')^2 = (p' - k)^2, \quad (4)$$

with the constraint $s + t + u = 2M^2 + 2m_e^2$. Furthermore, the variable ν is related to the Mandelstam variables by $\nu = (s - u)/(4M^2)$. The electron mass m_e can generally be ignored at the kinematics of interest here. In particular, there are no mass singularities in the limit $m_e \rightarrow 0$ in either the one-photon exchange amplitude or the *total* TPE amplitude.

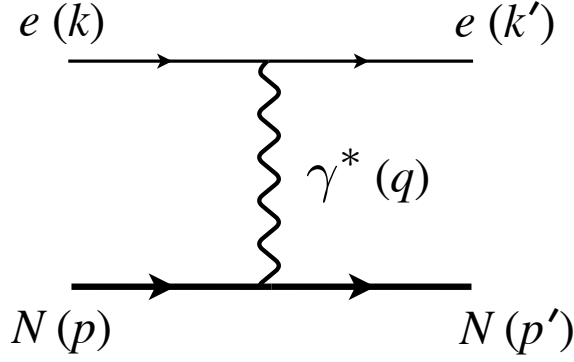


Figure 1: Elastic electron–nucleon scattering in the one-photon exchange (Born) approximation. Particle momentum is indicated in parentheses.

2.2 Born approximation

In the Born approximation (see Fig. 1), the electron–nucleon scattering invariant amplitude can be written as

$$\mathcal{M}_\gamma = -\frac{e^2}{q^2} j_{\gamma\mu} J_\gamma^\mu \quad (5)$$

where e is the electric charge, and the matrix elements of the electromagnetic leptonic and hadronic currents are given in terms of the lepton (u_e) and nucleon (u_N) spinors by

$$j_{\gamma\mu} = \bar{u}_e(k') \gamma_\mu u_e(k), \quad J_\gamma^\mu = \bar{u}_N(p') \Gamma_\gamma^\mu(q) u_N(p). \quad (6)$$

Our metric and other unstated conventions follow Ref. [4]. Note that other conventions for amplitudes have also been used in the TPE literature [5, 6, 7, 8, 9]. The electromagnetic hadron current operator Γ_γ^μ is parametrized by the Dirac (F_1) and Pauli (F_2) form factors as

$$\Gamma_\gamma^\mu(q) = \gamma^\mu F_1(q^2) + \frac{i\sigma^{\mu\nu} q_\nu}{2M} F_2(q^2), \quad (7)$$

where M is the nucleon mass. In terms of the amplitude \mathcal{M}_γ , the differential Born cross section is given by

$$\frac{d\sigma}{d\Omega} = \left(\frac{\alpha}{4MQ^2} \frac{E'}{E} \right)^2 |\mathcal{M}_\gamma|^2 = \frac{\sigma_{\text{Mott}}}{\varepsilon(1+\tau)} \sigma_R, \quad (8)$$

where $\alpha = e^2/4\pi$ is the electromagnetic fine structure constant, and the Mott cross section for the scattering from a point particle is

$$\sigma_{\text{Mott}} = \frac{\alpha^2 E' \cos^2(\theta/2)}{4E^3 \sin^4(\theta/2)}. \quad (9)$$

The reduced Born cross section σ_R is given by

$$\sigma_R = \varepsilon G_E^2(Q^2) + \tau G_M^2(Q^2), \quad (10)$$

where the Sachs electric and magnetic form factors $G_{E,M}(Q^2)$ are defined in terms of the Dirac and Pauli form factors as

$$G_E(Q^2) = F_1(Q^2) - \tau F_2(Q^2), \quad G_M(Q^2) = F_1(Q^2) + F_2(Q^2). \quad (11)$$

The form factors are normalized such that $G_E^{p(n)}(0) = 1(0)$ and $G_M^{p(n)}(0) = \mu_{p(n)} = 2.793(-1.913)$ for the proton (neutron).

2.3 Form factors in the Born approximation

The standard technique to extract the electric and magnetic form factors of the proton has been the Rosenbluth, or longitudinal-transverse (LT), separation method [10]. Using the fact that the Born level form factors in Eq. (10) are functions of Q^2 only, analyzing the cross section as a function of the longitudinal photon polarization ε at fixed Q^2 allows one to extract G_M^2 from the ε -intercept, and G_E^2 from the slope in ε , once standard radiative corrections have been applied. The cross section at $\theta = 180^\circ$ ($\varepsilon \rightarrow 0$) depends only on the magnetic form factor G_M , while the cross section at smaller angles ($\varepsilon \rightarrow 1$) is a combination of magnetic and electric contributions. Because of the ε/τ weighting of G_E^2 relative to G_M^2 , the contribution from the electric form factor to the cross section is suppressed at large Q^2 . The proton form factor ratios extracted via the Rosenbluth technique have generally been consistent with Q^2 scaling, $|G_E| \approx |G_M/\mu_p|$ [11, 12, 13, 14], where μ_p is the proton's magnetic moment. Note that because the cross sections are sensitive to the squares of the form factors, the signs on the form factors cannot be determined from Rosenbluth separations alone.

An alternative method of extracting the ratio R utilizes polarization degrees of freedom to increase the sensitivity to the electric form factor at large Q^2 . Here, longitudinally polarized electrons are scattered from an unpolarized proton target, with the polarization of the recoiling proton detected, $\vec{e}p \rightarrow e\vec{p}$. The polarization of the incident electron (or recoil proton) is characterized by the spin four-vector [6, 15]

$$s^\mu = \left(\frac{\boldsymbol{\zeta} \cdot \mathbf{k}}{m}; \boldsymbol{\zeta} + \mathbf{k} \frac{\boldsymbol{\zeta} \cdot \mathbf{k}}{m(m+E)} \right), \quad (12)$$

where m and E are the particle's mass and energy, and the three-dimensional spin vector $\boldsymbol{\zeta}$ specifies the spin direction in the rest frame. In the limit $\mathbf{k} \rightarrow 0$, the spin four-vector $s \rightarrow (0; \boldsymbol{\zeta})$. Since $\boldsymbol{\zeta}$ is a unit vector, $\boldsymbol{\zeta}^2 = 1$, and from Eq. (12) one has $s^2 = -1$ and $\mathbf{k} \cdot \mathbf{s} = 0$. For incident electron energies $E \gg m_e$, the electron spin four-vector s_e can be related to the electron helicity $h = \boldsymbol{\zeta}_e \cdot \hat{\mathbf{k}}$ by

$$s_e \approx h \frac{|\mathbf{k}|}{m_e}. \quad (13)$$

The coordinate axes are chosen so that the recoil proton momentum \mathbf{p}' defines the z axis, in which case for longitudinally polarized protons one has $\boldsymbol{\zeta}_p = \hat{\mathbf{p}}'$. In the Born approximation the elastic cross section for scattering a longitudinally polarized electron with a recoil proton polarized longitudinally is then given by

$$\frac{d\sigma^{(L)}}{d\Omega} = h \sigma_{\text{Mott}} \frac{E+E'}{M} \sqrt{\frac{\tau}{1+\tau}} \tan^2 \frac{\theta}{2} G_M^2. \quad (14)$$

For a proton detected with transverse polarization the x axis is defined to be in the scattering plane, $\hat{\mathbf{x}} = \hat{\mathbf{y}} \times \hat{\mathbf{z}}$, where $\hat{\mathbf{y}} = \hat{\mathbf{k}} \times \hat{\mathbf{k}}'$ defines the direction perpendicular, or normal, to the scattering plane. The cross section for producing a transversely polarized proton, $\boldsymbol{\zeta}_p \cdot \mathbf{p}' = 0$, is given by

$$\frac{d\sigma^{(T)}}{d\Omega} = h \sigma_{\text{Mott}} 2 \sqrt{\frac{\tau}{1+\tau}} \tan \frac{\theta}{2} G_E G_M, \quad (15)$$

while in the Born approximation, the normal polarization is identically zero. Taking the ratio of the transverse to longitudinal proton cross sections then yields the ratio of the electric to magnetic proton form factors,

$$-\mu_p \sqrt{\frac{\tau(1+\varepsilon)}{2\varepsilon}} \frac{P_T}{P_L} = -\mu_p \frac{E+E'}{2M} \tan \frac{\theta}{2} \frac{P_T}{P_L} = \mu_p \frac{G_E}{G_M}, \quad (16)$$

where P_L and P_T are the polarizations of the recoil proton longitudinal and transverse to the proton momentum in the scattering plane, proportional to the longitudinal and transverse cross sections in Eqs. (15) and (14), respectively.

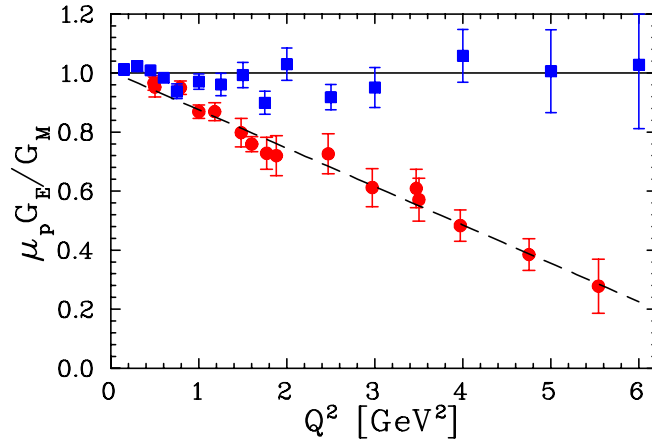


Figure 2: Ratio of proton electric to magnetic form factors as extracted using Rosenbluth (LT) separation [11] (squares) and polarization transfer measurements [16, 18] (circles). Figure adapted from Ref. [12].

In a series of recent experiments at Jefferson Lab [16, 17, 18, 19, 20, 21, 22, 23, 24, 25], the polarization transfer (PT) technique has been used to accurately determine the ratio G_E/G_M up to $Q^2 = 8.5 \text{ GeV}^2$. In addition, there have been complementary measurements using polarized targets at MIT-Bates [26] and Jefferson Lab [27]. The results, illustrated in Fig. 2, are in striking contrast to the ratio obtained via LT or Rosenbluth separations, showing an approximately linear decrease of R with Q^2 which is in strong violation of the Q^2 scaling behavior (see also Refs. [1, 2, 28, 29]).

The discrepancy between the LT and PT measurements of G_E/G_M has stimulated considerable activity, both theoretically and experimentally, over the past decade. Attempts to reconcile the measurements have mostly focused on improved treatments of radiative corrections, particularly those associated with two-photon exchange, which can lead to additional angular (and thus ε) dependence of the cross section. In the following sections we discuss experimental efforts to better understand the discrepancy, and then describe theoretical efforts to compute TPE corrections and assess their impact on various observables.

3 Experimental observables and measurements

3.1 Verification of the discrepancy

The striking difference between Rosenbluth [30] and the early polarization transfer [16, 18] measurements of the proton electromagnetic form factors shown in Fig. 2 led to significant activity aimed at understanding and resolving this discrepancy. It was noted early [16] that there was significant scatter between the results of different Rosenbluth extractions [11, 31, 32, 33, 34], as illustrated in Fig. 3, suggesting that the problem was related to the cross section measurements. At high Q^2 , G_E yields only a small, angle-dependent correction to the cross section, leading to the possibility that a systematic difference between small- and large-angle measurements could yield large corrections to G_E/G_M , which would increase in importance with increasing Q^2 . It was therefore argued that the observed difference may have been due to some experimental error in one or more of the cross section measurements that significantly change the high Q^2 extractions of G_E . Thus, the first step was a careful examination of the cross section data to determine if the observed discrepancy could be explained by problems with one or two experiments, or resolved by adjusting the normalization of some data sets within the assumed uncertainties.

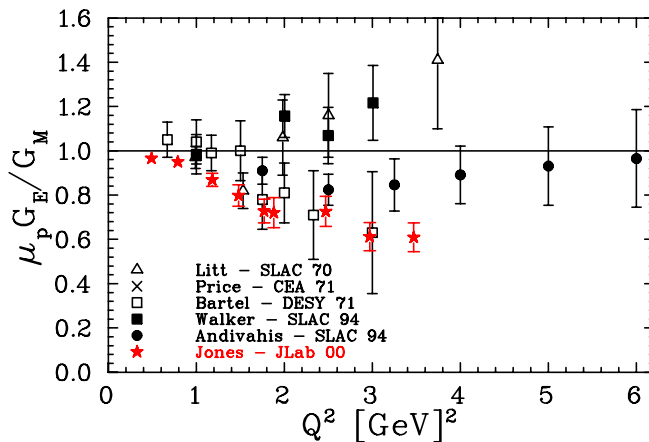


Figure 3: Ratio of proton electric to magnetic form factors as extracted from the initial high Q^2 polarization transfer measurement [16] (stars) and previous Rosenbluth (LT) separations [11, 31, 32, 33, 34].

Because G_E must be extracted by isolating a small, angle-dependent contribution to the cross section, global data analyses are sensitive to details of how data sets that cover different ranges of scattering angle are combined. Most extractions combining multiple data sets allowed the normalization of each experiment to vary as part of the fit, to improve consistency in the overlap regions. These normalizations were then fixed, and the uncertainty in the determination of the relative normalization factors was usually neglected. At high Q^2 , a change in the normalization between large- and small-angle measurements can systematically shift all of the high Q^2 results within the extraction.

A detailed reanalysis of the world's cross section data for moderate to high Q^2 values [12] showed that the cross sections were consistent when accounting for the quoted normalization uncertainties in the different data sets, except for some of the small-angle data from Ref. [11]. Excluding these data and performing a global extraction of G_E and G_M yielded results that were still in significant disagreement with the polarization transfer extractions. Furthermore, it was not possible to reproduce the polarization results by varying the normalization of the data sets within their quoted uncertainties, or by simply excluding one of the 20 data sets included in the analysis. However, it was noted that a systematic correction with an ε dependence of $\sim 5\%$ for $Q^2 \gtrsim 2 \text{ GeV}^2$ would be able to explain the discrepancy between the polarization measurements and the Rosenbluth extractions [12].

Shortly thereafter, a set of extremely high precision measurements of G_E/G_M was made using a modified Rosenbluth technique [14, 35]. Because the high Q^2 extraction is very sensitive to angle-dependent corrections, the measurement used detection of the recoil proton, rather than the scattered electron. In the traditional Rosenbluth separation, varying ε while keeping Q^2 fixed means that the scattered electron energy and angle vary with ε , as does the scattering cross section. This means that any momentum- or rate-dependent efficiencies or systematic corrections yield ε -dependent effects. With proton detection, the momentum of the detected particle does not vary for measurements at a fixed Q^2 value, and the cross section for detection of the recoil proton is only very weakly dependent on angle. These and several other corrections and systematic uncertainties are thus strongly suppressed in the extraction of G_E/G_M [14, 35]. In this measurement, care was taken to ensure that the *relative* cross section uncertainties were minimized, even though this could increase the absolute uncertainties, because only the relative uncertainties enter into the ratio G_E/G_M . The experiment yielded measurements for $2.64 < Q^2 < 4.1 \text{ GeV}^2$ with precision comparable to the recoil polarization results, as shown in Fig. 4. This confirmed a clear and significant discrepancy with the polarization measurements, which ruled out the possibility that the discrepancy was simply caused by a small systematic error in some of the earlier measurements.

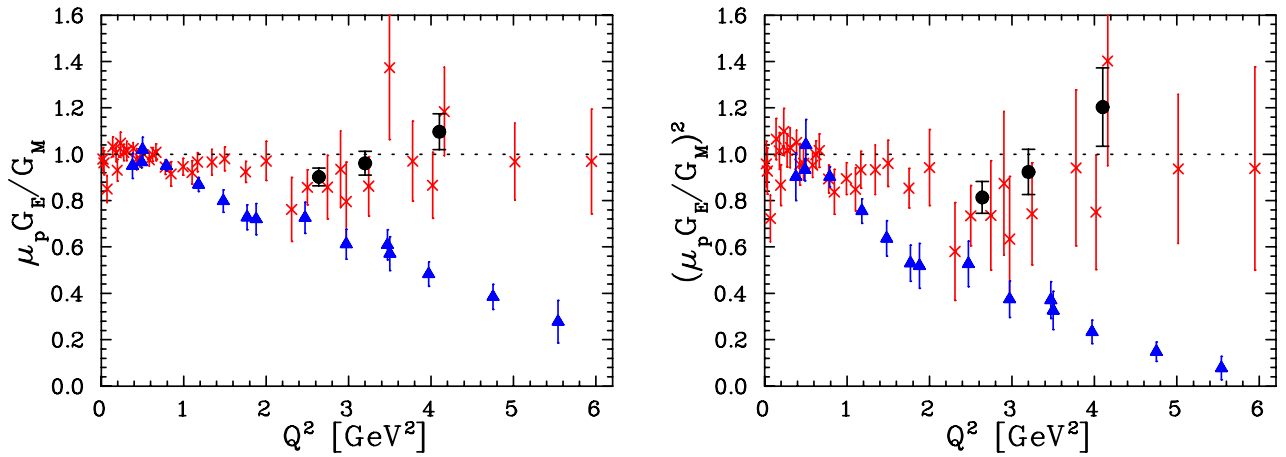


Figure 4: Proton electric to magnetic form factor ratio $\mu_p G_E / G_M$ (**left**) and $(\mu_p G_E / G_M)^2$ (**right**) extracted from the high-precision Super-Rosenbluth experiment [14] (filled circles), compared to polarization extractions [16, 18] (triangles) and a global analysis of previous cross section measurements [36] (crosses). Note that the slope of the reduced cross section in the Rosenbluth measurements is directly sensitive to $(\mu_p G_E / G_M)^2$, so the right figure best shows the significance of the discrepancy at the cross section level. Figure adapted from Ref. [14].

It is worth noting that the radiative corrections applied to the elastic scattering cross sections have evolved somewhat over time. While the work of Mo and Tsai [37, 38] is the standard formalism applied in the extraction of the Born cross section for most experiments over the last few decades, SLAC measurements in the 1990s [11, 34] included additional radiative correction terms such as vacuum polarization contributions from higher mass leptons. In the global analysis, these corrections were also included for older measurements to minimize the difference in the radiative correction procedures over the full body of data. However, the additional terms have essentially no dependence on the electron scattering angle, and therefore have minimal impact on the extraction of G_E at large Q^2 .

3.2 Early estimates of two-photon exchange corrections

Once it was clear that there was a systematic discrepancy between the techniques, it was important to determine how large of an effect would be needed to explain the discrepancy, and determine if TPE contributions of this size could be ruled out by existing measurements. Very early attempts to calculate the TPE contributions, using only the unexcited proton as an intermediate state [39], or including excited intermediate states [40, 41, 42, 43, 44, 45], yielded extremely small TPE contributions, typically well below one percent of the Born cross section,¹ but it was difficult to determine how reliable these estimates were, especially at large Q^2 values. Even before the form factor discrepancy was clear, there were additional works examining the radiative corrections [46] and TPE contributions [47]. Coulomb distortion was also investigated, both for low Q^2 [48] and higher Q^2 [49] values, but the effect is relatively small compared to the observed discrepancy at high Q^2 . For the most part, investigations have focused on the effect of TPE corrections [5, 50, 51, 52, 53] beyond those included in the traditional calculations of radiative corrections. Calculations of TPE corrections will be presented in detail in Sec. 4, and their impact on the measurements in Sec. 5.

Initial investigations focused on using measurements of the discrepancy to determine the nature of

¹The TPE diagram also contains an infrared-divergent contribution, which is canceled by a corresponding divergent term in bremsstrahlung emission, as discussed in more detail in Sec. 4.1.

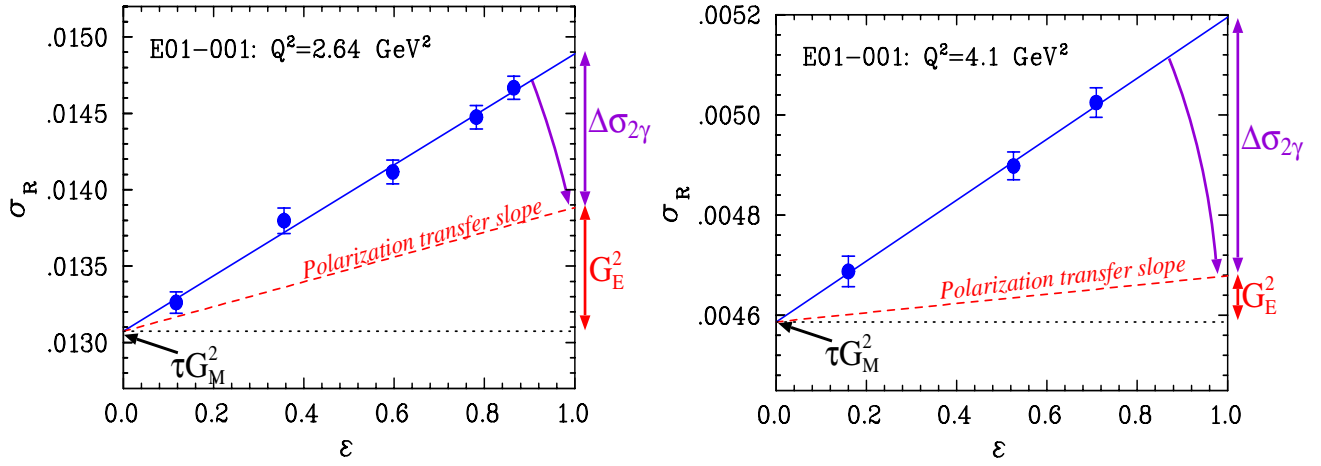


Figure 5: The ε dependence of the reduced cross section as predicted from the polarization transfer results for G_E/G_M (red dashed line), and as measured by Jefferson Lab experiment E01-001 [14] (circles). If the polarization transfer represents the true form factors, TPE yields more than half of the ε dependence at 2.64 GeV² (**left**), and 85% at 4.1 GeV² (**right**). The PT measurements give only the slope of σ_R , and the curve has been arbitrarily normalized to match the LT separations at $\varepsilon = 0$.

the corrections required to explain the data. Analyses of the discrepancy that assume it is due primarily to missing corrections in the cross section measurements [12, 36, 50] indicated that the difference could be explained by an error in the ε dependence of the cross section of approximately 5 – 8% for $Q^2 > 2 - 3$ GeV². Figure 5 shows the ε dependence observed in the Super-Rosenbluth experiment [14] and as expected based on the polarization transfer measurements [16, 18], assuming the Born approximation. The polarization transfer measurement constrains only the slope, not the value of the cross section, and has been arbitrarily normalized to agree with the Rosenbluth extraction at $\varepsilon = 0$ in Fig. 5. If some systematic correction to the cross section explains the difference, then the ε dependence shown by the dashed line is related to the contribution from the electric form factor, and the remaining slope must come from the missing correction. This correction should be close enough to linear that it does not spoil the linearity expected from the Rosenbluth formula, as the reduced cross section is consistent with a linear ε dependence within the current uncertainties. Note that if TPE corrections explain the difference, they must be zero at $\varepsilon = 1$, as explained in Sec. 4, and so one would expect the two lines to meet at $\varepsilon = 1$.

Early calculations were performed in hadronic [5] and partonic [53] frameworks, yielding corrections which could explain roughly half of the discrepancy at large Q^2 values. Calculations at the parton level in the double logarithm approximation [52] yielded a different form for the ε dependence, with nonlinearities appearing at large ε . Finally, invariance under C-parity and crossing symmetry were used [51] to argue that the TPE corrections should depend on $x = \sqrt{(1 + \varepsilon)/(1 - \varepsilon)}$. The range of predictions of these models is shown in Fig. 6 for $Q^2 \approx 2 - 3$ GeV², where each model has been scaled to give an overall ε dependence of the size needed to resolve the discrepancy between the Rosenbluth and polarization measurements. For the partonic model [53], the calculation is not expected to be valid at low Q^2 or ε values, indicated by the dashed extensions of the curve below $\varepsilon = 0.26$. Many of these calculations have been updated since, and the most recent results will be discussed in Sec. 4, but these were the models available at the time that measurements to further examine the TPE corrections were being considered.

While scaled to yield approximately the same ε dependence, they nonetheless would yield significantly different results for the extracted form factors. The Chen *et al.* calculation [53] has little ε

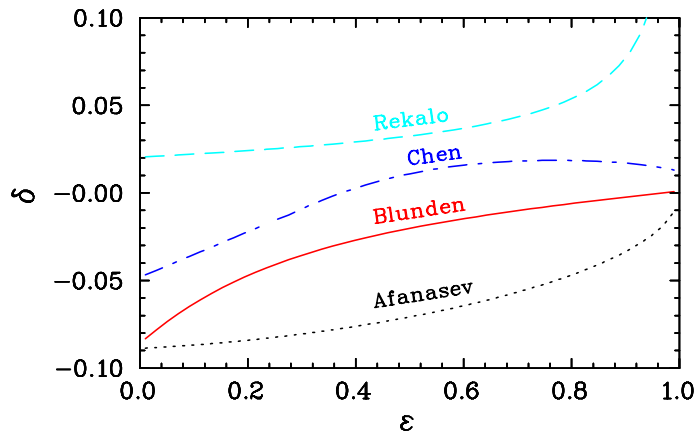


Figure 6: The TPE correction δ , defined via $\sigma = \sigma_0(1 + \delta)$, where σ_0 is the Born cross section, to the elastic ep cross section from the calculations of Rekalo *et al.* [51] (dashed), Chen *et al.* [53] (dot-dashed), Blunden *et al.* [5] (solid), and Afanasev *et al.* [52] (dotted) for $Q^2 \approx 5 \text{ GeV}^2$, after scaling the calculations to yield a ε dependence of approximately 6% over the ε range of existing data.

dependence for $\varepsilon > 0.5$, meaning that it would have little impact on Rosenbluth extractions if they did not have data at low ε . The form of the correction in Ref. [51] yields large effects for $\varepsilon \rightarrow 1$, but small corrections to G_M for measurements at low ε . The other calculations have the largest corrections at low ε , and thus larger corrections to direct measurements of G_M . In addition, some calculations predict large deviations from the linear ε dependence of the Born approximation at very high ε , while others predict the greatest deviations at low ε . Based on this large range of predictions, several experimental tests, using existing data or new measurements, were performed to provide independent constraints on any possible TPE contributions.

3.3 Experimental signatures of two-photon exchange contributions

Two-photon exchange contributions to elastic electron–proton scattering manifest themselves in several different ways. The real part of the TPE amplitude modifies both the unpolarized cross section and the polarization transfer components used to extract G_E/G_M , and thus measurements sensitive to the real part of TPE amplitudes yield constraints that are directly relevant to the form factor discrepancy. These contributions, however, must be disentangled from the dominant single-photon contributions. The imaginary part of the amplitudes, on the other hand, leads to non-zero values for the Born-forbidden normal asymmetries (Sec. 5.5), which allow two-photon effects to be directly isolated. However, since these are not directly connected to the form factor discrepancy, they were not the initial focus of experimental investigations. We summarize here some of the early experiments that provided constraints on the TPE contributions.

3.3.1 Comparisons of positron–proton and electron–proton scattering

In unpolarized electron–proton scattering the TPE contributions cannot in practice be separated from the Born cross section empirically. The cleanest way to identify TPE effects in unpolarized ep scattering is to compare positron–proton and electron–proton cross sections, where the interference between one- and two-photon exchange has the opposite sign for positron and electron beams (Sec. 4.1). While experimentally difficult, these were considered crucial tests of the electron scattering technique, and several experiments were performed in the 1960s to study possible TPE corrections. The comparisons

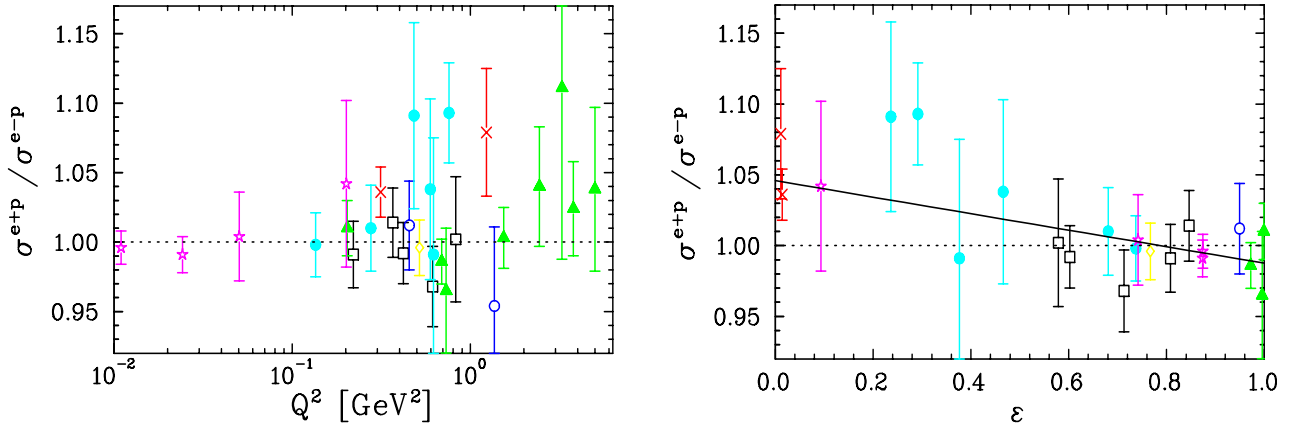


Figure 7: The ratio of positron–proton to electron–proton scattering as a function of Q^2 (**left**) and ε (**right**). The ε dependence plot includes only measurements below $Q^2 = 2 \text{ GeV}^2$. The solid curve is a linear fit to the data yielding a slope of $-0.057(18)$. Figure adapted from Ref. [62].

of e^+p and e^-p [54, 55, 56, 57, 58, 59, 60], and μ^+p and μ^-p [61], scattering were interpreted as supporting the conclusions of the early calculations that two-photon corrections were extremely small ($< 1\%$). Figure 7 (left panel) shows a compilation of all such measurements for elastic scattering as a function of Q^2 . However, the low intensity of e^+ (μ^+) beams made precise measurements nearly impossible for large Q^2 or small ε values.

More recently, the data were reexamined [62] in light of the form factor discrepancy, which suggested an ε -dependent effect. Measurements at high Q^2 were limited to small scattering angle (large ε) and so could not set a meaningful limit on angle-dependent TPE contributions if they were small at forward scattering angles. Figure 7 (right panel) shows the ratio of positron to electron cross section as a function of ε for measurements at $Q^2 \leq 2 \text{ GeV}^2$. There is some evidence of a charge-dependent term in the $e^\pm p$ elastic cross section ratio at small values of ε , although the data at low ε is not very precise. A linear fit yields a 6% ε dependence in the positron to electron ratio, implying a 3% ε dependence for the electron–proton cross section. This is roughly half of the ε dependence needed to explain the discrepancy at high Q^2 , but the average Q^2 value of the points showing nonzero TPE is $< 0.5 \text{ GeV}^2$, well below the region of the observed discrepancy. In addition, these measurements need to apply a model-dependent correction for the charge-dependent bremsstrahlung contributions to isolate TPE effects, and these corrections have not been applied in a consistent fashion for all of the measurements.

Because of the limited statistics, the low Q^2 values of the large angle measurements, and the model dependence in extracting the TPE contributions these data are insufficient to make a strong conclusion about the presence of TPE effects. There are three experiments which aim to improve the precision and kinematic coverage of $e^\pm p$ comparisons [63, 64, 65]. Two of the measurements [63, 64] have completed data taking, and the third is expected to begin in the near future. While all of these experiments will be limited to $Q^2 \lesssim 2 \text{ GeV}^2$, they will make precise measurements over a significant ε range, and allow direct tests of calculations of the TPE effects. Additional details on the planned measurements are presented in Sec. 5.2.

3.3.2 Improved measurements of the Rosenbluth–polarization discrepancy

Given the difficulty of making precise comparisons of positron and electron scattering at high Q^2 and large scattering angle, one must complement these direct measurement with other studies that can be used to constrain TPE contributions. The most compelling evidence to date is the discrepancy between

Rosenbluth and polarization measurements of the proton form factor ratio $\mu_p G_E/G_M$. These can only be used to constrain the overall size of the ε dependent TPE effects if we assume that TPE contributions fully explain the discrepancy.

Above $Q^2 = 4 \text{ GeV}^2$, the discrepancy is only at the 2–3 σ level when examined as a function of $(\mu_p G_E/G_M)^2$, Fig. 4 (right panel), which is directly related to the measured slope of the reduced cross section. Below $Q^2 = 1 \text{ GeV}^2$, the sensitivity to TPE corrections is smaller, and significant improvements in both the polarization and Rosenbluth measurements are necessary. Jefferson Lab experiment E05-017 [66] was approved to make an extended set of Super-Rosenbluth measurements, using the same technique as Ref. [14], but covering a much larger Q^2 range. At low Q^2 , extended Rosenbluth measurements at Jefferson Lab [66] and Mainz [67] and high-precision polarization measurements at Jefferson Lab [21, 23, 25] have been performed. The new data covering the range $0.3 < Q^2 < 0.8 \text{ GeV}^2$ show good agreement between Rosenbluth and polarization measurements, suggesting that TPE contributions may be small in this region. However, because the sensitivity to the TPE contributions is reduced at low Q^2 , and the Rosenbluth extractions [67] did include limited TPE corrections (using the Coulomb distortion correction of Ref. [37]), it is difficult to set precise limits in this region.

The high Q^2 Rosenbluth separations from Jefferson Lab experiment E05-017 will not only improve the determination of the discrepancy at low and high Q^2 , they potentially offer a clean and fairly direct measure of the TPE contributions. For $Q^2 > 4 - 5 \text{ GeV}^2$, the form factors extracted from the polarization measurements suggest that the maximum cross section contribution from G_E is $\lesssim 2\%$ (as illustrated in Fig. 5) and is relatively well measured. Thus, at high Q^2 the polarization measurements provide a reliable baseline for the ε dependence and any additional dependence on ε will be a direct measure of the TPE contribution, assuming that TPE fully explains the discrepancy. The results of experiment E05-017 are presently under analysis.

3.3.3 Experimental limits on nonlinearities

In the Born approximation, the reduced cross section at fixed Q^2 depends linearly on ε . Any deviation from linearity must come from terms that are not included in the standard radiative correction procedures. Thus, the difference between polarization and Rosenbluth measurements of the form factors is related to the average linear contribution of TPE, while any deviation from linearity is a clear indicator of effects beyond the Born approximation. At lower Q^2 values, observing such a deviation would provide a clear signature of effects beyond one-photon exchange and would provide quantitative information on the *nonlinear* component of the such effects. At large Q^2 , the contribution from G_E becomes small enough that almost all of the ε dependence comes from TPE (or other corrections), as shown in Fig. 5. In this region, the ε dependence of the reduced cross section allows us to isolate the full ε dependence of the contributions beyond the Born approximation.

A detailed examination of nonlinear contributions was performed by fitting the reduced cross section to the form

$$\sigma_R = P_0 [1 + P_1(\varepsilon - 0.5) + P_2(\varepsilon - 0.5)^2]. \quad (17)$$

Note that the quadratic term is expanded around $\varepsilon = 0.5$ such that P_2 represents the relative magnitude of the nonlinear term compared to the average cross section, rather than the $\varepsilon = 0$ cross section, which becomes extremely small at low Q^2 . The coefficient P_2 provides a simple measure of the relative size of nonlinear terms, and the uncertainty δP_2 can be used to set limits on ε^2 terms. Conventional Rosenbluth separation measurements have found P_2 to be consistent with zero, and the best constraint [34] yields $\delta P_2 \approx 10.5\%$. The recent Jefferson Lab E01-001 data [14] obtained improved limits on P_2 ($\delta P_2 = 4.4\%$) by detecting the struck proton rather than the scattered electron.

Figure 8 shows the reduced cross section as a function of ε for the best conventional Rosenbluth separation (SLAC NE11 [34]), and from the Super-Rosenbluth extraction in Jefferson Lab experiment

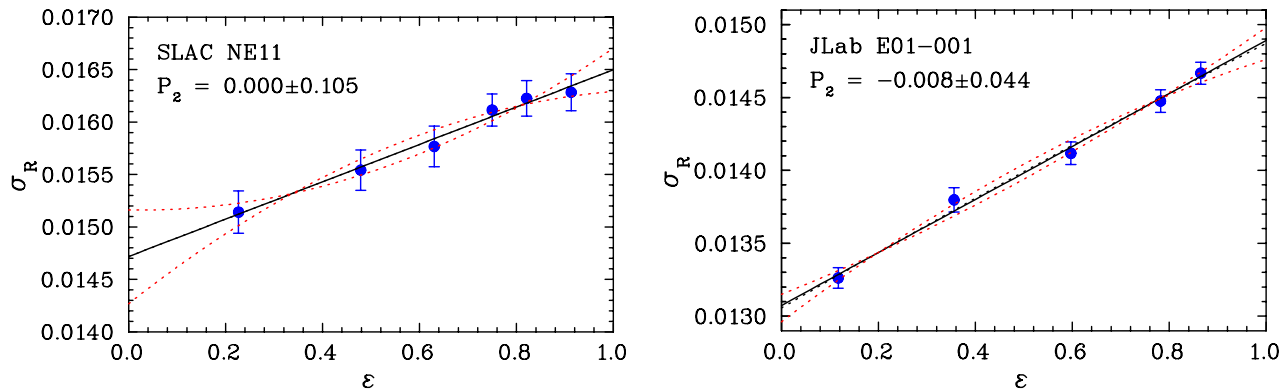


Figure 8: The ε dependence of the reduced cross section from SLAC NE11 [34] (using only data from the 8 GeV spectrometer) (**left**) and for Jefferson Lab experiment E01-001 [14] (**right**). The solid line is the linear fit, while the dotted lines are quadratic fits with $P_2 = \pm 0.105$ for NE11, $P_2 = -0.008 \pm 0.044$ for E01-001 (*i.e.* 1σ variations on the central value).

E01-001 [14]. The data are consistent with no nonlinear contributions. A global analysis of nonlinearities, including both elastic scattering, resonance region measurements, and deep-inelastic scattering was performed in Ref. [68]. This analysis concluded that all of the measurements are consistent with a linear ε dependence. For the elastic measurements, the limits on nonlinear contributions, shown in the left panel of Fig. 9, are not very significant except for $Q^2 = 2-4$ GeV², where there are recent high precision measurements [14]. The right panel shows the difference between the cross section measurements and the linear fits, averaged over all Q^2 , which gives an indication of how well the possible deviations from linearity are constrained as a function of ε .

Similar analyses were performed by other groups for ep [69] and ed elastic scattering [70]. In Ref. [69], the nonlinear contributions were parametrized using constraints from C-parity and crossing symmetry. However, the parametrization of the TPE contributions (relative to the Born cross section) was taken to be proportional to $x = \sqrt{(1+\varepsilon)/(1-\varepsilon)}$, which diverges for $\varepsilon \rightarrow 1$. Thus, any data with strong constraints at high ε yields a very tight constraint on the coefficient of the divergent TPE contributions, but still yields large nonlinear contributions at higher ε values. While this parametrization is consistent with the symmetries being considered by the authors, it is inconsistent with TPE contributions, as discussed in Ref. [71], and does not provide meaningful constraints on nonlinear TPE contributions.

The analysis of TPE effects in ed scattering by Rekaló *et al.* [70] has similar issues. Based on similar considerations, the TPE contributions were expanded there as a Taylor series in x . However, since x is always larger than unity, and in fact diverges as $\varepsilon \rightarrow 1$ ($\theta \rightarrow 0$), the expansion of the TPE contribution in powers of x does not provide a meaningful way to examine the data.

In Ref. [72] estimates were provided for P_2 based on the partonic TPE calculations [53, 73] (see Sec. 4.6). This work found that the calculated nonlinearities were of approximately the same size as the limits set by the global analysis [68], but had a large dependence on the model used for the calculation. While the limits on nonlinearity do not yet provide significant constraints, the improved measurements of Jefferson Lab experiment E05-017, presently being analyzed, should allow for significant constraints on TPE calculations over a range in Q^2 .

3.4 Conclusions from early experiments

While examinations of previous data and the early measurements aimed at understanding the discrepancy did not provide clear answers, they were consistent with the idea that larger than expected TPE

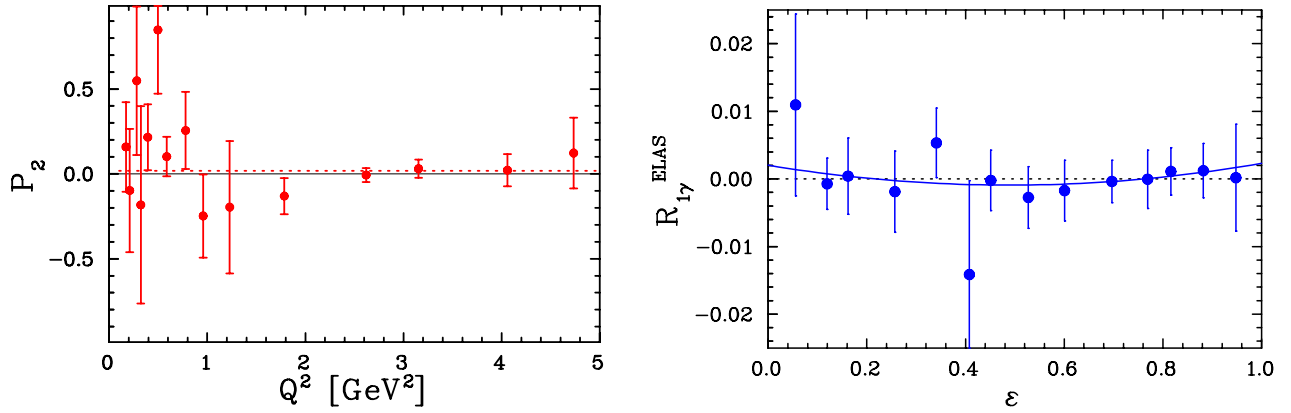


Figure 9: **(Left)** Nonlinearity parameter P_2 (see Eq. (8)) from a global analysis [68] of elastic cross section data. The dotted line indicates the global average, $\langle P_2 \rangle = 0.019 \pm 0.027$. **(Right)** Weighted average of the deviation of the cross section measurements from linear fits, $R_{1\gamma} = (\sigma_{\text{data}} - \sigma_{\text{fit}})/\sigma_{\text{fit}}$. The curve is a quadratic fit to the residual deviation yielding a quadratic term of $0.9 \pm 2.0\%$. Figure adapted from Ref. [68].

contributions could explain the discrepancy. The effect had to be small at forward scattering angles, to be consistent with comparisons of positron and electron scattering, and yield an angle dependence of $\sim 5\%$ at high Q^2 , approximately linear in ϵ , to resolve the discrepancy.

Because these corrections were larger than previous estimates of TPE, significant effort was put into understanding these theoretically and constraining them experimentally through new measurements. These efforts were not just limited to examining TPE corrections to the unpolarized cross sections; if TPE yields effects on the cross section on the order of a few percent, it may also enter into other observables at the same level and contribute to other reactions beyond elastic ep scattering. While experimental tests of TPE are for the most part limited to elastic ep scattering, measurements of several observables can be performed. With a range of measurements, one hopes to constrain models well enough that they can provide reliable, semi-quantitative estimates for TPE contributions in other reactions. This will allow one to determine where residual TPE effects may have a significant impact on other measurements.

As mentioned in Sec. 3.3, the initial experimental investigations focused on observables directly related to the cross section measurements. The initial investigations focused on existing data, while new measurements were being performed to improve the precision and kinematical coverage of Rosenbluth separations, polarization measurements, and comparisons of positron and electron scattering. Additional measurements were proposed to study at the ϵ dependence of the polarization observables [74] (Sec. 5.3), which are ϵ independent in the Born approximation, as well as observables which are forbidden in the Born approximation (Sec. 5.5). Before addressing these additional measurements, in the following sections we discuss calculations of TPE corrections within several theoretical frameworks (Sec. 4), comparisons of these calculations to additional measurements (Sec. 5), and estimates of TPE contributions in reactions beyond elastic ep scattering (Sec. 6).

4 Two-photon exchange

In view of the failure to understand the discrepancy between the Rosenbluth and polarization transfer measurements of G_E/G_M in terms of standard radiative corrections, the focus soon turned to revisiting the methodologies used in computing the box and crossed-box two-photon exchange corrections, illustrated in Fig. 10. An experimental–theoretical working group was established at Jefferson Lab, with the goal of identifying possible directions for resolving the discrepancy. The first quantitative calculation resulting from this renewed focus was made by Blunden *et al.* [5], who computed the effect on G_E/G_M from TPE, incorporating explicitly the nucleon’s substructure. Thereafter followed a number of other studies, examining TPE in a variety of frameworks, and exploring reactions beyond elastic ep scattering. In a parallel effort, Guichon and Vanderhaeghen [50] provided a generalized formalism for elastic scattering, allowing for possible TPE contributions, and demonstrated that it was natural to have TPE contributions which could significantly change the LT extraction of G_E with minimal impact on the PT measurements.

In this section we review these efforts, paying particular attention to the conventional hadronic-level calculations which are most applicable to data analysis at low to moderate Q^2 values. Before turning to the (model-dependent) TPE contributions, we first discuss some general properties of radiative corrections in order to set the stage for the recent improvements.

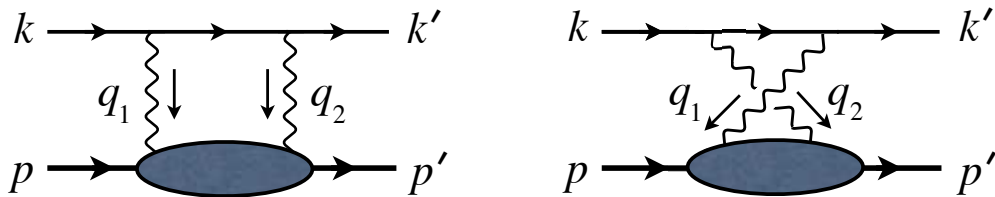


Figure 10: Box and crossed-box two-photon exchange contributions to elastic electron–nucleon scattering. The overall four-momentum transfer to the nucleon is $q = k - k' = q_1 + q_2$.

4.1 General properties of radiative corrections

At order α^2 , radiative corrections to the one-photon exchange cross section σ_R^0 , Eq. (8), include processes arising from the exchange of a second virtual photon, and inelastic scattering processes involving the emission of a real bremsstrahlung photon, so that

$$\sigma_R = \sigma_R^0 (1 + \delta_{\text{virt}} + \delta_{\text{brem}}). \quad (18)$$

In analyzing the virtual corrections for a ep scattering, it is convenient to separate terms into “soft” parts, which are independent of hadronic structure, and “hard” parts, which are model dependent. Soft here implies that any interaction of the second virtual photon with the proton occurs with vanishingly small momentum transfer. The soft parts are therefore the same for protons as they are for scattering from pointlike particles (*e.g.* in $e^- \mu^+$ scattering). All of the infrared (IR) divergences for the virtual diagrams are contained in the soft parts, and cancel in the total amplitude.

If we denote the amplitude for all one-loop virtual corrections, illustrated in Fig. 11, by $\mathcal{M}_{1\text{-loop}}$, then $\mathcal{M}_{1\text{-loop}}$ can be written as the sum of a “factorizable” soft term, proportional to the Born amplitude \mathcal{M}_γ , and a non-factorizable hard part $\mathcal{M}_{\text{hard}}$,

$$\mathcal{M}_{1\text{-loop}} = f(Q^2, \varepsilon) \mathcal{M}_\gamma + \mathcal{M}_{\text{hard}}, \quad (19)$$

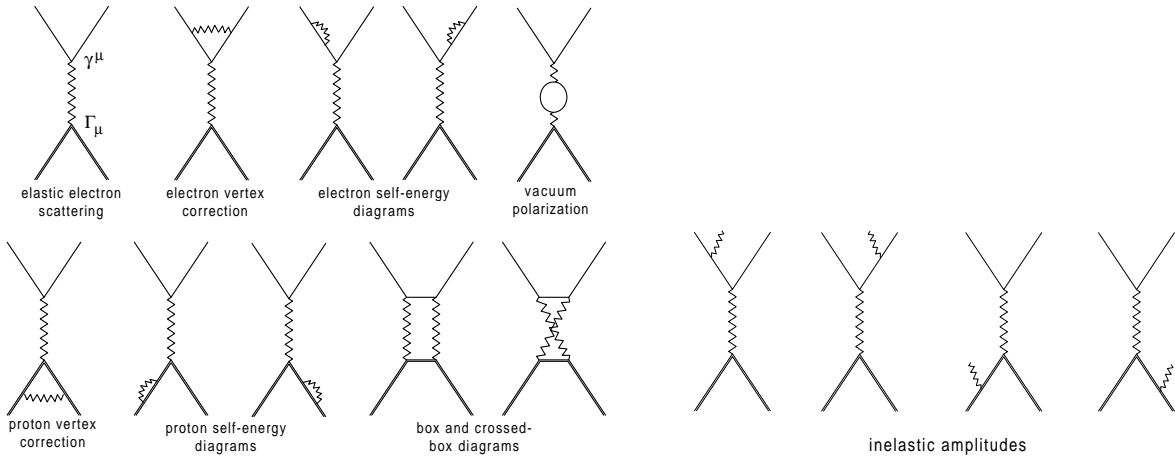


Figure 11: The complete set of diagrams to order α^2 , including the virtual (**left**) and bremsstrahlung (or inelastic) (**right**) contributions. Figure taken from Ref. [47].

with $f(Q^2, \varepsilon)$ a purely kinematic factor. Therefore δ_{virt} is given by

$$\delta_{\text{virt}} = 2f(Q^2, \varepsilon) + \frac{2\text{Re}\{\mathcal{M}_\gamma^* \mathcal{M}_{\text{hard}}\}}{|\mathcal{M}_\gamma|^2} \equiv \delta_{\text{soft}} + \delta_{\text{hard}}. \quad (20)$$

All of the virtual processes in Fig. 11 contribute to the soft terms in δ_{soft} . In practice these terms dominate, and are the ones accounted for in the standard radiative corrections of Mo and Tsai [37, 38]. Furthermore, the functions $f(Q^2, \varepsilon)$ for the vacuum polarization, self-energy, and vertex corrections are ε -independent (although the vertex terms are IR-divergent), and therefore have no relevance for the LT separation aside from an overall normalization factor. Hence, of the factorizable terms, only the TPE can contribute to the ε -dependence of the cross section (Fig. 10). It should be noted that the decomposition of the TPE effect into soft and hard parts is not unique, as discussed below.

The terms which depend on hadronic structure are contained in $\mathcal{M}_{\text{hard}}$, and arise from the proton vertex and TPE corrections. For the proton, the hadronic vertex correction was analyzed by Maximon and Tjon [47], and found to be $< 0.5\%$ in magnitude for $Q^2 < 6 \text{ GeV}^2$. Since the proton vertex correction does not have a strong ε -dependence, it will not affect the LT analysis, and can be safely neglected in examining the form factor discrepancy.

For the inelastic bremsstrahlung contribution, illustrated in Fig. 11, the amplitude for real photon emission can also be written in the form of Eq. (19). In the soft photon approximation (SPA) one again keeps only the factorizable terms that are independent of hadron structure, in which case the cross section is a simple kinematic factor times the Born cross section, Eq. (8). A significant ε -dependence arises from this contribution due to the frame dependence of the angular distribution of the emitted photon.

Typically an infinitesimal photon mass λ is introduced in the photon propagator as a bookkeeping device to regulate the IR divergences. For the box and crossed-box TPE diagrams in Fig. 10, this λ dependence is cancelled by the bremsstrahlung interference contribution with a soft-photon emitted from the electron and proton (*i.e.* by cutting one of the (soft) photon propagators). This produces a correction to the cross section depending on the proton charge Z . A similar cancellation occurs for the IR divergences in the electron vertex and proton vertex corrections, which depend on Z^0 and Z^2 , respectively. For positron-proton scattering one can take $Z = -1$, so that only the TPE (and bremsstrahlung interference) terms are relevant in comparison with the electron-proton case.

Although the standard radiative corrections are model independent, there have been significant improvements to the original work of Mo and Tsai [37, 38], removing many of the mathematical and

other approximations used in that work. An important contribution was the calculation of Maximon and Tjon [47], whose analysis differs from that of Refs. [37, 38] in two substantive aspects. First, they evaluated the inelastic bremsstrahlung cross section without any approximation, using integrals given in closed form by 't Hooft and Veltman [75]. The exact expressions are simpler in form than the approximate ones given in Ref. [38]. In the limit $M \rightarrow \infty$, corresponding to a static Coulomb potential, they reproduce exactly the result first given by Schwinger [76]. Second, in the evaluation of the contribution of the TPE diagrams, they make a less drastic approximation than that made in [37]. Specifically, in the integrands corresponding to the relevant IR-divergent amplitudes, they make a soft-photon approximation for the matrix elements of the current appearing in the numerator (as in [37]), but not for the propagators, which appear in the denominator. The required integrals (scalar four-point functions) have also been given in [75, 77]; the resulting expressions are again considerably simpler than those obtained in [37], where the soft-photon approximation is also made in the denominators.

Other improvements have also been made to the work of Mo and Tsai [38]. These include higher mass vacuum polarizations terms (not just e^+e^-) from Ref. [11], improved implementation of multi-photon exchange and angle-dependent bremsstrahlung for coincidence reactions [46, 78], and improved treatment of multi-photon exchange in the structure function method [79]. The first three were simply improvements to the Mo-Tsai framework, made independently of the form factor discrepancy. The last [79] was an attempt to explain the discrepancy. While they found differences between their results and Mo-Tsai based radiative corrections, the comparison was not made for identical conditions, and more work is required to determine whether there is really any substantial difference.

4.2 Soft two-photon exchange effects

The improvements in the computation of the radiative corrections made by Maximon and Tjon [47] have a number of important effects on the corrections of order Z . The form of the bremsstrahlung correction depends on whether the scattered electron or the recoil proton is detected. For the detection of the scattered electron, the bremsstrahlung correction in the SPA is found to be

$$\delta_{\text{brem}}(\text{MTj}) = \frac{2\alpha Z}{\pi} \left[\ln \eta \ln \left(\frac{(2\eta\Delta E)^2}{y\lambda^2} \right) + \text{Li}_2 \left(1 - \frac{\eta}{y} \right) - \text{Li}_2 \left(1 - \frac{1}{\eta y} \right) \right], \quad (21)$$

with $\eta = E/E'$ the ratio of incident to final electron energies, Li_2 is the dilogarithm function, and $y = 1 + 2\tau + 2\sqrt{\tau(1+\tau)}$. Here ΔE is the maximum allowable energy loss in the lab frame due to detector acceptance or experimental cuts, below which one cannot determine that a soft photon has been emitted. This exact expression is simpler in form than the approximate one of Mo and Tsai [37, 38]. Their expression is too long to reproduce here, but it takes the form

$$\delta_{\text{brem}}(\text{MoT}) = \frac{2\alpha Z}{\pi} \ln \eta \ln \left(\frac{\Delta E^2}{\lambda^2} \right) + \text{finite terms}. \quad (22)$$

From this it is clear that the logarithmic dependence on both ΔE and λ in Eqs. (21) and (22) is the same, and so the difference between the two treatments is a finite kinematic factor.

The IR-divergent part of the box amplitude can be separated from the IR-finite part by analyzing the structure of the photon propagators in the integrand. The two poles, where the photons are soft, occur at $q_1 = 0$ ($q_2 = q$) and at $q_1 = q$ ($q_2 = 0$). Evaluating the *numerator* of the integral at either value gives a contribution to the TPE amplitude for the box diagram as

$$\begin{aligned} \mathcal{M}_{\gamma\gamma}^{\text{box}} &= -\frac{Z\alpha}{2\pi} (s - M^2) q^2 \mathcal{M}_\gamma \frac{1}{i\pi^2} \int d^4q_1 \frac{1}{[q_1^2 - \lambda^2] [(q - q_1)^2 - \lambda^2] [(k - q_1)^2 - m_e^2] [(p + q_1)^2 - M^2]} \\ &= -\frac{Z\alpha}{2\pi} (s - M^2) q^2 \mathcal{M}_\gamma D_0(s; m_e, \lambda, M, \lambda), \end{aligned} \quad (23)$$

where $s = M^2 + 2ME$ is the Mandelstam variable in the laboratory frame. The integral over the product of four propagators is expressed in terms of the four-point Passarino-Veltman function $D_0(s)$ [77], which can be evaluated numerically using the program LoopTools [80]. General expressions for the asymptotic expansion of all four-point IR-divergent integrals have been given by Beenakker and Denner [81], who find

$$D_0(s; m_e, \lambda, M, \lambda) = \frac{2}{(s - M^2)q^2} \ln \left(\frac{M^2 - s}{m_e M} \right) \ln \left(\frac{-q^2}{\lambda^2} \right), \quad (24)$$

in the limit $(s - M^2) \gg m_e^2, m_e M$. Here one is only interested in the real part of this expression. The convention for the logarithm is $\ln(-z) = \ln(z) - i\pi$ when $z < 0$, which is achieved by setting $z \rightarrow z + i0^+$. For the crossed-box one can make use of crossing symmetry. This requires that the crossed-box amplitude $\mathcal{M}_{\gamma\gamma}^{\text{xbbox}}$ obey the relation

$$\mathcal{M}_{\gamma\gamma}^{\text{xbbox}}(u, t) = + \mathcal{M}_{\gamma\gamma}^{\text{bbox}}(s, t)|_{s \rightarrow u}. \quad (25)$$

where $t = q^2$. Thus the total box plus crossed-box amplitude must be even under the interchange $s \leftrightarrow u$, or equivalently $E \leftrightarrow -E'$. Note that since $M^2 - u > 0$, the crossed-box amplitude has no imaginary part. Combining these expressions, and taking the real part only, the final result for the soft virtual correction is [47]

$$\delta_{\text{IR}}(\text{MTj}) = -\frac{2\alpha Z}{\pi} \ln \eta \ln \frac{Q^2}{\lambda^2}. \quad (26)$$

Note that the dependence on the electron mass m_e has dropped out in the final expression, and the logarithmic IR singularity in λ is exactly cancelled when added to Eq. (21).

By contrast, in earlier treatments [37, 44, 82] the SPA is also applied to one of the propagators, for example replacing $1/(q - q_1)^2$ by $1/q^2$ when $q_1 \rightarrow 0$, and $1/q_1^2$ by $1/q^2$ when $q_1 \rightarrow q$. Hence the IR-divergent contribution is

$$\begin{aligned} \mathcal{M}_{\gamma\gamma}^{\text{bbox}} &= -2 \frac{Z\alpha}{2\pi} (s - M^2) \mathcal{M}_\gamma \frac{1}{i\pi^2} \int d^4 q_1 \frac{1}{[q_1^2 - \lambda^2] [(k - q_1)^2 - m_e^2] [(p + q_1)^2 - M^2]} \\ &= -2 \frac{Z\alpha}{2\pi} (s - M^2) \mathcal{M}_\gamma C_0(s; m_e, \lambda, M), \end{aligned} \quad (27)$$

where $C_0(s)$ is the three-point Passarino-Veltman function [77], and a factor of 2 accounts for the contribution from both poles. To facilitate comparison, note that Tsai [37] introduces the function $K(-k, p)$ in evaluating this integral, which is equal to $(s - M^2)C_0(s)$, with $s = (k + p)^2$. In this approximation one therefore expects

$$\begin{aligned} \delta_{\text{IR}} &= -\frac{2\alpha Z}{\pi} [(s - M^2)C_0(s) - (u - M^2)C_0(u)], \\ &= \frac{2\alpha Z}{\pi} \left[\text{Li}_2 \left(1 + \frac{M}{2E} \right) - \text{Li}_2 \left(1 - \frac{M}{2E'} \right) - \frac{1}{2} \ln(-\eta) \ln \left(\frac{-4M^2 E E'}{\lambda^4} \right) \right], \end{aligned} \quad (28)$$

for which the crossing symmetry property is manifest. In writing the last line we have again used the asymptotic expansion of three-point IR-divergent functions given in Beenakker and Denner [81]. Equation (28) is equivalent to the form given by Meister and Yennie [82], which was used in Refs. [53, 73]. Equation (28) is larger than Eq. (26) by a finite amount of approximately $\alpha\pi$ – a point that was also noted in Refs. [53, 73].

Tsai [37] makes a further mathematical approximation, to replace $p \rightarrow -p$ in the *box contribution only*, or equivalently $s \rightarrow M^2 - 2ME$. Although this additional approximation spoils the crossing symmetry, it eliminates the term $(i\pi)^2$ that arises in Eq. (28) from the product of logarithms with negative argument, and is therefore closer to the result of Maximon and Tjon, Eq. (26). At the time,

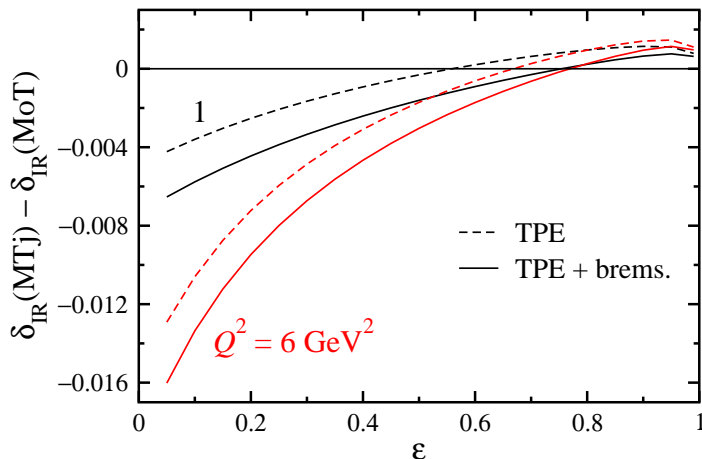


Figure 12: Difference between the model-independent corrections of Maximon-Tjon [47] and Mo-Tsai [37, 38] for virtual TPE (dashed curves) and virtual+real (solid). The upper (lower) dashed and solid curves correspond to $Q^2 = 1$ (6) GeV^2 .

Mo and Tsai argued that the resulting expression is closer to the exact calculations of ee scattering [38]. The final result for the Mo-Tsai soft virtual correction can then be expressed as

$$\delta_{\text{IR}}(\text{MoT}) = \frac{2\alpha Z}{\pi} \left[\text{Li}_2 \left(1 - \frac{M}{2E} \right) - \text{Li}_2 \left(1 - \frac{M}{2E'} \right) - \frac{1}{2} \ln \eta \ln \left(\frac{4M^2 E E'}{\lambda^4} \right) \right], \quad (29)$$

which is clearly no longer asymmetric under $E \leftrightarrow -E'$.

Because the Mo-Tsai result is the one generally used in existing experimental analyses calculations of the full TPE contribution presented here will be taken with respect to $\delta_{\text{IR}}(\text{MoT})$ rather than $\delta_{\text{IR}}(\text{MTj})$ (except where indicated). It is useful to compare the ϵ -dependence of these two treatments of the soft virtual corrections. The difference $\delta_{\text{IR}}(\text{MTj}) - \delta_{\text{IR}}(\text{MoT})$ is independent of λ , and is shown in Fig. 12 (dashed curves) as a function of ϵ for $Q^2 = 1$ and 6 GeV^2 . Note that the difference vanishes as $Q^2 \rightarrow 0$. The different treatments of the IR-divergent terms already have significance for the LT separation, resulting in roughly a 1% change in the cross section over the range of ϵ . Also shown in Fig. 12 is a comparison for the total correction linear in Z (solid curves), which includes the improvements to the bremsstrahlung correction, *viz.* $[\delta_{\text{IR}}(\text{MTj}) + \delta_{\text{brem}}(\text{MTj})] - [\delta_{\text{IR}}(\text{MoT}) + \delta_{\text{brem}}(\text{MoT})]$. This is appropriate when the scattered electron is detected, and is the procedure adopted in the generalized parton distribution calculations of Refs. [53, 73]. From these curves it is clear that most of the difference arises from the treatment of the TPE diagrams rather than the bremsstrahlung correction.

4.3 Hadron structure effects

Going beyond the Mo-Tsai [37, 38] and Maximon-Tjon [47] approximations, Blunden *et al.* [5] proceeded to evaluate the box and crossed-box TPE diagrams without resorting to any of the soft-photon approximations discussed above. In particular, they considered explicitly the effects of incorporating the hadronic structure of the nucleon, parametrized through hadronic electromagnetic form factors. Specifically, Blunden *et al.* computed [5, 6, 83] the total TPE amplitude

$$\mathcal{M}_{\gamma\gamma} = \mathcal{M}_{\gamma\gamma}^{\text{box}} + \mathcal{M}_{\gamma\gamma}^{\text{xbox}}, \quad (30)$$

where

$$\mathcal{M}_{\gamma\gamma}^{\text{box (xbox)}} = -ie^4 \int \frac{d^4 q_1}{(2\pi)^4} L_{\mu\nu}^{\text{box (xbox)}} H_N^{\mu\nu} \Delta_F(q_1, \lambda) \Delta_F(q_2, \lambda), \quad (31)$$

with the box and crossed-box leptonic tensors given by

$$L_{\mu\nu}^{\text{box}} = \bar{u}_e(k') \gamma_\mu S_F(k - q_1, m_e) \gamma_\nu u_e(k), \quad L_{\mu\nu}^{\text{xbox}} = \bar{u}_e(k') \gamma_\nu S_F(k - q_2, m_e) \gamma_\mu u_e(k). \quad (32)$$

Alternatively, one can obtain the crossed-box term directly from the box term by applying the crossing symmetry relation Eq. (25). The electromagnetic nucleon elastic hadronic tensor $H_N^{\mu\nu}$ is given by

$$H_N^{\mu\nu} = \bar{u}_N(p') \Gamma_\gamma^\mu(q_2) S_F(p + q_1, M) \Gamma_\gamma^\nu(q_1) u_N(p). \quad (33)$$

Here the electromagnetic current operator Γ_γ^μ is given in Eq. (7), and the fermion (electron and nucleon) and gauge boson (photon) propagators are given by

$$S_F(k, m) = \frac{\not{k} + m}{k^2 - m^2 + i\epsilon}, \quad \Delta_F(k, \lambda) = \frac{1}{k^2 - \lambda^2 + i\epsilon}, \quad (34)$$

respectively. The infinitesimal photon mass λ is introduced to regulate the infrared divergences. One can verify explicitly that the integrals in Eq. (31) satisfy the crossing symmetry constraint in Eq. (25).

The relative correction to the elastic Born cross section, Eq. (8), due to the interference of the one- and two-photon exchange amplitudes (Figs. 1 and 10) is given by

$$\delta_{\gamma\gamma} = \frac{2\text{Re}(\mathcal{M}_\gamma^* \mathcal{M}_{\gamma\gamma})}{|\mathcal{M}_\gamma|^2}. \quad (35)$$

Typically, experimental analyses of form factor data apply radiative corrections based on the Mo-Tsai prescription [37, 38] or modified approaches based on the same general framework [11, 46], which include approximating the TPE contribution by the IR prescription $\delta_{\text{IR}}(\text{MoT})$ in Eq. (29). To determine the effect of the full, hadron-structure dependent correction $\delta_{\gamma\gamma}$ on the data, one must therefore compare the ε -dependence of the full calculation with that of $\delta_{\text{IR}}(\text{MoT})$. A meaningful comparison can be made by considering the difference

$$\bar{\delta} \equiv \delta_{\gamma\gamma} - \delta_{\text{IR}}(\text{MoT}), \quad (36)$$

in which the IR divergences cancel, and which is independent of λ .

The results for the difference $\bar{\delta}$ between the full calculation and the MT approximation are shown in Fig. 13 as a function of ε for several values of Q^2 from 0.001 to 1 GeV² (left panel) and 1 to 6 GeV² (right panel). The hadron structure dependent corrections are most significant at low ε , where they range from 2% to $\sim 6\%$ over this Q^2 range. At the lower Q^2 values, $\bar{\delta}$ is approximately linear in ε , but significant deviations from linearity are observed with increasing Q^2 , especially at small ε .

Note that assuming that the current operator Γ_γ^μ in $\mathcal{M}_{\gamma\gamma}$ has a similar structure off-shell as on-shell, with phenomenological form factors at the γNN vertices, introduces model dependence into the calculation, as the radiative corrections are used to determine the experimental form factors in the first place. In principle this dependence could be removed by iteratively extracting the form factors with the inclusion of TPE corrections and feeding those form factors into subsequent TPE calculations. Even without iterating, however, because $\delta_{\gamma\gamma}$ is a ratio, the model dependence mostly cancels, provided the same phenomenological form factors are used for both \mathcal{M}_γ and $\mathcal{M}_{\gamma\gamma}$. This was demonstrated in Ref. [6] by comparing the results with those obtained using a dipole form

$$G_D(Q^2) = \left(1 + \frac{Q^2}{\Lambda_D^2}\right)^{-2}, \quad (37)$$

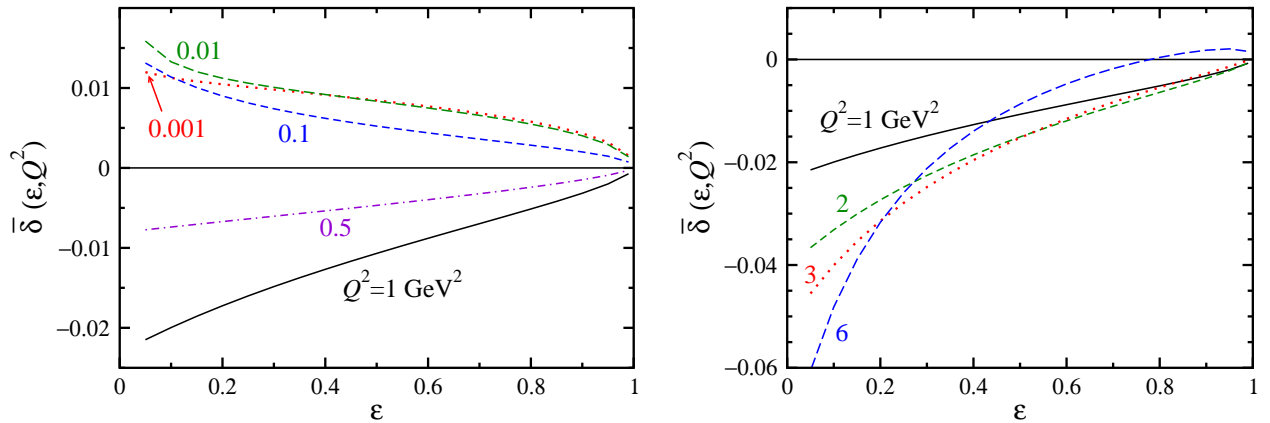


Figure 13: Difference $\bar{\delta}$ between the full TPE correction to the elastic cross section [5] and the commonly used Mo-Tsai approximation (29) [37, 38], for $Q^2 = 0.001\text{--}1 \text{ GeV}^2$ (**left**), and for $Q^2 = 1\text{--}6 \text{ GeV}^2$ (**right**).

with mass $\Lambda_D = 0.84 \text{ GeV}$. The model dependence is very weak at the lower Q^2 value, with virtually no effect on the ϵ slope. At larger Q^2 values the differences increase, but the general trend of the correction remains unchanged, so that one can conclude that the model dependence of the calculation is quite modest. At $Q^2 \gtrsim 6 \text{ GeV}^2$, which will be accessible in future experiments at Jefferson Lab, significant deviations from linearity are expected over the entire ϵ range.

The TPE correction $\bar{\delta}$ is also found to be insensitive to the high- Q^2 behavior of the G_E/G_M ratio. Using form factor inputs from parametrizations obtained by fitting only LT-separated data [36, 84] and those in which G_E is constrained by the polarization transfer data [36, 85], the differences are almost indistinguishable up to $Q^2 = 6 \text{ GeV}^2$ [6]. (Note that the G_M form factor itself also differs by a few percent between the various parametrizations.)

4.4 Inelastic contributions

While the TPE diagrams in Fig. 10 contain contributions from intermediate states containing all possible excitations of the nucleon, the above discussion has thus far been restricted to the nucleon elastic component. In view of the prominent role of the $\Delta(1232)$ resonance, for example, in many hadronic reactions, it is important to evaluate its contribution to the TPE amplitude, as well as the possible role of other inelastic intermediate states.

4.4.1 Δ intermediate states

The first estimate of the possible role played by excitations of the nucleon in elastic ep scattering was by Drell and Fubini [41]. Using dispersion theory methods within a nonrelativistic approximation, they found that for energies up to $E \sim 1 \text{ GeV}$, the $\Delta(1232)$ resonance contribution increased the Born cross section by $\sim 1\%$. Later, Campbell [43, 44] used relativistic Rarita-Schwinger spinors for the Δ , but retained the soft-photon approximation [38], together with the assumption of $M1$ transition dominance. For large scattering angles, the correction from the Δ was found to be non-negligible for $Q^2 \sim 1\text{--}5 \text{ GeV}^2$, but the estimate was limited by the uncertainty in the $\gamma N \Delta$ form factor. Partial cancellation between the nucleon and Δ contributions for center of mass energies above 500 MeV was observed by Greenhut [45], who used the second Born approximation, neglecting recoil, and assuming magnetic only coupling. The conclusion of this work was that the combined N and Δ channels were not expected to exceed $\sim 1\%$ of the cross section, although the approximations inherent in the calculation

rendered it less reliable for energies above 1 GeV [45].

More recently, Kondratyuk *et al.* [7] computed the $\Delta(1232)$ resonance contribution within the same relativistic framework that was used to compute the nucleon intermediate states in Sec. 4.3, without invoking any of the approximations of the earlier studies [41, 43, 44, 45]. Following Refs. [86, 87], the $\gamma N\Delta$ vertex is defined as

$$\begin{aligned} \Gamma_{\gamma N \rightarrow \Delta}^{\alpha\mu}(p_\Delta, q) &= \frac{1}{2M_\Delta^2} \sqrt{\frac{2}{3}} \left\{ g_1(Q^2) [g^{\alpha\mu} \not{p}_\Delta - \not{q} \gamma^\alpha p_\Delta^\mu - \gamma^\alpha \gamma^\mu q \cdot p_\Delta + \not{p}_\Delta \gamma^\mu q^\alpha] \right. \\ &\quad \left. + g_2(Q^2) [q^\alpha p_\Delta^\mu - g^{\alpha\mu} q \cdot p_\Delta] + \frac{g_3(Q^2)}{M_\Delta} [q^2 (\gamma^\alpha p_\Delta^\mu - g^{\alpha\mu} \not{p}_\Delta) + q^\mu (q^\alpha \not{p}_\Delta - \gamma^\alpha q \cdot p_\Delta)] \right\} \gamma_5, \end{aligned} \quad (38)$$

where p_Δ and q are the momenta of the *outgoing* Δ and *incoming* photon, with corresponding Lorentz indices α and μ , respectively. The factor $\sqrt{2/3}$ is the $N \rightarrow \Delta$ isospin transition factor. Electromagnetic gauge invariance requires that $q_\mu \Gamma_{\gamma N \rightarrow \Delta}^{\alpha\mu}(p_\Delta, q) = 0$. The coupling constants $g_i \equiv g_i(Q^2 = 0)$ for $i = 1, 2, 3$ can be related to the magnetic, electric and Coulomb components of the $\gamma N\Delta$ vertex by $g_1 = g_M$, $g_2 = g_M + g_E$, $g_3 = g_C$ [7, 83]. The corresponding conjugate vertex can be obtained from the relation [7, 88]

$$\Gamma_{\Delta \rightarrow \gamma N}^{\mu\alpha}(p_\Delta, q) = \gamma_0 [\Gamma_{\gamma N \rightarrow \Delta}^{\alpha\mu}(p_\Delta, q)]^\dagger \gamma_0, \quad (39)$$

where p_Δ and q are the momenta of the *incoming* Δ and *outgoing* photon.

The amplitude of the box diagram with a Δ intermediate state can then be written as [7, 83]

$$\mathcal{M}_{\gamma\gamma}^{(\Delta)} = -ie^4 \int \frac{d^4 q_1}{(2\pi)^4} L_{\mu\nu} H_\Delta^{\mu\nu} \Delta_F(q_1, 0) \Delta_F(q_2, 0), \quad (40)$$

where $L_{\mu\nu}$ is the leptonic box tensor of Eq. (32), and the crossed-box is obtained by crossing symmetry, Eq. (25). The Δ hadronic tensor is given by

$$H_\Delta^{\mu\nu} = \bar{u}_N(p') \Gamma_{\Delta \rightarrow \gamma N}^{\mu\alpha}(p + q_1, -q_2) S_{\alpha\beta}(p + q_1, M_\Delta) \Gamma_{\gamma N \rightarrow \Delta}^{\beta\nu}(p + q_1, q_1) u_N(p), \quad (41)$$

where the Δ propagator is given by

$$S_{\alpha\beta}(p_\Delta, M_\Delta) = -S_F(p_\Delta, M_\Delta) \mathcal{P}_{\alpha\beta}^{3/2}(p_\Delta), \quad (42)$$

where the projection operator

$$\mathcal{P}_{\alpha\beta}^{3/2}(p_\Delta) = g_{\alpha\beta} - \frac{1}{3} \gamma_\alpha \gamma_\beta - \frac{1}{3p_\Delta^2} (\not{p}_\Delta \gamma_\alpha p_{\Delta\beta} + \gamma_\beta \not{p}_\Delta p_{\Delta\alpha}) \quad (43)$$

ensures that only spin-3/2 components are present. Suppression of the unphysical spin-1/2 contributions also leads to the condition on the vertex $p_{\Delta\alpha} \Gamma_{\gamma N \rightarrow \Delta}^{\alpha\mu}(p_\Delta, q) = 0$. Note that the mass difference $M_\Delta - M$ between the initial and intermediate hadronic states renders the integral (41) IR-finite, so that in contrast to Eq. (30), a photon mass parameter λ is not needed to regulate divergences.

In Refs. [7, 83] the three $\gamma N\Delta$ transition form factors $g_i(Q^2) \equiv g_i F_V^\Delta(Q^2)$ ($i = 1, 2, 3$) were assumed to have dipole shapes, $F_V^\Delta(Q^2) = (1 + Q^2/\Lambda_\Delta^2)^{-2}$, with a dipole mass $\Lambda_\Delta = 0.84$ GeV for each. The electric and magnetic couplings were taken to have the values $g_M = 7$ and $g_E = 9$ [7], obtained from a K-matrix analysis of pion photoproduction data [87]. A more realistic πN coupled channel quasi-potential study [89] gives similar values, $g_M = 6.3$ and $g_E = 3.4$. The Coulomb coupling g_C is not as well constrained as the electric and magnetic couplings, and Kondratyuk *et al.* [7] considered the range between $g_C = -2$ to 0. Tjon *et al.* [83] used an estimate from the nucleon- Δ E2/M1 transition strength, $g_C = 5.8$, but found the sensitivity to variations of g_C small. Similar values for the couplings were also used by Zhou *et al.* [88], although defined with different normalizations. The sensitivity to g_C was found

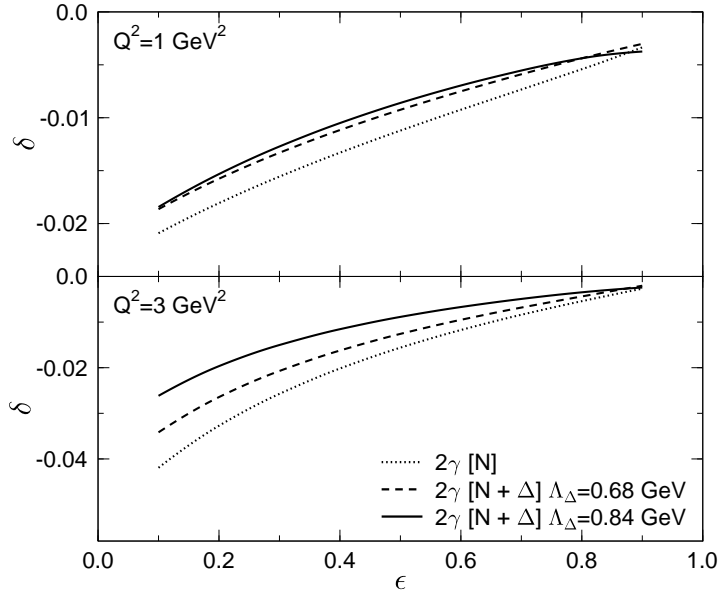


Figure 14: Sum of the nucleon and $\Delta(1232)$ contributions to the TPE correction to the ep elastic cross section for two values of the cut-off mass Λ_Δ . Figure taken from Ref. [7].

to be weak at low Q^2 and ϵ , becoming stronger at forward angles and large Q^2 ($Q^2 \gtrsim 3 \text{ GeV}^2$, $\epsilon \sim 1$) [88].

The ϵ dependence of the relative Δ and nucleon TPE contributions to the elastic cross section from Ref. [7], for $g_C = 0$, is shown in Fig. 14 at $Q^2 = 1$ and 3 GeV^2 . The most striking feature of Δ corrections is its positive sign, in agreement with the early estimates [41, 43, 44, 45], which is opposite to that of the nucleon, and the corresponding *negative* slope in ϵ . This has the effect of attenuating the (negative) nucleon TPE correction, making it somewhat smaller especially at backward angles. The magnitude of the Δ correction is considerably smaller than the nucleon, however, so that the general features of the TPE correction in Fig. 13 are not affected by the Δ .

These features are also largely insensitive to the details of the $\gamma N \Delta$ form factor, particularly at low Q^2 , as the comparison of the results in Fig. 14 with cut-offs $\Lambda_\Delta = 0.84$ and 0.68 GeV illustrates [7]. At higher Q^2 , on the other hand, both the magnitude of the Δ correction and its dependence on the form factor model increase, although for very large Q^2 the pure resonance calculation itself becomes more questionable.

4.4.2 Nucleon resonances

If the $\Delta(1232)$ resonance makes a non-negligible contribution to the TPE correction, at least in some kinematic regions, the question naturally arises whether other, higher-mass resonances could also play some role. Kondratyuk and Blunden [90] extended the formalism of Refs. [5, 7], generalizing it to include the full spectrum of the most important hadron resonances as intermediate states involving spin $1/2$ and $3/2$ resonances. The masses of the resonances and their nucleon-photon coupling constants are based on dynamical multichannel calculations [87, 91, 92] of nucleon Compton scattering at low and intermediate energies. The resonance TPE effects turn out to be not too sensitive to the details of these models.

In general the contributions of all the heavier resonances are much smaller than those of the nucleon and Δ (P_{33}) [7]. However, there is an interesting interplay between the contributions of the spin $1/2$ and spin $3/2$ resonances, which is analogous to the partial cancellation of the two-photon exchange effects of the nucleon and Δ intermediate states, found in Ref. [7]. Notwithstanding the smallness of the resonance

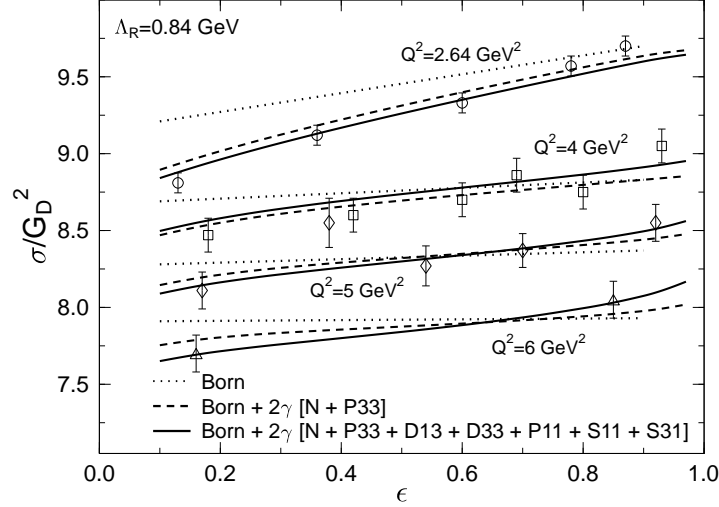


Figure 15: Reduced cross section, scaled by the dipole form factor squared, showing the effect of adding TPE corrections to the Born cross section. The intermediate state includes a nucleon and the indicated hadron resonances. The curves for $Q^2 = 2.64, 4$ and 6 GeV^2 have been shifted vertically by $-0.04, +0.04$ and $+0.09$, respectively, for clarity, and are compared with data from Refs. [11, 14]. The nucleon-only result is slightly larger than the $N + \Delta(P_{33})$, lying close to the full calculation. Figure taken from Ref. [90].

contributions, their inclusion in the TPE diagrams leads to a better agreement between the Rosenbluth and polarization transfer data analyses, especially at higher values of the momentum-transfer squared Q^2 .

The total TPE correction is given by the sum of the separate hadron contributions,

$$\delta = \delta^N + \delta^\Delta + \delta^{D_{13}} + \delta^{D_{33}} + \delta^{P_{11}} + \delta^{S_{11}} + \delta^{S_{31}}. \quad (44)$$

The coupling constants in the vertices are taken from the Dressed K-Matrix Model, whose essential ingredients are described in Ref. [87]. The calculated two-photon corrections to the reduced cross section are displayed in Fig. 15. The one-photon exchange cross sections are shown by the dotted lines. The cross sections including additional TPE corrections are shown by the dashed lines for the sum of the nucleon and Δ contributions, and by the solid lines for the full result with all resonances. In general, each resonance two-photon correction is proportional to a sum of squares of the nucleon-photon coupling constants of that resonance. This sets the scale of the magnitude of the resonance contributions.

As an example at the moderately high value $Q^2 = 4 \text{ GeV}^2$, the TPE corrections from the included resonances can be classified by their signs and orders of magnitude as follows. For $0 < \epsilon < 1$, the corrections change smoothly between the values

$$\begin{aligned} -5.0 \lesssim \delta^N \lesssim 0\%, & \quad 1.9 \gtrsim \delta^\Delta \gtrsim 0\%, & \quad -0.7 \lesssim \delta^{D_{13}} \lesssim 0\%, \\ -0.3 \lesssim \delta^{D_{33}} \lesssim 0\%, & \quad -0.15 \lesssim \delta^{P_{11}} \lesssim 0\%, & \quad 0.06 \gtrsim \delta^{S_{11}} \gtrsim 0\%, & \quad 0.01 \gtrsim \delta^{S_{31}} \gtrsim 0\%, \end{aligned}$$

listed in order of decreasing magnitude. Inclusion of the excited state resonance contributions therefore effectively reduces the nucleon elastic TPE correction by $\sim 15\%$ at this Q^2 value. At lower Q^2 the resonance contributions are even less important relative to the nucleon-only contribution.

Figure 15 shows that at low to moderate Q^2 the total TPE corrections as a function of ε lie between those of the nucleon and Δ intermediate states. In addition to the dominant nucleon and Δ contributions, the D_{13} gives the most important correction among the remaining resonances. This is consistent with the well-known prominence of the D_{13} in the second resonance region of the Compton scattering cross section (*e.g.* see Ref. [91, 92] and references therein).

Inclusion of contributions of intermediate states with masses larger than ~ 2 GeV becomes impractical within a hadronic approach when one moves into the deep-inelastic continuum. Here it becomes more efficient to use either partonic degrees of freedom, discussed in Sec. 4.6, or dispersion relations, discussed in Sec. 4.7

4.5 Electron–muon scattering

It is useful to examine the TPE corrections to elastic scattering for a structureless pointlike target, such as $e\mu^+$ scattering, or in the limit of hard scattering from quarks in the nucleon. The pointlike limit is realized by setting $F_1 = 1$ and $F_2 = 0$ in the electromagnetic current operator appearing in Eq. (33), or equivalently by replacing $\Gamma_\gamma^\mu(q) \rightarrow \gamma^\mu$. The reduced cross section is then $\sigma_R^0 = \tau + \varepsilon$. In this case, we take the IR divergent part of the TPE correction to be the model-independent Maximon-Tjon result of Eq. (26); the remainder is denoted as δ_{hard} , *viz.* $\delta_{\gamma\gamma} = \delta_{\text{IR}}(\text{MTj}) + \delta_{\text{hard}}$.

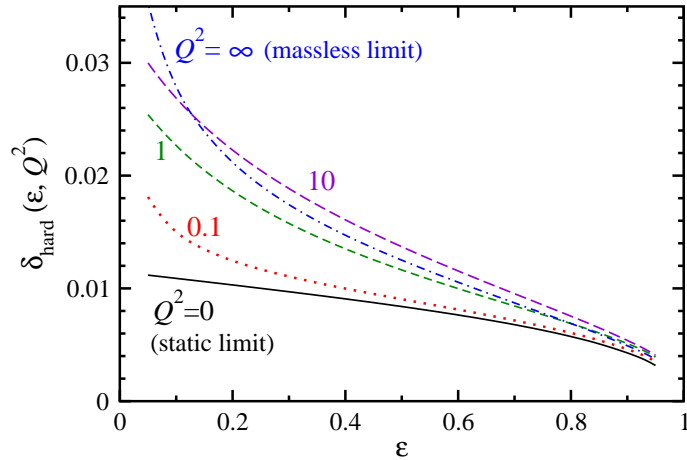


Figure 16: TPE corrections to scattering from a particle of mass $M = 0.939$ GeV for various values of Q^2 (in GeV^2). Note that the limit $Q^2 \rightarrow 0$ also corresponds to the static limit $M \rightarrow \infty$ for any finite Q^2 , and the limit $Q^2 \rightarrow \infty$ also corresponds to the massless limit $M \rightarrow 0$ for any finite Q^2 .

Figure 16 shows the result for δ_{hard} as a function of ε for various values of Q^2 ranging from 0 to ∞ . Clearly δ_{hard} is a positive quantity which generally increases with Q^2 between the two limiting cases. In both limits simple expressions for δ_{hard} exist in terms of a single variable. For a pointlike target the results should exhibit a scale invariance under the appropriate dimensionless variable, which can be taken to be τ and ε .

- (i) The limit $\tau \rightarrow 0$ is the same as either $Q^2 \rightarrow 0$ or the static limit $M \rightarrow \infty$ with Q^2 finite. In this case δ_{hard} is a function of a single variable. Making use of the asymptotic expansions of the Passarino-Veltman functions, a particularly simple expression exists in this limit, namely

$$\delta_{\text{hard}} = \frac{\alpha\pi}{x+1}, \quad (45)$$

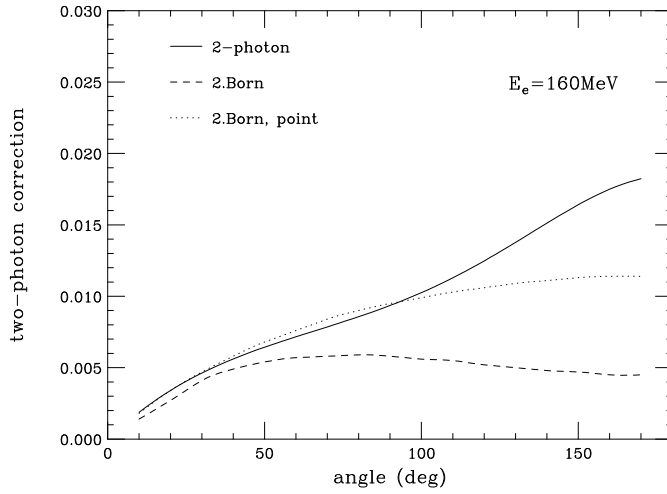


Figure 17: Relative contribution of TPE to elastic ep scattering at $E = 160$ MeV. The results in second Born approximation account for the Coulomb distortion (exchange of second soft photon) only. Figure taken from Ref. [96].

with $x = \sqrt{(1 + \varepsilon)/(1 - \varepsilon)}$. This static limit is also realized in the second Born approximation, which we discuss in the next section.

- (ii) The limit $\tau \rightarrow \infty$ is the same as either $Q^2 \rightarrow \infty$ or the limit $M \rightarrow 0$ with Q^2 finite. Once again δ_{hard} is a function of a single variable only, and can be expressed as

$$\delta_{\text{hard}} = \frac{\alpha}{\pi(x^2 + 1)} \left\{ \ln\left(\frac{x+1}{x-1}\right) + x \left[\pi^2 + \ln^2\left(\frac{x+1}{2}\right) + \ln^2\left(\frac{x-1}{2}\right) - \ln\left(\frac{x^2-1}{4}\right) \right] \right\}. \quad (46)$$

This expression, plus the soft IR contribution $\delta_{\text{IR}}(\text{MTj})$, agrees with that for scattering from massless quarks given in Eq. (27) of Ref. [73], and also in earlier work. However, those results were not expressed in terms of a single variable.

The behavior of TPE for hard scattering from a pointlike target stands in stark contrast to the ep elastic scattering results, shown in Fig. 13, which is larger and has the opposite sign at high Q^2 . However, as one decreases Q^2 , the ep TPE correction becomes smaller, eventually switching sign from negative to positive as Q^2 decreases. For $Q^2 \rightarrow 0$, the hadronic result reproduces the pointlike limit shown in Fig. 16 (and given in Eq. (45)) – independent of the anomalous magnetic form factor F_2 . (Note that $\delta_{\text{IR}}(\text{MTj}) \rightarrow \delta_{\text{IR}}(\text{MoT})$ in the limit $Q^2 \rightarrow 0$, so that $\bar{\delta} \rightarrow \delta_{\text{hard}}$). This suggests that the magnetic interaction is unimportant in this limit. This is consistent with the low- Q^2 analysis of Ref. [93].

Kuraev and Tomasi-Gustafsson [94] have suggested that $e\mu$ scattering should be a function of x , and that it represents an “upper limit” for the hadronic TPE corrections. In the context of the discussion here, while this may be a positive upper bound, at high Q^2 the full calculation gives a correction larger in magnitude but opposite in sign.

To fully understand the underlying reasons for this behavior, one can invoke the second Born approximation. In the static limit, equivalent to the case where the proton has infinite mass, the scattering amplitude for TPE coincides with the amplitude for electron scattering in a Coulomb potential in second Born approximation. This limit was first considered by Dalitz [95].

In Fig. 17 the TPE correction is shown as a function of θ for a typical electron energy involving a range of low Q^2 values [96]. The TPE contribution is compared to the contribution involving only the Coulomb distortion of the electron, arising from a second *soft* photon, calculated according to Ref. [97] in second Born approximation. The same contribution, but for a point nucleus, is given for comparison.

Remarkably good agreement between the two approaches is obtained at forward angles. Figure 17 shows that at forward angles the TPE contribution is dominated by the Coulomb distortion, while at backward angles the exchange of two hard photons contributes appreciably. This is consistent with the observations about the pointlike limit, and the independence of this limit from F_2 .

The behavior shown in Fig. 13 (left) can also be understood from the second Born approximation [98]. The second interaction provides a “focusing effect” — accelerating electrons towards the target. For a pointlike target this should increase scattering at backward angles. However, because of an increased momentum transfer there is a competing effect from a reduction in cross section due to the proton electric and magnetic form factors. At larger Q^2 this reduction wins out, and the total cross section is reduced at backward angles. For positrons, the opposite effect is expected.

4.6 High Q^2 partonic models

In the regime of high Q^2 , two approaches to the TPE effect on elastic scattering have been taken by different groups. In Refs. [53, 73], the hard scattering part of TPE was studied in a partonic approach using different models for generalized parton distributions (GPDs). In this approach it is assumed that both photons interact with the same quark. The results of these calculations on the cross sections and other observables have been examined in detail in Ref. [99], and the details will not be duplicated here.

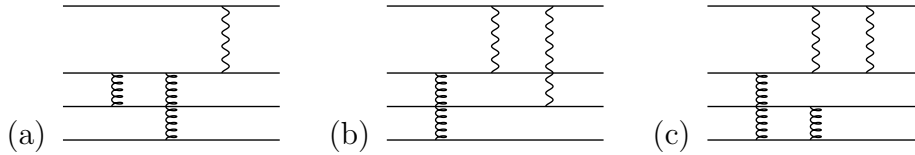


Figure 18: Typical pQCD diagrams for **(a)** one-photon exchange, **(b)** leading order TPE involving 1 hard gluon, and **(c)** subleading order TPE involving 2 hard gluons. Figure adapted from Ref. [100].

Our observations about the pointlike limit in Sec. 4.5 suggest that hard TPE corrections involving both photons interacting with the same particle have the opposite sign to the hadronic calculations at backward angles. Borisyyuk and Kobushkin [100] studied TPE in the framework of perturbative QCD (pQCD). In this approach, it turns out that the most important diagrams for backward angle scattering are the ones where the two photons interact with different quarks. This allows the possibility to generate a hard TPE correction that is negative at backward angles. The argument given by Borisyyuk and Kobushkin is as follows.

Referring to the diagrams in Fig. 18, one-photon exchange diagrams like (a) need 2 hard gluons to turn the momentum of all 3 quarks, and are therefore of order $\alpha\alpha_s^2/Q^6$, where α_s is the strong coupling. The TPE diagrams like (b), involving 2 quarks, need only 1 hard gluon, and are of order $\alpha^2\alpha_s/Q^6$. Therefore the ratio of two-photon to one-photon exchange is not of order α , as one might expect, but of order α/α_s . By contrast, diagrams like (c), where both photons interact with the same quark, require 2 hard gluons, and are therefore suppressed by an additional factor of α_s .

Numerically, Borisyyuk and Kobushkin [100] express the cross section correction in terms of the relative TPE amplitude $\delta G_M/G_M$, where $G_M = G_M^{\text{Born}} + \delta G_M$, which has linear ε dependence. This amplitude grows logarithmically with Q^2 , reaching 3.5% at $Q^2 = 30 \text{ GeV}^2$. This may offer an interesting avenue to merge the hadronic approach, valid at low to moderate Q^2 , with the pQCD approach at high Q^2 . Figure 19 shows how the hadronic and pQCD results seem to connect smoothly at around $Q^2 = 3 \text{ GeV}^2$ for two values of ε . A complementary pQCD analysis by Kivel and Vanderhaeghen [101] also finds a comparable effect.

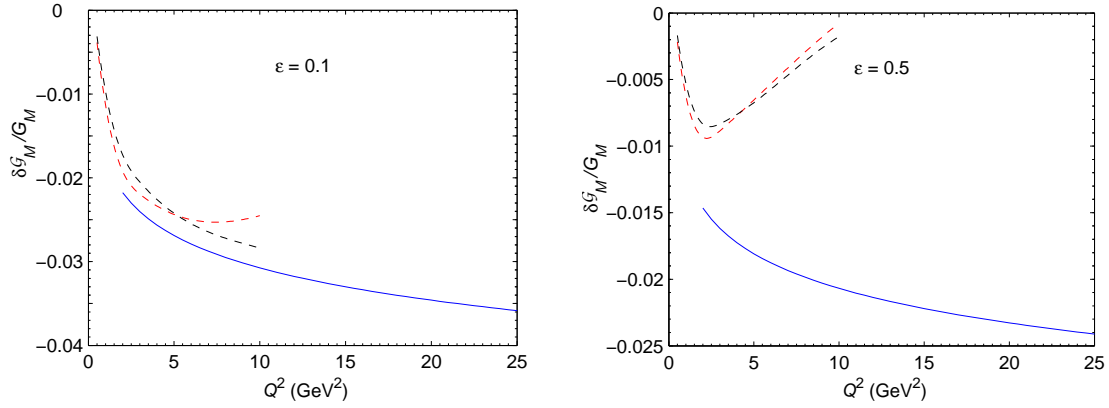


Figure 19: TPE amplitude vs. Q^2 for two values of ε . The dashed curves are the hadronic calculation using two different form factors, and solid curves are the pQCD results. Figure taken from Ref. [100].

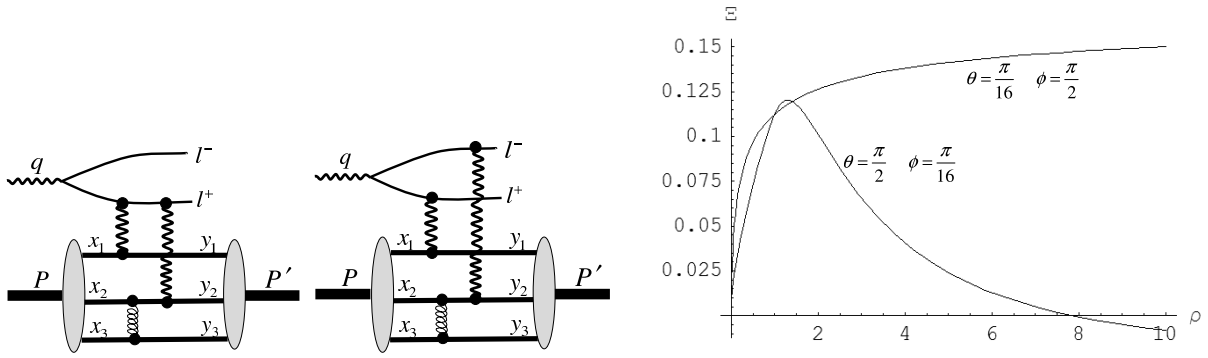


Figure 20: Typical TPE diagrams for lepton pair production involving two photons and one hard gluon (**left**). The graph shows the resulting lepton pair asymmetry at select angles (**right**). Figures taken from Ref. [102].

Two-photon effects also manifest in the production of lepton-antilepton pairs from a hadronic target by real photons. The interference of one- and two-photon exchange amplitudes leads to a charge asymmetry term that can be calculated explicitly in the large- t limit. This was studied using pQCD by Hoodbhoy [102] in the region of high center of mass energy s ($s \gg -t \gg M^2$). Typical diagrams involving 2 photons and 1 hard gluon exchange are shown in Fig. 20, analogous to the corresponding diagrams in elastic ep scattering discussed previously. The lepton pair asymmetry for select angles in the lepton pair center of mass is also shown as a function of $\rho \equiv -t/M^2$. Note that Hoodbhoy's calculation and observations about the leading contribution involving different quarks actually predates the work of Refs. [100, 101].

4.7 Dispersion relations

One of the sources of model dependence in the calculation of the real parts of the TBE amplitudes arises from the intermediate state in the box diagrams being off-shell. For the nucleon elastic contribution, for example, this can be parametrized through the off-shell dependence of the nucleon electromagnetic form factors, where one of the nucleons is off its mass shell, $W^2 = (p+q_1)^2 \neq M^2$, see Fig. 10. In this case the vertex form factors are in general functions of *two* variables, q_1^2 and W^2 , which in the limit $W^2 \rightarrow M^2$

reduce to the on-shell values. Outside of a field-theoretical calculation of the amplitudes from first principles, however, it is not possible to determine the (unphysical) dependence on W^2 independently of a specific model. This model dependence invariably introduces additional uncertainties into the calculation.

One way to avoid the off-shell ambiguities is through the use of dispersion relations [103], which are based on general principles such as unitarity and analyticity of scattering amplitudes, and can in principle relate real and imaginary parts of amplitudes for on-shell processes. The conservation of total probability in a scattering process implies that the scattering matrix, \mathcal{S} , is unitary, $\mathcal{S}^\dagger \mathcal{S} = 1$. In general the S-matrix element $\mathcal{S}_{fi} = \langle f | \mathcal{S} | i \rangle$ between initial state i (with total momentum p_i) and final state f (total momentum p_f) can be written in terms of the invariant amplitude as

$$\mathcal{S}_{fi} = \delta_{fi} + i(2\pi)^4 \delta^4(p_f - p_i) \mathcal{M}_{fi}. \quad (47)$$

Unitarity then requires that

$$2\mathcal{I}m \mathcal{M}_{fi} = \sum_n \int d\rho \mathcal{M}_{nf}^* \mathcal{M}_{ni}, \quad (48)$$

where $d\rho$ is the covariant phase-space factor for a complete set of intermediate states n . In the limit of forward elastic scattering, $i = f$, the product of amplitudes in (48) becomes diagonal, and can be expressed as a directly measurable cross section. This allows loop integrations to be evaluated in terms of on-shell states, so that empirical *data* can be used as input in the calculation of the imaginary part.

The Cauchy integral formula allows the amplitude $\mathcal{M}_{fi}(s)$ to be determined as a function of a real s -channel variable s from the structure of its singularities in the complex plane. The real and imaginary parts of $\mathcal{M}_{fi}(s)$ can be related by

$$\mathcal{R}e \mathcal{M}_{fi}(s) = \frac{1}{\pi} \mathcal{P} \int_{-\infty}^{\infty} ds' \frac{\mathcal{I}m \mathcal{M}_{fi}(s')}{s' - s}, \quad (49)$$

where \mathcal{P} denotes the principal value of the integral.

The dispersion approach has been applied in various studies in the literature of TPE corrections to elastic ep scattering, starting with some early attempts in the late 1950s [40, 41, 42] to compute $\mathcal{O}(e^4)$ corrections to elastic ep cross sections. More recently, Borisjuk and Kobushkin [104] used dispersion relations to compute the contribution to TPE amplitudes arising from nucleon elastic intermediate states, in terms of elastic on-shell nucleon form factors parametrized as a sum of monopoles [5]. Interestingly, the results of the dispersive calculations were found to be very similar numerically to the direct loop computation [6, 105], especially at low Q^2 . This suggests that the prescription of taking on-shell values for the half off-shell form factors in the direct calculations provided a very good approximation. At larger Q^2 ($Q^2 \gtrsim 6 \text{ GeV}^2$) the agreement between the two approaches deteriorates, possibly hinting at the need to account for the off-shell dependence of the form factors; at such Q^2 values the reliability of the hadronic approach itself may be more questionable. In Ref. [106] the authors applied the same method to also compute the TPE corrections to the pion form factor (see Sec. 6.4 below), again finding very similar results to the direct loop calculations [9].

Elastic scattering from hadrons at forward angles was analyzed some time ago within a dispersive approach by Bernabéu and collaborators [107, 108], and more recently by Gorchtein [109]. We sketch here the relevant details (in the notation of this article), noting the overlap with the discussion of forward-angle parity-violating γZ interference in Sec. 7.3. In the forward angle limit ($q_1 \approx -q_2$ in Fig. 10) the imaginary part of the TPE amplitude, by virtue of the intermediate state being on-shell, is related via the optical theorem (48) to the inclusive electromagnetic structure functions of the nucleon,

$$2\mathcal{I}m \mathcal{M}_{\gamma\gamma} = 4\pi M e^4 \int \frac{d^3l}{(2\pi)^3 2E_l} \frac{1}{Q_1^4} L_{\mu\nu} W^{\mu\nu}, \quad (50)$$

where $l = k - q_1$ is the momentum of intermediate state electron, $E_l = \sqrt{(\mathbf{k} - \mathbf{q}_1)^2 + m_e^2}$ its energy, and $Q_1^2 = -q_1^2$ is the virtuality of exchanged photon. The factor $4\pi M$ arises from the definition of the hadronic tensor. The leptonic tensor in (50) is given by $L_{\mu\nu} = \bar{u}_e(k') \gamma_\mu (\not{l} + m_e) \gamma_\nu u_e(k)$, where the scattered lepton momentum has been set to $k' = k - q$, with q kept small but finite. The nucleon hadronic tensor can be written in terms of the inclusive F_1 and F_2 structure functions as

$$MW^{\mu\nu} = -g^{\mu\nu} F_1(W^2, Q_1^2) + \frac{p^\mu p^\nu}{p \cdot q_1} F_2(W^2, Q_1^2), \quad (51)$$

dropping terms proportional to $q_{\mu,\nu}$ which vanish when contracted with $L_{\mu\nu}$. Using Eq. (35) the relative correction from TPE to the elastic cross section can then be written as

$$\mathcal{I}m \delta_{\gamma\gamma}(E) = -\frac{\alpha t}{(2ME)^2} \int_{M^2}^s dW^2 \int_0^{Q_{1,\max}^2} \frac{dQ_1^2}{Q_1^2} \left[F_1 + \frac{s(Q_{1,\max}^2 - Q_1^2)}{Q_1^2(W^2 - M^2 + Q_1^2)} F_2 \right], \quad (52)$$

where the upper limit on the Q_1^2 integration is $Q_{1,\max}^2 = 2ME(1 - W^2/s)$, with $s = M^2 + 2ME$ the total center of mass energy squared, and $t = q^2$. Note that the factor t in Eq. (52) implies that formally this contribution vanishes at $t = 0$.

The real part of $\delta_{\gamma\gamma}(E)$ at a given electron energy E is then evaluated from the imaginary part (52) using the fixed- t dispersion relation

$$\mathcal{R}e \delta_{\gamma\gamma}(E) = \frac{1}{\pi} \mathcal{P} \int_{-\infty}^{\infty} dE' \frac{\mathcal{I}m \delta_{\gamma\gamma}(E')}{E' - E}. \quad (53)$$

Note that the contribution to the integral from the region $E' < 0$ corresponds to the crossed-box diagram in Fig. 10. Invoking the crossing symmetry property discussed earlier in Eq. (25), one can write

$$\mathcal{R}e \delta_{\gamma\gamma}(E) = \frac{2E}{\pi} \mathcal{P} \int_0^{\infty} dE' \frac{1}{E'^2 - E^2} \mathcal{I}m \delta_{\gamma\gamma}(E'). \quad (54)$$

Bordes *et al.* [108] applied this formalism to the case of elastic electron and muon scattering from the spin-0 ^4He and ^{12}C nuclei at low energy, focusing in particular on the nuclear finite size effects. For electrons, assuming the dominant matrix elements correspond to electric dipole intermediate transitions, which are dominated by low values of Q_1^2 , the nuclear finite size effects are found to be small for kinetic energies up to ≈ 50 MeV, but increase to $\approx 30\%$ of the total forward amplitude at energies ≈ 100 MeV [108]. In the case of muon scattering, the nuclear finite size effects were found to be more significant.

More recently, Gorchtein [109] applied the forward dispersion formalism to study the effect of TPE on the e^+p to e^-p cross section ratio at higher energies. Using phenomenological structure functions in the deep-inelastic scattering region [110], the ratio of e^+p to e^-p cross sections is found to be larger than unity, with effects ranging from $\lesssim 1.5\%$ for incident energy $E = 3$ GeV to $\lesssim 2.5\%$ for $E \approx 10$ GeV.

Overall, the dispersion approach provides a unique method to compute amplitudes from empirical inputs, in principle free of model dependent ambiguities associated with off-shell effects of intermediate states, particular at high mass W^2 . On the other hand, this virtue is at times somewhat negated by the need to know the inputs at all energies, which are often not well determined at very high energy. Uncertainties in the high energy behavior of the input cross sections can in some cases be as large as the off-shell uncertainties in the direct, non-dispersive approaches. Furthermore, at scattering angles away from the forward limit the imaginary parts of TPE amplitudes are no longer related to inclusive structure functions, but are given by nonforward virtual Compton scattering amplitudes, for which there are considerably fewer phenomenological constraints. The dispersive framework therefore provides a useful *complement* to the other methods discussed in this section.

5 Impact of two-photon exchange on observables

Having outlined the theoretical developments in the computation of TPE corrections to elastic scattering, in this section we review the implications of the corrections for observables. Starting with the most topical case of TPE effects on the proton electric to magnetic form factor ratio (Sec. 5.1), we also consider the impact that TPE corrections have on electron to positron elastic cross sections (Sec. 5.2), on the global analysis of form factor data (Sec. 5.4), as well as on polarization observables (Sec. 5.3 and 5.5). To simplify the discussion, unless otherwise indicated we restrict the hadronic calculations to the nucleon elastic intermediate states only (which provides a reasonable approximation to the total had

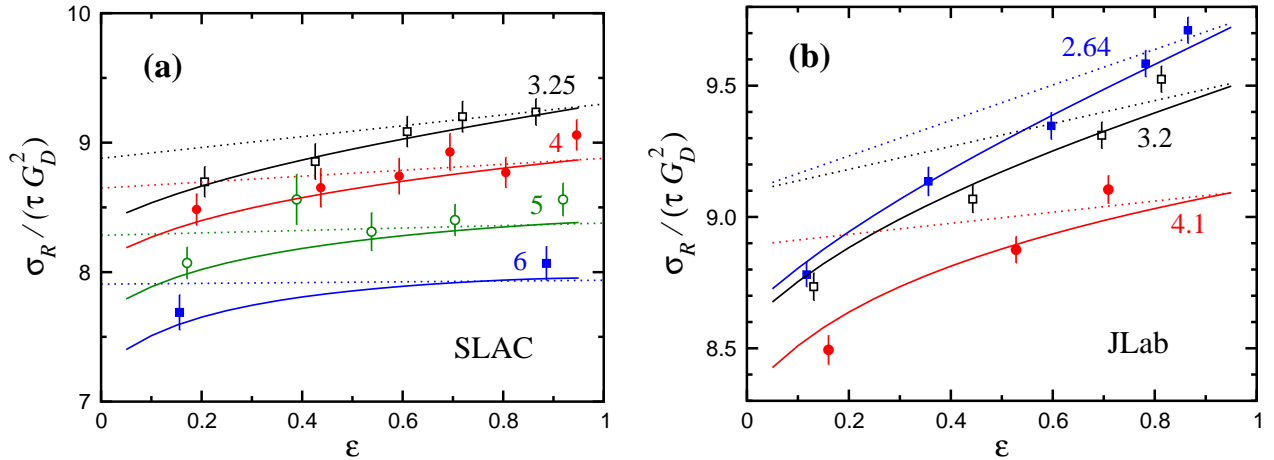


Figure 21: Comparison of the Born (dotted) and TPE (solid) calculations to measurements of $\sigma_R/(\tau G_D^2)$ for several values of Q^2 : **(a)** SLAC data [34] at $Q^2 = 3.25 - 6$ GeV²; **(b)** Jefferson Lab data [14] at $Q^2 = 2.64 - 4.1$ GeV². The Born cross section is evaluated using the form factors from Ref. [85] which use PT extractions of G_E . The curves in (b) have been shifted by (+1.0%, +2.1%, +3.0%) for $Q^2 = (2.64, 3.2, 4.1)$ GeV². Figure adapted from Ref. [6].

5.1 Cross sections and Rosenbluth separations

The effect of the TPE corrections on the Rosenbluth separations, calculated within the hadronic formalism of Sec. 4.3, is illustrated in Fig. 21. The data points are the reduced cross sections σ_R scaled by the square of the dipole form factor (37), multiplied by τ , from SLAC [34] and the Jefferson Lab “Super-Rosenbluth” experiment [14]. Here the Born-level prediction (dotted line) is obtained using the form factor parametrization of Ref. [85] in which G_E is fitted to the polarization transfer data, while the full result (solid) includes the TPE corrections. The TPE contributions yield a significant increase of the slope, with some nonlinearity evident at small ε . The corrected results are clearly in better agreement with the data, although some residual difference between the Rosenbluth and polarization measurements remain at the higher Q^2 values.

To obtain a rough estimate of the influence of these corrections on the electric to magnetic proton form factor ratio $R = \mu_p G_E/G_M$, Blunden *et al.* [5, 6] considered a simplified analysis in which the effective ε slope was approximated by a linear fit to the full TPE corrections. Such an analysis may not provide an accurate estimate at very low ε or high Q^2 where strong deviations from linearity arise; however, it is still instructive to obtain an estimate of the effect on R by taking the slope over several ranges of ε . Blunden *et al.* [6] fit the relative correction to the Born cross section ($1 + \bar{\delta}$) to a linear

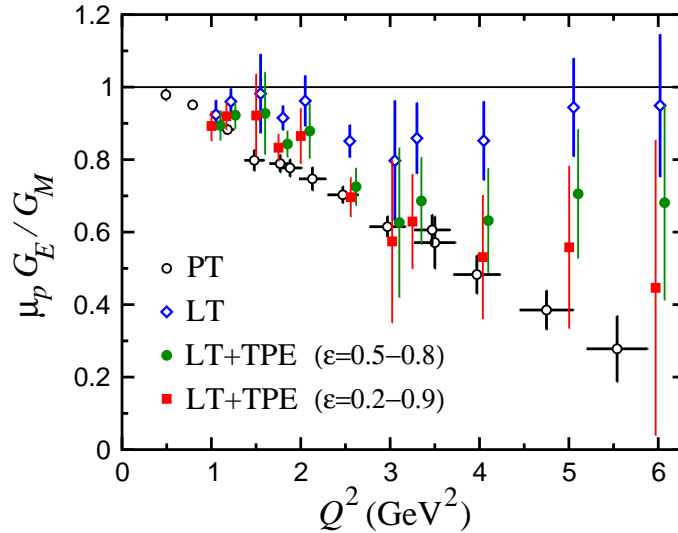


Figure 22: The ratio of proton electric and magnetic form factors $\mu_p G_E/G_M$ measured using LT separation (open diamonds) [12] and polarization transfer (PT) (open circles) [16]. The LT points corrected for TPE are shown assuming a linear slope for $\varepsilon = 0.2 - 0.9$ (filled squares) and $\varepsilon = 0.5 - 0.8$ (filled circles) (offset for clarity). Figure adapted from Ref. [6].

function of ε , of the form $a + b\varepsilon$, for each value of Q^2 at which the ratio R is measured. The corrected reduced cross section in Eq. (10) then becomes [6]

$$\sigma_R \approx a\tau G_M^2(Q^2) \left[1 + \frac{\varepsilon}{\mu^2\tau} (R^2 [1 + \varepsilon b/a] + \mu^2\tau b/a) \right], \quad (55)$$

where

$$R^2 = \frac{\tilde{R}^2 - \mu^2\tau b/a}{1 + \bar{\varepsilon}b/a} \quad (56)$$

is the “true” form factor ratio, corrected for TPE effects, and \tilde{R} is the “effective” ratio, contaminated by TPE. Note that in Eqs. (55) and (56) the term quadratic in ε has effectively been linearized by averaging ε over the range fitted, $\varepsilon \rightarrow \bar{\varepsilon}$. The approximation in Eq. (55) is reasonable provided $b/a \ll 1$, which is more valid at high Q^2 values.

Considering two ranges for ε , namely a large range $\varepsilon = 0.2 - 0.9$ and a more restricted range $\varepsilon = 0.5 - 0.8$, the resulting shift in R is shown in Fig. 22, together with the polarization transfer data. The linear ε approximation to the TPE correction should be better for the latter, even though in practice experiments typically sample values of ε near its extrema.

The effect of TPE on R is clearly significant. In particular, the corrections have the proper sign and magnitude to resolve a large part of the discrepancy between the LT and PT techniques. While the early analysis of Ref. [5] using simple monopole form factors found a shift similar to that in for the $\varepsilon = 0.5 - 0.8$ range in Fig. 22, which resolves around 1/2 of the discrepancy, the nonlinearity at small ε makes the effective slope somewhat larger if the ε range is taken between 0.2 and 0.9. The magnitude of the effect in this case is sufficient to bring the LT and PT points almost to agreement. A more detailed analysis, where the TPE correction is applied directly to the experimentally measured cross sections, is discussed in Sec. 5.4.2.

Note that for the high Q^2 points, the value of $\mu_p G_E/G_M$ decreases but the uncertainty on the ratio increases when TPE corrections are applied. This is because the quantity directly constrained by the experiment is the slope of the reduced cross section, which is related to $(\mu_p G_E/G_M)^2$, rather than $\mu_p G_E/G_M$. So while the absolute uncertainty on the slope, and thus $(\mu_p G_E/G_M)^2$, is unchanged, the

uncertainty that this translates to for $\mu_p G_E/G_M$ depends on the value, and increases when $\mu_p G_E/G_M$ decreases.

The results in Fig. 22 are representative of most calculations of the TPE corrections within the conventional hadronic approach. Qualitatively similar results are also obtained in the GPD-based approach [53, 73], whose applicability is limited, however, at low Q^2 and ε values (*cf.* Fig. 19). Note that since the hard electron–quark scattering amplitude gives a *negative* slope in ε , Fig. 16, agreement with data suggests an important role played by soft physics.

5.2 e^+p/e^-p ratios

As previewed in Sec. 3.3.1, direct experimental evidence for TPE effects can be obtained by comparing elastic e^+p and e^-p cross sections. The ratio of these is defined as

$$R^{e^+e^-} = \frac{\sigma^{e^+p}}{\sigma^{e^-p}} \approx \frac{|\mathcal{M}_\gamma^{e^+}|^2 + 2\mathcal{R}e\left(\mathcal{M}_\gamma^{e^+*}\mathcal{M}_{\gamma\gamma}^{e^+}\right)}{|\mathcal{M}_\gamma^{e^-}|^2 + 2\mathcal{R}e\left(\mathcal{M}_\gamma^{e^-*}\mathcal{M}_{\gamma\gamma}^{e^-}\right)}, \quad (57)$$

where $\sigma^{e^\pm p} \equiv d\sigma^{e^\pm p}/d\Omega$. Whereas the electron Born amplitude $\mathcal{M}_\gamma^{e^-}$ changes sign under the interchange $e^- \rightarrow e^+$, the TPE amplitude $\mathcal{M}_{\gamma\gamma}^{e^-}$ does not. The interference of the Born and TPE amplitudes therefore has the opposite sign for electron and positron scattering, so that the cross section ratio can be written as

$$R^{e^+e^-} \approx 1 - 2\bar{\delta}, \quad (58)$$

where $\bar{\delta}$ is defined in Eq. (36). The hadronic TPE calculation of $\bar{\delta}$ is illustrated for a range of Q^2 values in Fig. 13. Since the finite part of the TPE contribution is negative over most of the range of ε , one would expect to see an enhancement of the ratio of e^+ to e^- cross sections.

Existing data on elastic e^-p and e^+p scattering are sparse, although some constraints exist from early measurements at SLAC [55, 60], Cornell [56], DESY [57] and Orsay [59], as discussed in Sec. 3.3.1. The data are predominantly at low Q^2 and at forward scattering angles, corresponding to large ε ($\varepsilon \gtrsim 0.7$), where the TPE contributions to the cross section are small ($\lesssim 1\%$). Nevertheless, the overall trend in the data reveals a small enhancement in $R^{e^+e^-}$ at the lower ε values, as shown in Fig. 7.

The measurements of $R^{e^+e^-}$ are compared to the hadronic TPE calculations [6] in Fig. 23, which generally predict a slight enhancement in the ratio at the experimental kinematics. Overall, the TPE corrections agree reasonably well with the data, although the experimental uncertainties are quite large, especially where there are indications of a nonzero TPE effect. Interestingly, the GPD-based calculations [53, 73] predict a suppression of $R^{e^+e^-}$ at large ε in the $Q^2 \sim \text{few GeV}^2$ range. Better quality data, particularly at backward angles, where an enhancement of up to $\sim 10\%$ is predicted, is needed for a more definitive test of the TPE mechanism.

Recently three new measurements have been made comparing e^+p and e^-p scattering. The first is at the VEPP-3 storage ring at Novosibirsk [63], which uses an internal target in a positron/electron storage ring to extract the ratio at $Q^2 = 1.6 \text{ GeV}^2$ and $\varepsilon \approx 0.4$ [111]. The analysis yields a raw e^+p/e^-p ratio of 1.056 ± 0.011 , but only preliminary corrections for charge-dependent bremsstrahlung, estimated to be $\sim 3\%$, have to be applied [112].

Another experiment [64], using a mixed beam of e^+ and e^- generated via pair production from a secondary photon beam, recently completed data taking at Jefferson Lab. In this experiment, e^-p and e^+p elastic scattering are measured simultaneously, using detection of both the scattered lepton and struck proton to reconstruct the initial lepton energy. Cross sections can be measured for $0.5 < Q^2 < 2.0 \text{ GeV}^2$ and $\varepsilon \gtrsim 0.2$, and the analysis is currently underway. The use of a lepton beam with a large range of energies allows for a mapping out of the ε dependence at fixed Q^2 values over the kinematic range of the experiment.

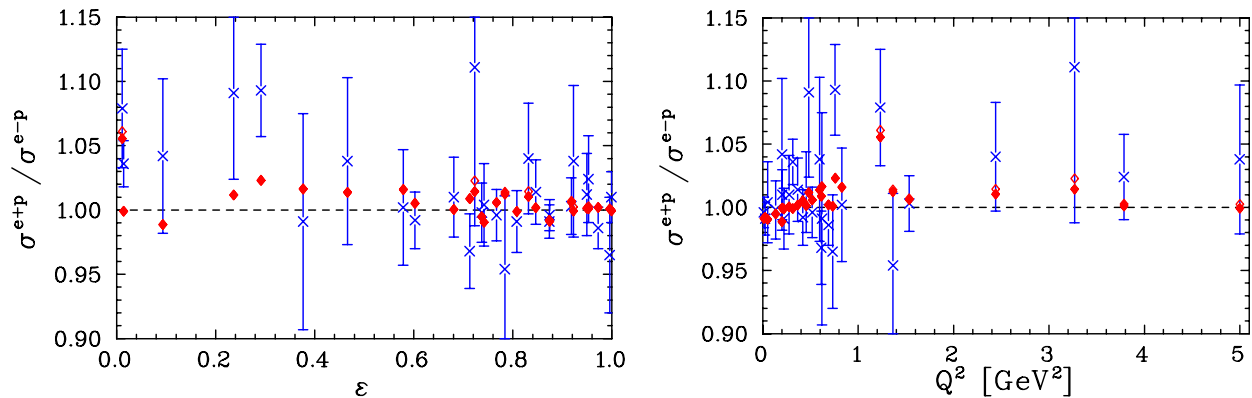


Figure 23: Measured ratio of elastic e^+p to e^-p cross sections (crosses), compared to the hadronic TPE calculations [6] (diamonds), presented as a function of ε (**left**) and Q^2 (**right**).

Finally, the OLYMPUS experiment [65] will use the DORIS lepton storage ring at DESY to make measurements with a fixed lepton energy, yielding e^+p/e^-p ratios at several points from $Q^2 = 2.2 \text{ GeV}^2$, $\varepsilon = 0.35$, to $Q^2 = 0.6 \text{ GeV}^2$, $\varepsilon = 0.9$. The experiment is currently being installed and is scheduled to run in 2012.

5.3 Polarization measurements

While the results of the modern TPE calculations give a clear indication of a sizable correction to the LT-separated data, the obvious question which arises is to what extent does TPE affect the polarization transfer results themselves. The expectation is that since the PT measurements involve ratios of cross sections, most of the radiative effects, including TPE, should cancel.

The polarization transfer experiment involves the scattering of longitudinally polarized electrons from an unpolarized proton target, with the detection of the polarization of the recoil proton, $\vec{e} + p \rightarrow e + \vec{p}$. (The analogous process whereby a polarized electron scatters elastically from a polarized proton leaving an unpolarized final state gives rise to essentially the same information.) The calculation of the TPE corrections to the cross sections with longitudinally or transversely polarized recoil protons follows that of Sec. 4.3, with the spin traces evaluated using the explicit expression for the spin-vectors of the incident electron and recoil proton in Eqs. (12) and (13).

In the standard radiative corrections using the Mo-Tsai prescription [37, 38], the corrections to the transverse and longitudinal polarization are identical, so that no additional corrections beyond hard bremsstrahlung are necessary [15]. For the TPE corrections, in analogy with the unpolarized case, Eq. (35), the spin-dependent TPE corrections to the longitudinal ($\bar{\delta}_L$) and transverse ($\bar{\delta}_T$) cross sections are defined as the finite parts of the TPE contributions relative to the IR expression from Mo and Tsai [37, 38] in Eq. (29), which are independent of polarization,

$$\bar{\delta}_{L,T} = \delta_{L,T} - \delta_{\text{IR}}(\text{MoT}). \quad (59)$$

In the polarization transfer measurements of the form factor ratio $\mu_p G_E/G_M$, one usually measures the ratio of the longitudinal or transverse cross section to the unpolarized cross section, P_L or P_T , respectively. The TPE correction to the polarization transfer ratio can therefore be incorporated as [6]

$$\frac{P_{L,T}}{P_{L,T}^0} = \frac{1 + \bar{\delta}_{L,T}}{1 + \bar{\delta}}, \quad (60)$$

where $P_{L,T}^0$ are the polarized Born cross sections, and the correction to the unpolarized cross section $\bar{\delta}$ is given in Eq. (36). Polarized target measurements make similar comparisons of beam-target cross section

asymmetries for two different target spin orientations, yielding two different combinations longitudinal and transverse spin asymmetries.

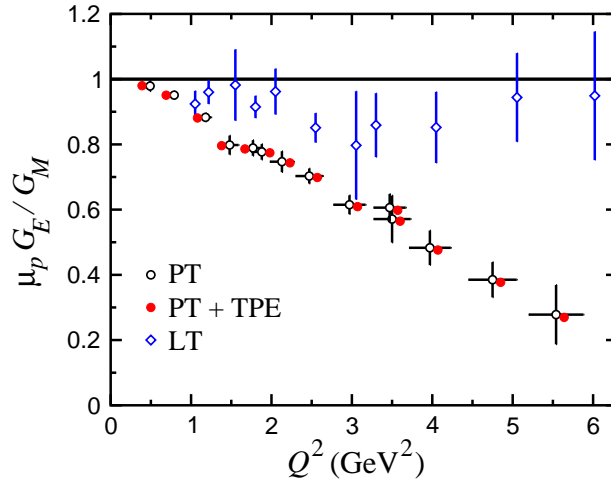


Figure 24: Proton electric to magnetic form factor ratio obtained from the PT measurements [16], with (solid circles) and without (open circles) TPE corrections. The corrected values have been offset for clarity. The LT-separated ratio (open diamonds) from Fig. 22 is shown for comparison. Figure adapted from Ref. [6].

Taking $R = -\mu_p \sqrt{\tau(1 + \varepsilon)}/2\varepsilon (P_T/P_L)$ to be the corrected (“true”) electric to magnetic form factor ratio (see Eq. (56)), the experimentally measured PT ratio is

$$\tilde{R} = R \left(\frac{1 + \bar{\delta}_T}{1 + \bar{\delta}_L} \right). \quad (61)$$

Inverting Eq. (61), the shift in R is illustrated in Fig. 24, relative to the uncorrected results and the LT separated data. Clearly the effect of TPE on the form factor ratio is a very small, $\lesssim 3\%$ suppression at the larger Q^2 values, which is well within the experimental uncertainties. Note that the shift in R in Eq. (61) does not include corrections due to hard photon bremsstrahlung, which are part of the standard radiative corrections. Since these would increase both the numerator and denominator in Eq. (61), the correction in Fig. 24 represents an upper limit on the shift in R .

Although the TPE effects on the PT ratio R are very small, this is mostly because those measurements were typically performed at large ε ($\varepsilon \approx 0.7 - 0.8$) [16], where the TPE corrections are minimal. At lower ε , or for $\varepsilon \sim 1$, the effects on the polarizations can be significant. This can be seen in Fig. 25, which shows the longitudinal and transverse polarizations from nucleon elastic intermediate states relative to the Born terms. The correction $\bar{\delta}_L$ to the longitudinal cross section is approximately the same as the correction $\bar{\delta}$ to the unpolarized cross section, so that TPE correction to the longitudinal polarization P_L is extremely small. In fact, at extreme backward angles ($\varepsilon = 0$) the unpolarized and longitudinal corrections $\bar{\delta}$ and $\bar{\delta}_L$ must be identical [6], and there is no TPE contribution to P_L . In contrast, the combined effects of an increasing $\bar{\delta}_T$ at large Q^2 and $\bar{\delta}$ becoming more negative mean that the correction to the transverse polarization P_T is enhanced at backward angles, and grows with Q^2 , as Fig. 25 (b) illustrates.

In a recent Jefferson Lab experiment the ratios R and P_L/P_L^0 were measured at three ε values for a fixed $Q^2 = 2.5 \text{ GeV}^2$ [74]. In the Born approximation both of these should be independent of ε , so that any observed angular dependence would be an indication of TPE contributions. The results

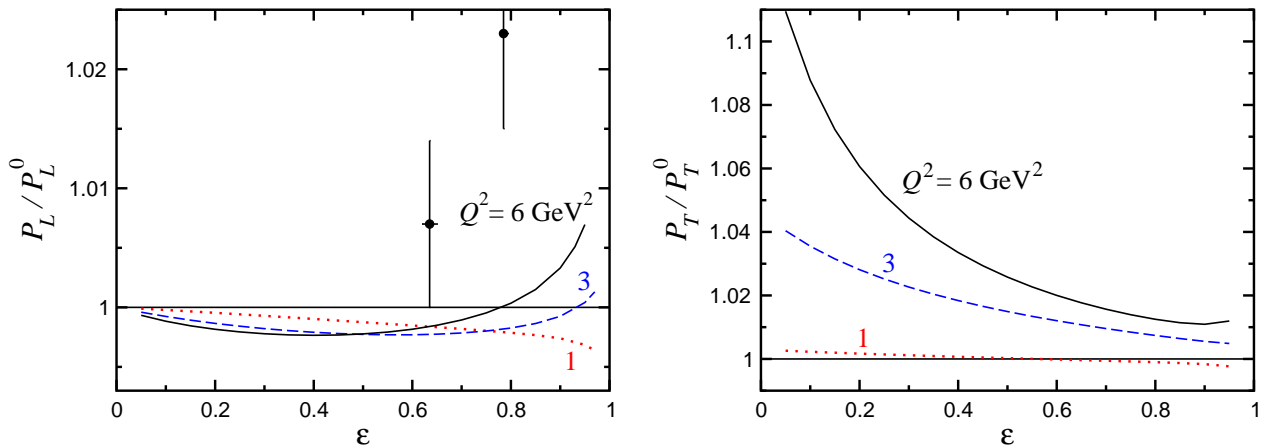


Figure 25: Ratio of the finite part (with respect to the Mo-Tsai IR contribution (29)) of the Born+TPE correction relative to the Born term, for **(left)** longitudinal and **(right)** transverse recoil proton polarization, at $Q^2 = 1$ (dotted), 3 (dashed) and 6 GeV^2 (solid). The longitudinal polarization data are from Ref. [74], and have an overall normalization uncertainty of 0.01. Figure adapted from Ref. [6].

for the longitudinal polarization ratio in Fig. 25 (left) are consistent with no TPE effect at $\varepsilon = 0.635$, but indicate an $\approx 2\%$ enhancement at the larger $\varepsilon = 0.785$ value (note that an overall normalization uncertainty of 0.01 applies to the data). While a rise as $\varepsilon \rightarrow 1$ is predicted at larger Q^2 , the magnitude of the effect is difficult to reconcile with the calculation [6] and possibly suggests the need to include higher-mass intermediate states in the TPE amplitude. The results in the GPD-based approach [53, 73] give a similarly small effect, but with opposite sign compared with the hadronic calculation [6].

Data taken on the PT ratio R at $Q^2 = 2.5 \text{ GeV}^2$ are also consistent with no significant ε dependence over the range $0.15 \lesssim \varepsilon \lesssim 0.8$, and hence in the transverse ratio P_T/P_T^0 . The hadronic calculation with elastic nucleon intermediate states predicts a $\sim 2 - 3\%$ enhancement, which once again may indicate a role played by the higher-mass resonances; the $\Delta(1232)$ contribution, for example may cancel some of the rise at $\varepsilon \rightarrow 0$ (Sec. 4.4.1). It is interesting to observe that the GPD-based model predicts a large *decrease* in the ratio R (or transverse polarization) at low ε , opposite to the hadronic model. Further measurements of the ε dependence of the P_T/P_T^0 ratio over a range of Q^2 values would be very helpful in constraining the magnitude and sign of the TPE effects.

Finally, two recent analyses [113, 114] have attempted to extract from the new data individual contributions to TPE amplitudes. Because data exist for a limited set of Q^2 values, and because the effect on the cross section is only inferred from the discrepancy between LT and PT measurements, such analyses at present require assumptions about the ε dependence of the amplitudes. Although different decompositions of the amplitudes are used in Refs. [113, 114], the extracted amplitudes are found to be similar when the different definitions are accounted for.

5.4 Global form factor analysis

With the realization that the Rosenbluth separations of elastic cross section data were significantly affected by TPE, came the need to ensure that for reliable extractions of the nucleon form factors the TPE corrections must be incorporated in the analysis. Initial efforts focused on minimizing the impact of TPE in the extractions, based on the assumption that TPE was the likely explanation for the LT/PT form factor discrepancy, and that all observables (cross sections and polarization components)

were affected at a similar level. Given that the various calculations of TPE corrections give qualitatively consistent estimates and are consistent with existing e^+p/e^-p data, more recent efforts have focused on including the calculated contributions *a priori* in the combined analysis of all form factor measurements.

5.4.1 Initial attempts to combine Rosenbluth and polarization data

Because the Rosenbluth extractions at high Q^2 are very sensitive to any small, angle-dependent systematic effects, it was generally believed that the polarization measurements provided a more reliable way to extract G_E at large Q^2 , where it has minimal contribution to the cross section. Many early attempts to extract form factors using both unpolarized cross section and polarization transfer measurements therefore assumed that G_M could be reliably extracted from the Rosenbluth results, and G_E could best be extracted using polarization measurements of G_E/G_M , combined with the Rosenbluth extractions of G_M .

This corresponds to the assumption, illustrated in Fig. 5, that whatever was deficient in the cross section measurements led to a linear ε dependence which had no impact at $\varepsilon = 0$, and thus the value of G_M extracted from Rosenbluth separations was unmodified. However, if the discrepancy is caused by TPE contributions, then it is $\varepsilon = 1$ where these contributions must be negligible, and thus there will be both a large change in G_E and a smaller change in G_M . While the size of the discrepancy suggests that the impact on G_M would be on the order of 2 – 3%, this is large compared to the precision with which G_M extractions were quoted and thus needs to be taken into account.

In practice, different combined analyses made assumptions that led to somewhat different results. Because the polarization measurements were only available with precision at high Q^2 , some analyses [115] used G_M from LT separations, while taking G_E from LT separations at low Q^2 and polarization measurements at high Q^2 . A slightly different approach was taken in Ref. [85]. Rather than fitting the extracted values of G_E and G_M from a mix of cross section and polarization measurements, the slope of the reduced cross section was fixed from polarization measurements, and G_M varied to best match the reduced cross section over the entire ε range. This corresponds to taking the slope predicted by polarization transfer in Fig. 5 and varying the normalization so that it gives the best reproduction, on average, of the cross section measurement. In this case, the slope will match the data at a weighted average value of ε , typically reproducing the cross section at a point in $0.5 < \varepsilon < 0.8$. This is closer to what one expects from TPE, where the agreement would occur at $\varepsilon = 1$, but still yields a value of G_M that is too small.

A later analysis [36] applied a 6% ε -dependent correction to the cross sections, before performing a combined fit to the cross section and polarization transfer data. The size of this correction was chosen to yield consistency between the measurements at large Q^2 , and the constrained to vanish in the $\varepsilon = 1$ limit. This analysis was consistent with what was known about the discrepancy at high Q^2 , assuming TPE explained the entire difference, although the same 6% ε -dependent correction was applied at all Q^2 , yielding a very large TPE correction for $Q^2 < 1 \text{ GeV}^2$ compared to the predictions of present calculations.

In addition to the dependence of the G_M extraction on the various prescriptions adopted in these analysis, they also assume no TPE contributions to the polarization measurements. The overall impact of TPE on the polarization observables can be comparable to the impact on the cross sections, and could modify the form factors extracted from polarization measurements at the the few percent level.

Furthermore, the extracted form factors all modify the ε dependence of the cross section measurements, and thus will not reproduce the empirical elastic cross sections unless the corrections to the ε dependence, which were often not explicitly given, are put back. This scenario can be seen from Fig. 5, where G_M is determined from the extrapolation of the cross section measurements to $\varepsilon = 0$, and then the polarization measurements used to give the ε dependence of the reduced cross section. The form factors thus obtained, if treated in the Born approximation, will yield the correct cross section only

for scattering at 180° , and produce the maximum deviation from the measured cross section at small angles, where a large fraction of the high-precision measurements are taken. If these form factors are used as input in the analysis of other measurements, such as when calculating the ep elastic cross section in the analysis of quasielastic proton knockout from a nucleus [36, 49, 116] and the deuteron elastic form factors [117], then this error in the cross section can yield incorrect results.

Note that this is not simply because of the inconsistencies of the early extractions, although the impact is more significant in some of these analyses. The problem arises because the form factors yield the cross section in the Born approximation, and the additional TPE contributions must be included along with the traditional radiative corrections to obtain the observed cross section. Because of the model dependence of the TPE corrections, and the concern that one must apply consistent TPE corrections in extracting the form factors and obtaining the cross section from these form factors, some analyses provide both an extraction of the TPE-corrected form factors and a fit to the total (Born+TPE) elastic cross section [36, 118, 119].

There were also attempts to extract the TPE amplitudes from the available data [50, 120], driven mainly by the form factor discrepancy. However, the extraction of the amplitudes required strong assumptions about their ε dependence. While these analyses yielded consistent TPE corrections to the cross sections (up to an overall difference in the normalization), using these amplitudes to make predictions for other observables was extremely unreliable. These analyses are in practice similar to that of Ref. [36], which used a simple TPE correction to the cross section based on the LT/PT discrepancy, although they allowed for an extraction of the Q^2 dependence of the TPE contributions to the cross section, and an estimate of the uncertainties in the extraction of the TPE corrections based solely on the LT/PT form factor discrepancy.

5.4.2 Extraction of form factors including TPE contributions

Given that modern TPE calculations appear able to resolve most or all of the form factor discrepancy (left panel of Fig. 26), the next step is to apply these corrections to the experimental observables and see if the results are consistent. If so, then a combined extraction of the form factors from all available data can be performed.

Such an analysis was performed in Ref. [118] using the hadronic TPE calculations with nucleon elastic intermediate states [6], as outlined in Sec. 4.3. The hadronic TPE corrections have the advantage that they are applicable at ε and Q^2 values where most of the data exist, although they may be incomplete at higher Q^2 . For $Q^2 \lesssim 2 - 3 \text{ GeV}^2$, the TPE corrections to the cross section bring the form factor ratio extracted from Rosenbluth separations into excellent agreement with the polarization transfer measurements (middle panel of Fig. 26). At higher Q^2 , there is a small residual, systematic disagreement. Here a small additional phenomenological correction was applied, linear in ε and with magnitude comparable with estimates [7, 53, 90] of higher-mass intermediate state contributions (right panel of Fig. 26).

For the combined analysis of cross section and polarization measurements, TPE corrections were applied to the extracted cross sections. Most experiments assumed a 1–2% uncertainty due to radiative corrections, with the dominant contribution coming from TPE corrections. Clearly, this was an underestimate of the uncertainty when no TPE corrections were applied, and was taken to be an appropriate uncertainty after applying the hadronic correction of the TPE effects. For the additional TPE contribution associated with higher-mass intermediate states, 100% of the correction was applied as an additional uncertainty to the cross section to reflect the impact of the poorly constrained TPE corrections at high Q^2 . While the TPE calculation [6] provides predictions for the impact on the polarization transfer measurement, most of the data are at large ε , where the impact is extremely small compared to the statistical uncertainties of the measurements. In addition, while the hadronic and partonic calculations yield similar results for the correction to the unpolarized cross sections, they yield corrections

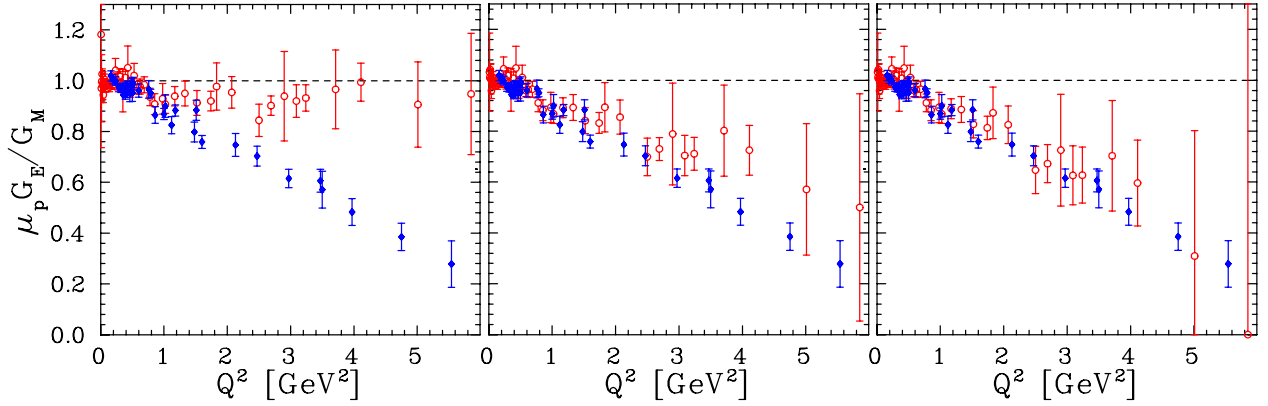


Figure 26: Comparison of polarization measurements (filled diamonds) and LT separations (open circles) with no TPE corrections (**left**), TPE corrections from Ref. [6] (**center**), and with the additional high- Q^2 correction applied in Ref. [118] (**right**).

to the polarization measurements with opposite sign at large Q^2 . The analysis [118] therefore did not to include any TPE corrections to the polarization measurement, as either calculation would have had an extremely small impact on the final result.

The extracted form factors from the combined analysis of polarization measurements and TPE-corrected cross sections is show in Figure 27. Since this publication, there have been updated polarization results at high Q^2 [22, 24] and very low Q^2 [21, 23, 25, 121], as well as an extensive set of cross section measurements at low Q^2 [67]. The global fit of Ref. [118] has been updated in Refs. [23, 121] to include the new polarization measurements, and inclusion of the new cross section measurements is in progress [122].

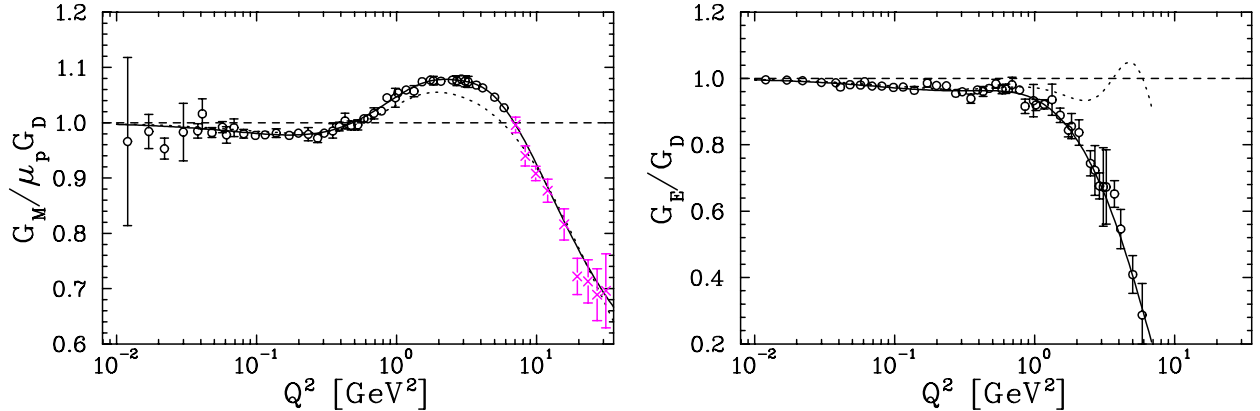


Figure 27: Proton G_M (**left**) and G_E (**right**) form factors from the global fit in Ref. [118], scaled by the dipole form factor (37). Note that above $Q^2 = 6 \text{ GeV}^2$ there were no direct measurements of G_E and G_M was extracted from the cross section data with an additional uncertainty related to the uncertainty in G_E . The solid line is the final fit, while the points are from direct extractions from data in small Q^2 bins. The short-dashed line shows the fit from the cross sections with no TPE corrections applied.

5.4.3 Impact on the extracted charge radius of the proton

The proton charge radius is related to the low Q^2 behavior of the charge form factor. In both electron scattering and atomic physics extractions, the root-mean-square radius R_E is defined in terms of the

slope of the form factor at $Q^2 = 0$,

$$G_E(Q^2) = 1 - \frac{Q^2 R_E^2}{6} + \dots; \quad R_E^2 = -6 \left. \frac{dG_E}{dQ^2} \right|_{Q^2=0}. \quad (62)$$

Because the TPE corrections are finite and Q^2 -dependent in the limit $Q^2 \rightarrow 0$, as seen in Fig. 13, they can impact the electron scattering extractions of the charge radius. These corrections were first included in the second Born (static) approximation by Rosenfelder [48], who found that these increase the charge radius by about 0.01 fm. More recently, the full hadronic calculations were evaluated [96] and compared to the Coulomb distortion correction [48]. The additional impact of the TPE was again very small, yielding an additional increase of 0.002 fm.

Since G_E dominates the cross section at low Q^2 , it is relatively insensitive to the large scattering angle TPE corrections, and one can see from Fig. 17 that the main difference between the second Born approximation and the full hadronic TPE calculation is most important at large angles. Note that for the extraction of the magnetic radius, made more feasible with the addition of new, high-precision data [23, 67], these effects may be significantly more important. In the Rosenbluth extractions, one typically extrapolates the reduced cross section to $\varepsilon = 0$ to extract G_M , and because the $\varepsilon = 0$ cross section becomes extremely small, this extrapolation is very sensitive to any ε -dependent effects, especially at large angle. Thus, the full TPE contribution will be significantly more important in this case, and the impact will be very dependent on the exact kinematics of the experiment, as the uncertainty due to the extrapolation is very sensitive to the angular coverage of the measurements. This is one possible contribution to the discrepancy in the magnetic radii obtained in the recent measurements [23, 67].

5.5 Normal asymmetries

The TPE exchange process gives rise to a nonzero contribution to the elastic cross section for a recoil proton polarized normal to the scattering plane. By time reversal invariance this is also equivalent to scattering (unpolarized) electrons from a target polarized normal to the scattering plane [123]. Normal polarization observables vanishes in the Born approximation, and their measurement directly accesses the imaginary part of the TPE amplitude.

The target normal asymmetry A_N is defined as [99, 123]

$$A_N = \frac{\sigma^\uparrow - \sigma^\downarrow}{\sigma^\uparrow + \sigma^\downarrow}, \quad (63)$$

where $\sigma^{\uparrow(\downarrow)}$ is the cross section for unpolarized electrons scattering from a proton target with spin parallel (antiparallel) to the direction normal to the scattering plane, defined by the spin vector $\zeta_N = \mathbf{k} \times \mathbf{k}' / |\mathbf{k} \times \mathbf{k}'|$ (see Eq. (12)).² At order α in the electromagnetic coupling, the target normal asymmetry is given by [123]

$$A_N = \frac{2 \text{Im}(\mathcal{M}_\gamma^* \mathcal{M}_{\gamma\gamma})}{|\mathcal{M}_\gamma|^2}, \quad (64)$$

providing a direct measure of the imaginary part of $\mathcal{M}_{\gamma\gamma}$.

In Fig. 28 (left) the ratio $\bar{\delta}_N$ of the TPE normal contribution from nucleon elastic intermediate states relative to the unpolarized Born cross section is shown as a function of ε for several values of Q^2 . Note that there is no IR contribution to the normal polarization. The normal polarization contribution is very small numerically, $\delta_N \lesssim 1\%$, and has a very weak ε dependence. In contrast to the TPE longitudinal and transverse polarization corrections δ_L and δ_T in Sec. 5.3, the normal polarization ratio is smallest at low ε , becoming larger with increasing ε .

²Equivalently, by time reversal invariance, A_N would be the asymmetry for scattering unpolarized electrons from an unpolarized proton target, with the recoil proton polarized normal to the scattering plane.

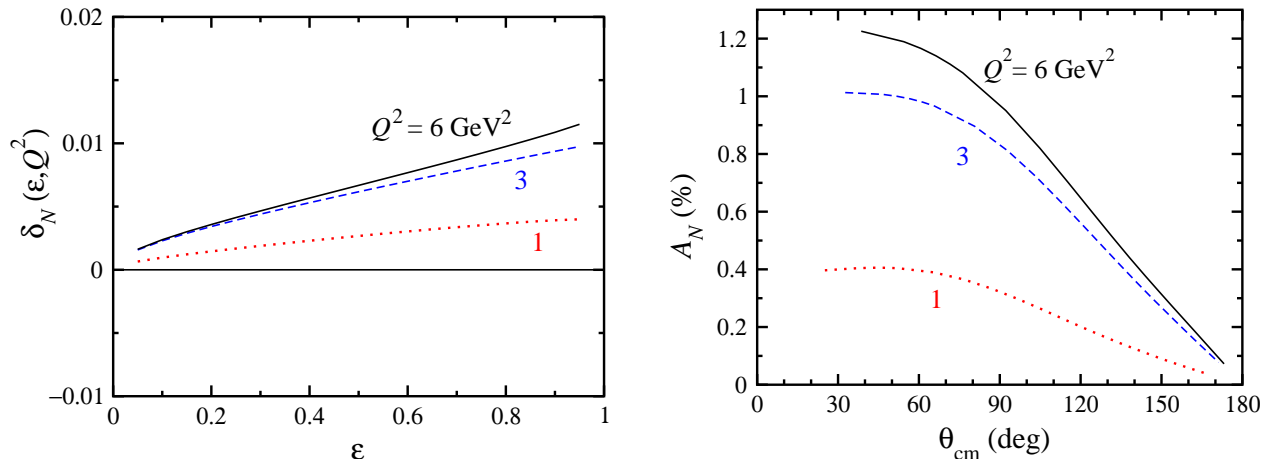


Figure 28: **(Left)** Ratio of the TPE normal polarization correction to the unpolarized Born contribution as a function of ϵ , for $Q^2 = 1$ (dotted), 3 (dashed) and 6 GeV^2 (solid). **(Right)** Target normal polarization asymmetry, as a percentage, as a function of the center of mass scattering angle, θ_{cm} , for $Q^2 = 1$ (dotted), 3 (dashed) and 6 GeV^2 (solid). Figures adapted from Ref. [6].

The target normal asymmetry A_N in Eq. (64) is shown in Fig. 28 (right) as a function of the center of mass scattering angle, θ_{cm} , for several values of Q^2 . The asymmetry is relatively small, of the order of 1% at low θ_{cm} for $Q^2 \sim 3 \text{ GeV}^2$, but grows with Q^2 [6]. The magnitude of the elastic contribution to A_N is relatively model independent (see also Refs. [73, 123]), as it is determined mostly by the (on-shell) proton electromagnetic form factors, which are reasonably well determined. Estimates of contributions from higher-mass intermediate states have been made within the GPD approach [73], and suggest that these may be as significant as the elastic at forward angles θ_{cm} , but very small at backward angles.

Unfortunately no data on target normal asymmetries have been collected for normal-polarized target or recoil nucleons. Experiments have been proposed at Jefferson Lab to measure the target normal asymmetry of the neutron on a ^3He target for deep-inelastic scattering [124] and quasi-elastic neutron knockout [125]. Note that the observation of nonzero effects here would not necessarily signal TPE effects, as there are likely to be nuclear final state interaction effects which can also produce a nonzero asymmetry.

Although not directly relevant to the elastic form factor extraction, the observation of nonzero target normal asymmetries would provide direct evidence of TPE in elastic scattering. Knowledge of the imaginary part of the TPE amplitude could be used to constrain models of Compton scattering, or as input into dispersion relations to obtain the real part of the TPE amplitude from the imaginary part (see Sec. 4.7).

The imaginary part of the TPE amplitude can also be accessed by measuring the electron beam asymmetry for electrons polarized normal to the scattering plane scattering from unpolarized targets. The corresponding beam normal asymmetry B_N is then defined analogously to Eq. (63), with the electron spin parallel or antiparallel to the normal polarization vector ζ_N . Since the beam normal asymmetry involves flipping the helicity of the electron, is it zero in the limit $m_e \rightarrow 0$. Further discussion about the theoretical and experimental status of beam normal asymmetries can be found in Ref. [99].

6 Two-photon exchange in other reactions

While the effect of TPE has been most dramatically illustrated for extraction of proton electric and magnetic form factors using the LT separation method, TPE has also been studied for its effect on the extraction of observables, ranging from elastic neutron and transition form factors, to the pion and nuclear form factors.

6.1 Neutron form factors

Because the magnitude of the electric form factor of the neutron is relatively small compared to that of the proton, especially at low Q^2 the effects of TPE may be even more important for G_E^n than for G_E^p especially at large Q^2 . Within the hadronic framework of Sec. 4, the relative TPE correction to the neutron elastic cross section is shown in Fig. 29 as a function of ε for $Q^2 = 1, 3$ and 6 GeV^2 [6], using input neutron form factors from Ref. [84]. For comparison the correction at $Q^2 = 6 \text{ GeV}^2$ is also computed with the parametrization from Ref. [30], with the difference between these indicative of the model dependence of the calculation.

Since there is no IR-divergent contribution to the TPE correction for the neutron, the *total* correction δ^n is displayed in Fig. 29. Similarly, we note that as $Q^2 \rightarrow 0$, the TPE correction vanishes for neutrons. As explained in Sec. 4.5, for $Q^2 \rightarrow 0$ the TPE correction depends only on $F_1(0)$, and is independent of the anomalous magnetic form factor F_2 .

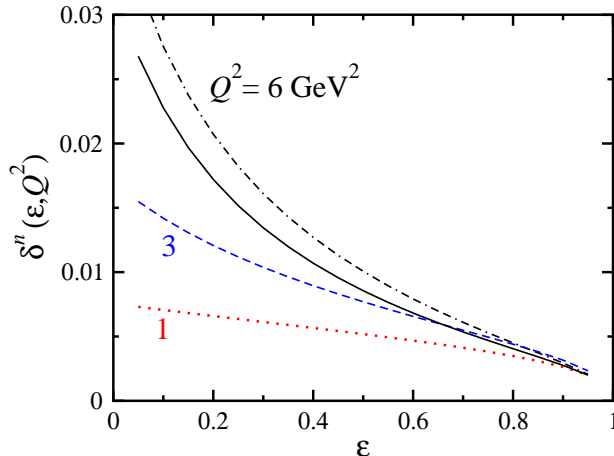


Figure 29: TPE correction δ^n to the unpolarized electron–neutron elastic scattering cross section at $Q^2 = 1$ (dotted), 3 (dashed) and 6 GeV^2 (solid and dot-dashed). The dot-dashed curve corresponds to the form factor parametrization of Ref. [30], while the others are from Ref. [84]. Figure adapted from Ref. [6].

The most notable difference with respect to the proton (Fig. 13) is the sign and slope of the TPE correction. In particular, the magnitude of the neutron correction is around 3 times smaller than for the proton, and the negative slope arises from the negative anomalous magnetic moment of the neutron μ_n [6]. While the correction for the neutron is smaller for the proton, the value of G_E^n is small at all Q^2 values for the neutron, and so the effect of the TPE correction on an LT separation is magnified at all Q^2 values. Figure 30 (left panel) shows the impact that TPE correction would have on a Rosenbluth extraction of $\mu_n G_E^n / G_M^n$. The “uncorrected” values are taken from a global fit [84], and the filled circles show the modification after applying the TPE corrections from Fig. 29, assuming that the initial value came from an LT separation covering two different ε ranges. Inclusion of this correction would

improve the significance of the upper limits on G_E^n from the SLAC Rosenbluth extraction [126] up to $Q^2 = 4 \text{ GeV}^2$, as well as yielding a small correction to G_M^n .

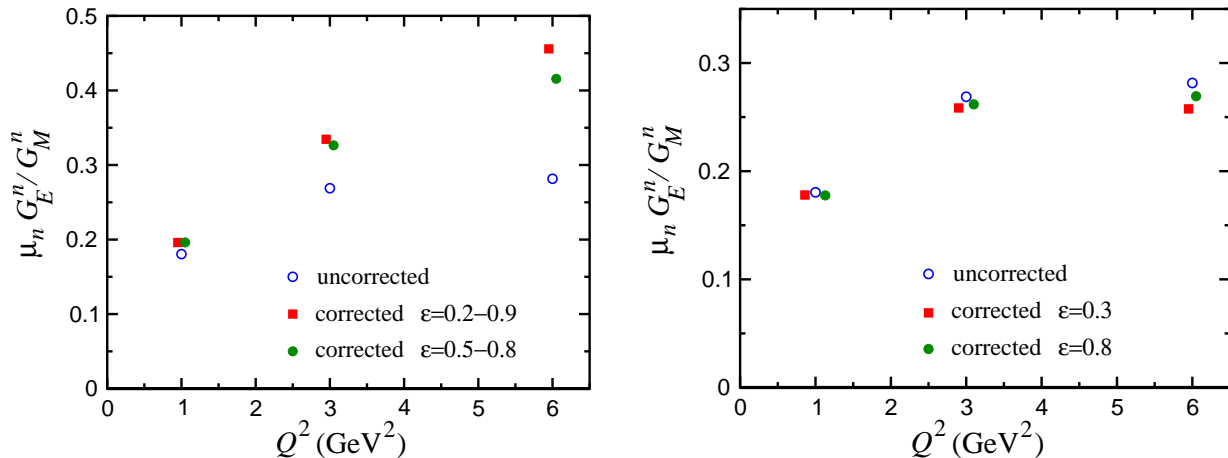


Figure 30: **(Left)** Effect of TPE on the ratio of neutron form factors $\mu_n G_E^n / G_M^n$ using LT separation. The uncorrected points (open circles) are shifted by taking linear fits to the TPE correction in Fig. 29 over the quoted ϵ ranges. **(Right)** TPE effect on polarization transfer measurements. The corrected points correspond to $\epsilon = 0.3$ (filled squares) and $\epsilon = 0.8$ (filled circles) (offset for clarity). Figure taken from Ref. [6].

While the TPE corrections to the form factor ratio from LT separations are significant at large Q^2 , the neutron G_E^n form factor is typically extracted in polarization transfer experiments. To compare the TPE effects on the ratio $\mu_n G_E^n / G_M^n$ extracted using the polarization transfer method, we take the same “uncorrected” starting values for $\mu_n G_E^n / G_M^n$, and show the impact of TPE corrections under the assumption that they were extracted from polarization transfer measurements at $\epsilon = 0.3$ or 0.8 (right panel of Fig. 30). The points are shifted by the $\bar{\delta}_L^n$ and $\bar{\delta}_T^n$ corrections as in Eq. (61) corresponding to the assumed ϵ value. The shift is considerably smaller than that from the LT method, and below the present experimental uncertainties, but nevertheless represents a 3 – 4% suppression at $Q^2 = 3 \text{ GeV}^2$ and 5–10% at $Q^2 = 6 \text{ GeV}^2$.

For kinematics typical of neutron form factor experiments at Jefferson Lab, the ratio G_E^n / G_M^n was recently measured in experiment E93-038 [127] at $Q^2 = 1.45 \text{ GeV}^2$ for $\epsilon \approx 0.9$, at which the TPE correction was $\approx 2.5\%$. In the subsequent extension E04-110 [128] at $Q^2 \approx 4.3 \text{ GeV}^2$, the TPE correction for $\epsilon \approx 0.82$ is expected to be around 3%. While small, these corrections will be important to take into account in order to achieve precision at the several percent level. Two-photon exchange effects will also need to be taken into account when extracting the neutron magnetic form factor G_M^n from cross section data, if precision at the $\sim 1 - 2\%$ level is sought. In particular, in measurements of the ratio of neutron to proton cross sections, the neutron cross section is obtained by multiplying the ratio by the total measured proton cross section which depends on both the Born form factors and TPE corrections. The extracted neutron cross section must then be corrected for TPE effects in the neutron to obtain the Born form factors.

6.2 Electroproduction of resonances

Beyond elastic final states, inelastic electroproduction channels provide additional information on hadron structure, from mapping out the spectrum of states in QCD, to probing the spatial distributions

of hadrons. Of particular interest is the reaction whereby the produced final state is in the $\Delta(1232)$ resonance region, which has been recently studied both experimentally [68, 129] and theoretically [130].

At the Born level, Δ electroproduction is parametrized by the same electromagnetic $N \rightarrow \Delta$ transition amplitudes that enter the calculation of the Δ intermediate state contribution to the TPE corrections in elastic ep scattering in Sec. 4.4.1. It therefore provides an important consistency check on the role of the Δ resonance in electron scattering. Kondratyuk and Blunden [131] computed the TPE corrections to the unpolarized cross section for Δ production in electron-proton collisions, including both nucleon and Δ contributions in the intermediate states in the one-loop diagrams. As in the case of elastic scattering, the TPE effects from the intermediate nucleon and Δ have opposite signs in most kinematical regimes, and are pronounced even at low energies.

It is straightforward to show that the sum of the box and crossed-box amplitudes with an intermediate Δ is gauge invariant by itself. For the nucleon intermediate state, an additional $\gamma\gamma N\Delta$ contact term has to be added to the box and crossed-box diagrams. Such a term is required for gauge invariance, and can be constructed by the standard procedure of minimal substitution [132].

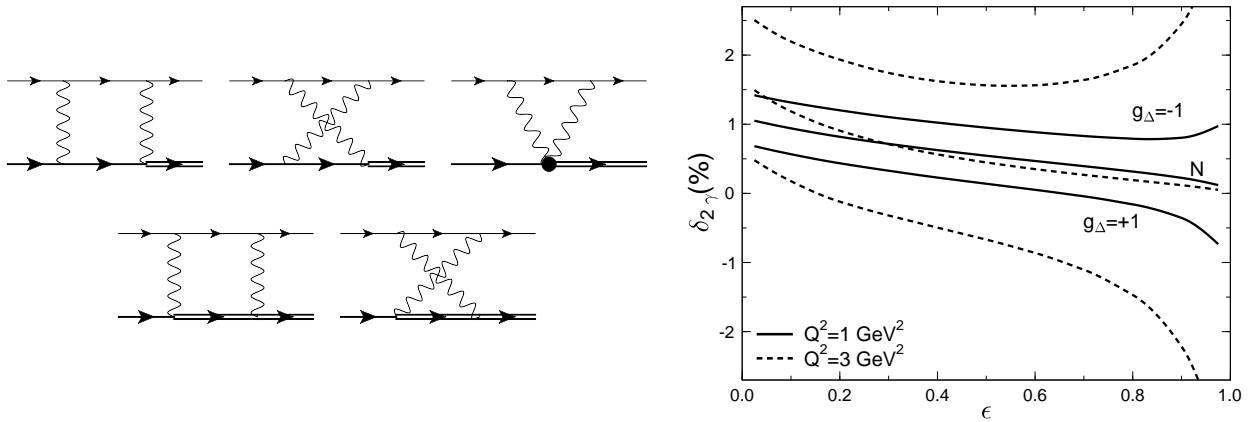


Figure 31: **(Left)** Two-photon exchange graphs for the $ep \rightarrow e\Delta$ reaction. The loop diagram with the $\gamma\gamma N\Delta$ contact term (denoted by the black circle) ensures gauge invariance of the calculation. **(Right)** Two-photon exchange correction to the unpolarized cross section for Δ production in electron-proton collisions, calculated for $Q^2 = 1 \text{ GeV}^2$ (solid) and $Q^2 = 3 \text{ GeV}^2$ (dashed). The upper, middle and lower pairs of lines are labeled by the values of the $\gamma\Delta\Delta$ coupling constant g_{Δ} (“N” corresponding to $g_{\Delta} = 0$, *i.e.* to the absence of an intermediate Δ state). Figures adapted from Ref. [131].

An important theoretical ingredient of the calculation is the $\gamma\Delta\Delta$ vertex form factor. Various forms of this vertex feature prominently in the studies of electromagnetic interactions of the deuteron [133] and three-nucleon bound states [134], as well as in the recent extraction [135] of the Δ magnetic dipole moment.

The TPE corrections in Δ electroproduction are, as expected, generally much smaller than the Born contribution [131], but can be important for a precise analysis of ep scattering in the resonance region. Results for $Q^2 = 1 \text{ GeV}^2$ and $Q^2 = 3 \text{ GeV}^2$ are shown in Fig. 31. Kondratyuk and Blunden [131] find a pronounced ϵ dependence of the TPE correction to the value and sign of the (dominant) $\gamma\Delta\Delta$ magnetic coupling constant. A current analysis [68] of experimental Rosenbluth separations in ep scattering provides strong constraints on the nonlinearity in ϵ , although additional high-precision data would allow more definite conclusions to be reached.

For further progress in the evaluation of higher-order effects in electron-nucleon collisions, a more detailed knowledge of the $\gamma\Delta\Delta$ vertex is needed. Being formulated in terms of hadronic degrees of

freedom, this model is somewhat complementary to the approach of Ref. [130], where TPE effects were calculated using the formalism of generalized parton distributions.

6.3 Timelike form factors

Electromagnetic form factors in the space-like ($Q^2 > 0$) and time-like ($Q^2 < 0$) regions both yield information on the structure of hadrons. The form factors are real in the space-like region, while the time-like form factors have a phase structure reflecting the final-state interactions of the outgoing hadrons, and are therefore complex.

The interference of one- and two-photon exchange can be studied in the process $e^+e^- \rightarrow p\bar{p}$, and is related by crossing symmetry to the elastic ep interaction. The interference manifests as an angular asymmetry in the differential cross section. This was studied recently by Chen *et al.* [136] in a hadronic model with essentially the same ingredients as the ep calculations. The corrections are again at the few percent level, and are shown in Fig. 32 for $Q^2 = 4 \text{ GeV}^2$. A search for TPE effects in BABAR $e^+e^- \rightarrow p\bar{p}$ data [137] showed no indication of the expected forward-backward asymmetry within the precision of the data [138].

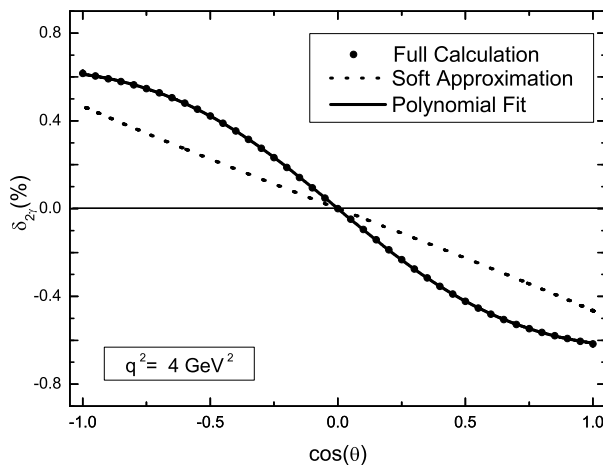


Figure 32: Angular dependence of the TPE contribution to the differential cross section for $e^+e^- \rightarrow p\bar{p}$. Figure taken from Ref. [136].

In addition to the unpolarized differential cross section, Chen *et al.* [136] considered the single-spin polarization observable P_y , and the double-spin polarization observables P_x and P_z , which require the incoming electron to be polarized. They suggested that P_z in particular should be considered in future experiments looking for TPE effects.

6.4 Pion form factor

As the lightest bound state of quarks and antiquarks, the pion plays a unique role in QCD, and determining its electromagnetic structure is of great importance for understanding the realization of chiral symmetry in nature. Extractions of the pion form factor $F_\pi(q^2)$ in the space-like region from measurements of the pion electroproduction reaction $ep \rightarrow e\pi^+n$ have recently provided data on the Q^2 dependence of F_π up to values of $Q^2 \sim 2.5 \text{ GeV}^2$ [139, 140, 141], and higher Q^2 measurements are planned to $Q^2 \sim 6 \text{ GeV}^2$. The role of TPE in electromagnetic scattering from the pion was recently investigated by several authors [9, 106, 142, 143]. The analysis of TPE from a spin-0 target is, in fact, considerably simpler than that for spin- $\frac{1}{2}$ targets.

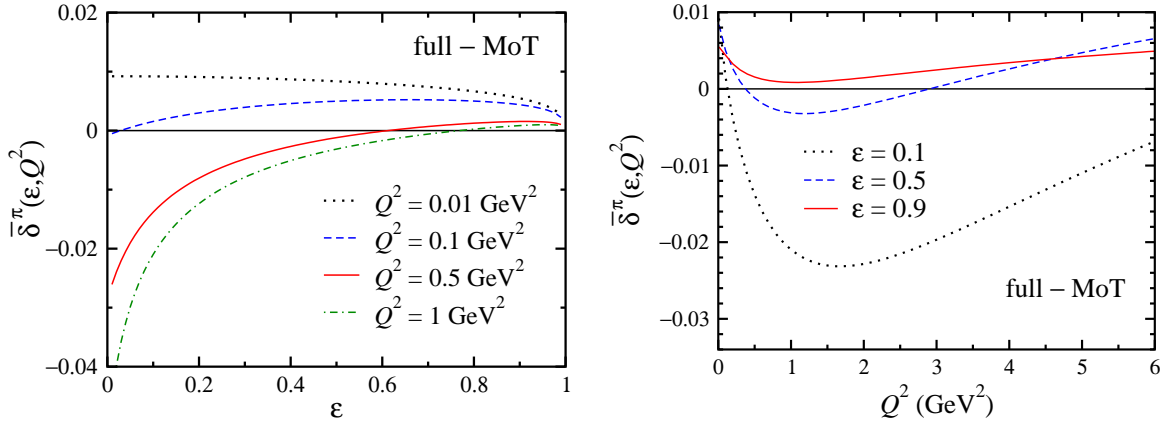


Figure 33: Two-photon exchange correction $\bar{\delta}^\pi$ to the pion form factor squared, relative to the Mo-Tsai (MoT) contribution [37, 38], as a function of ϵ for various Q^2 (**left**), and of Q^2 for various ϵ (**right**). Figures adapted from Ref. [9].

The form factor of the pion is defined through the matrix element of the pion current,

$$\langle \pi(p') | J^\mu(0) | \pi(p) \rangle = (p + p')^\mu F_\pi(q^2). \quad (65)$$

In the Born approximation the amplitude for an electron scattering from a π^+ is given by

$$\mathcal{M}_\gamma^\pi = -\frac{e^2}{q^2} \bar{u}_e(k') \gamma_\mu u_e(k) (p + p')^\mu F_\pi(q^2), \quad (66)$$

and the Born cross section in the target rest frame is

$$\frac{d\sigma^{e\pi}}{d\Omega} = \sigma_{\text{Mott}} F_\pi^2(q^2), \quad (67)$$

where σ_{Mott} is given in Eq. (9).

The TPE amplitude for the box diagram has the form [9, 106]

$$\mathcal{M}_{\gamma\gamma}^\pi = -ie^4 \int \frac{d^4 q_1}{(2\pi)^4} L_{\mu\nu} H_\pi^{\mu\nu} \Delta_F(q_1, \lambda) \Delta_F(q_2, \lambda), \quad (68)$$

where the leptonic tensor $L_{\mu\nu}$ is given in Eq. (32), and the crossed-box is obtained using crossing symmetry. The pion hadronic tensor $H_\pi^{\mu\nu}$ in principle contains contributions from all hadronic excitations in the intermediate state. For the dominant pion elastic contribution, one has

$$H_\pi^{\mu\nu} = (2p + q_1 + q)^\mu F_\pi(q_1^2) \Delta_F(p + q_1, m_\pi) (2p + q_1)^\nu F_\pi(q_2^2). \quad (69)$$

The pion form factor is then modified according to $F_\pi^2(q^2) \rightarrow F_\pi^2(q^2) (1 + \delta^\pi)$, where, as for the nucleon TPE correction in Eq. (35), the relative correction δ^π is given by

$$\delta^\pi = \frac{2\text{Re}(\mathcal{M}_\gamma^{\pi*} \mathcal{M}_{\gamma\gamma}^\pi)}{|\mathcal{M}_\gamma^\pi|^2}. \quad (70)$$

As in the case of the nucleon electromagnetic form factors, experimental analyses of pion form factor data typically use radiative corrections computed by Mo and Tsai in the soft-photon approximation [37, 38] (see Sec. 4.1). The effect of the IR-finite, structure-dependent contribution is illustrated in

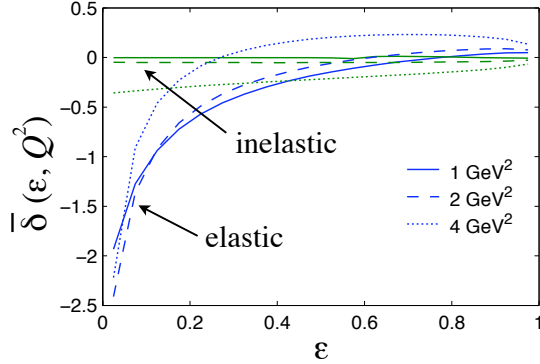


Figure 34: Elastic and inelastic (ρ and $b_1(1235)$) contributions to the TPE correction $\bar{\delta}^\pi$ (in percent) relative to the Maximon-Tjon result [47], as a function of ε for $Q^2 = 1, 2$ and 4 GeV^2 . Figure adapted from Ref. [106].

Fig. 33, where the difference between the full TPE correction and the Mo-Tsai prescription [37, 38], $\bar{\delta}^\pi = \delta^\pi - \delta_{\text{IR}}(\text{MoT})$, is shown as a function of ε and Q^2 . Here a monopole parametrization for the “bare” pion form factor in Eq. (68) is used,

$$F_\pi(q^2) = \left(1 - \frac{q^2}{\Lambda_\pi^2}\right)^{-1}, \quad (71)$$

with the cut-off parameter $\Lambda_\pi = 770 \text{ MeV}$ corresponding to the ρ -meson mass. The sensitivity of the results to the input pion form factor was studied in Ref. [9], using an alternative parametrization [144] which gives a better description of the available data and builds in gauge invariance constraints for the $Q^2 \rightarrow 0$ limit and perturbative QCD expectations for the $Q^2 \rightarrow \infty$ behavior. The differences at low Q^2 are negligible, but become noticeable at high Q^2 , although do not affect the results qualitatively.

At low Q^2 ($Q^2 \sim 0.01 \text{ GeV}^2$) the TPE correction is positive and of the order of 1% at backward angles (small ε), decreasing to zero as $\varepsilon \rightarrow 1$. For larger Q^2 the correction becomes more negative up to $Q^2 \sim 1\text{--}2 \text{ GeV}^2$, especially at backward angles, but changes sign at intermediate ε . Unlike for ep scattering, the $e\pi$ cross section vanishes in the extreme backward limit ($\varepsilon \rightarrow 0$). Above $Q^2 \sim 2 \text{ GeV}^2$ the correction grows once again, reaching $\sim 1\%$ at $Q^2 = 10 \text{ GeV}^2$ [9]. Interestingly, the TPE correction is most positive at very small Q^2 ($Q^2 \ll 1 \text{ GeV}^2$) and at large Q^2 ($Q^2 \gg 1 \text{ GeV}^2$), reaching its minimum values at $Q^2 \sim 1\text{--}2 \text{ GeV}^2$.

The contributions from higher-mass intermediate states to the pion hadronic tensor were considered in Ref. [106] within a dispersion relations approach. Because the mass difference between the pion and the next excited resonant state, the ρ meson, is ~ 5 times as large as the pion mass, one would not expect large contributions from excited hadronic intermediate states. This was indeed confirmed in explicit calculations of the ρ and $b_1(1235)$ meson contributions, which were found to be negligible for $Q^2 \lesssim 2 \text{ GeV}^2$, as Fig. 34 illustrates. At larger Q^2 ($\gtrsim 4 \text{ GeV}^2$) the inelastic contributions become comparable to the elastic for $\varepsilon \gtrsim 0.2$; however, in the region at low ε where the TPE effect is greatest, these are still significantly smaller than the elastic components.

In contrast to the proton form factor case, where the TPE effects give large corrections to the elastic form factors extracted from LT separated cross sections at large Q^2 [118], the TPE corrections to the pion form factor are relatively small. This stems from the fact that electron scattering from a scalar target is described by a single form factor, with no LT separation necessary. On the other hand, since F_π is extracted via LT separation of the pion electroproduction cross section, TPE with one photon

attached to the pion and the other to the initial proton or final neutron could modify the longitudinal cross section, and may need to be considered. Furthermore, the effects on the pion form factor from nonresonant contributions in the intermediate state have not yet been evaluated, and may also need to be considered in future analyses.

6.5 Electron–nucleus scattering

6.5.1 TPE in deuteron form factors

The TPE corrections to the (spin-1) deuteron (D) elastic electromagnetic form factors and to the $e^+e^- \rightarrow D\bar{D}$ process have been discussed in Refs. [145, 146, 147, 148, 149]. The reaction amplitude contains six generalized form factors, but only three linearly independent combinations of them (generalized charge G_C^D , quadrupole G_Q^D , and magnetic G_M^D form factors) contribute to the cross section [145].

Dong and collaborators [146, 147, 149] estimated all the TPE corrections to the conventional form factors of the deuteron using an effective Lagrangian approach. In this model, the two photons couple to one of the two nucleons in the deuteron. Dong found the TPE corrections to be small (less than 1% for $Q^2 < 2 \text{ GeV}^2$), and most significant for G_M^D [146]. He also suggested that two of the additional form factors could be tested in measurements of the double and single polarization observables [146]. The effect makes a sizable contribution at backward angles to the polarization observable P_y of eD scattering, which vanishes in the Born approximation [149].

Kobushkin *et al.* [148] also discuss elastic electron-deuteron scattering beyond the Born approximation. They included contributions where the two photons can also interact with different nucleons. They conclude that TPE *may* give a large contribution to elastic eD scattering, but point out that their estimates have large uncertainties. The most important source of uncertainty comes from the short-range part of the deuteron wave function. It is suggested that experimental study of TPE in elastic eD scattering for Q^2 in the few GeV^2 range can give important information about the deuteron structure at short distances.

6.5.2 ^3He elastic form factors

The hadronic formalism of Sec. 4 has also been applied to the case of elastic scattering from the spin-1/2 ^3He nucleus [6], where contributions of unexcited ^3He intermediate states were computed. Of course these are likely to constitute only a part of the entire TPE effect, as contributions from break-up channels may also be important. Nevertheless, a comparison of the size and magnitude of the TPE corrections from elastic intermediate states in ^3He relative to those in the proton illustrates a number of features of TPE.

The expressions used to evaluate the TPE contributions to the ^3He correction $\delta^{^3\text{He}}$ are similar to those for the nucleon in Sec. 4.3, but with some important differences. The charge of the nucleus is Ze , with $Z = 2$ for ^3He , and the mass $M_{^3\text{He}}$ is approximately 3 times larger than the nucleon mass, while the anomalous magnetic moment is $\kappa_{^3\text{He}} = -4.185$. The internal photon– ^3He form factors are also softer than the corresponding proton form factor (the charge radius of the ^3He nucleus is $\approx 1.88 \text{ fm}$), and have zeros at $Q^2 \approx 0.45$ and 0.7 GeV^2 for the charge and magnetic form factors, respectively [150].

The TPE correction $\bar{\delta}^{^3\text{He}}$, relative to the Mo-Tsai IR-divergent result, is shown in Fig. 35 as a function of ε for several values of Q^2 , using the ^3He form factors from Ref. [150]. As for the proton, the correction is negative at low Q^2 , and generally increases in magnitude with increasing Q^2 . On the other hand, the larger charge of the ^3He nucleus makes the TPE effect larger by a factor ~ 4 , while the larger mass squared suppresses it by a factor ~ 9 . The dramatic change of sign in $\bar{\delta}^{^3\text{He}}$ at $Q^2 = 0.5 \text{ GeV}^2$ stems from the presence of the zeros in the form factors at $Q^2 \sim 0.5 \text{ GeV}^2$.

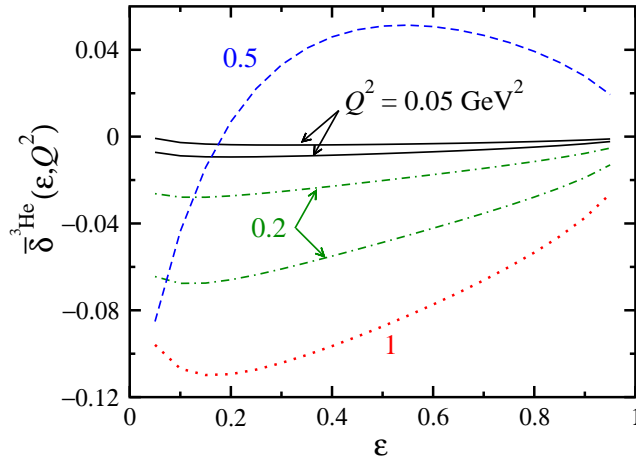


Figure 35: TPE contribution to the unpolarized electron- ${}^3\text{He}$ cross section, with the ${}^3\text{He}$ elastic intermediate state, as a function of ϵ , for $Q^2 = 0.05$ (solid), 0.2 (dot-dashed), 0.5 (dashed) and 1 GeV^2 (dotted). A parameterization of the form factor from Ref. [150] is used in all cases, except for the upper solid and dot-dashed curves, which uses a dipole with mass $\Lambda_{3\text{He}} = 0.37 \text{ GeV}$. Figure adapted from Ref. [6].

To estimate the model dependence of the results, Blunden *et al.* also calculated $\bar{\delta}^{{}^3\text{He}}$ assuming a dipole shape with a cut-off mass $\Lambda_{3\text{He}} = 0.37 \text{ GeV}$, fitted to the ${}^3\text{He}$ radius, which gives a reasonable approximation at low Q^2 ($\lesssim 0.05 \text{ GeV}^2$). The results with this form factor are about a factor 2 smaller in magnitude than for the form factor from Ref. [150]. At larger Q^2 the dipole shape is a less reliable representation of the ${}^3\text{He}$ form factor, making it difficult to estimate the model dependence of $\delta^{{}^3\text{He}}$. The results in Fig. 35 illustrate the potential relevance of TPE effects for future ${}^3\text{He}$ form factor measurements, which may reveal interesting TPE effects at larger Q^2 [151].

7 Parity-violating electron scattering

In addition to the exchange of one or more virtual photons between the electron and nucleon, the Standard Model allows the scattering to take place via the exchange of a neutral Z boson. Because the Z boson mass is some two orders of magnitude larger than the proton mass, the weak exchange process is strongly suppressed relative to the electromagnetic reaction. Nevertheless, asymmetries sensitive to the γZ interference amplitude, which are of the order of several parts per million (ppm), have been measured in modern accelerator facilities. These have been used to probe the strangeness content of the proton, through measurements of the strange electric and magnetic form factors [152, 153, 154, 155, 156, 157, 158, 159, 160, 161], as well as to measure the weak charge of the proton [162].

The γZ interference term is isolated by polarizing the incident electron and measuring the difference between right- and left-handed electrons scattering from unpolarized protons. A parity-violating (PV) asymmetry can then be defined in terms of the differential cross sections as

$$A_{\text{PV}} = \frac{\sigma_+ - \sigma_-}{\sigma_+ + \sigma_-}, \quad (72)$$

where σ_h is the cross section for a right-hand (helicity $h = +1$) or left-hand (helicity $h = -1$) polarized electron. The numerator in the asymmetry is sensitive to the interference of the vector and axial-vector currents, and hence violates parity. The natural size of the PV asymmetry is $\sim Q^2/M_Z^2$, which for $Q^2 \sim 0.1 \text{ GeV}^2$ is of the order $10^{-5} - 10^{-6}$ — values that can be routinely measured at current facilities such as Jefferson Lab or MAMI at Mainz [163].

In view of the large TPE effects on electromagnetic form factors discussed in the proceeding sections, the question naturally arises of what effect the exchange of two bosons (γ or Z) may have on PV asymmetries. Because both the strange form factors and the proton weak charge are numerically small quantities, these contributions could affect their extraction significantly.

One should note that the “standard electroweak radiative corrections” already include a contribution from two-boson exchange (TBE) effects. These are usually taken from the classic calculation of Marciano and Sirlin [164, 165], and include γZ , ZZ , and WW exchange box and crossed-box diagrams. Because of the large masses of the Z and W bosons, the box diagrams contain contributions for virtual four-momenta of all mass scales. For the ZZ and WW boxes, the high mass scales dominate, and a calculation in terms of the quark structure of the nucleon is reliable. However, for the γZ diagram both high and low mass scales contribute. The high-mass scale, calculated in terms of quarks, accounts for most of the effect, but the low momentum contribution in terms of a hadronic picture is not negligible. The quark-based calculation is discussed in more detail in Sec. 7.3.

In this section we review the TBE corrections to PV asymmetries arising from the interference between single Z boson and $\gamma\gamma$ exchange amplitudes (which we denote by “ $Z(\gamma\gamma)$ ”), and between the one-photon exchange and γZ interference amplitudes (denoted by “ $\gamma(Z\gamma)$ ”). Because PV electron scattering experiments are typically performed at Q^2 values $\lesssim 1 \text{ GeV}^2$, the hadronic formalism described in Sec. 4 is the more natural implementation of hadronic structure effects. For a detailed examination of the GPD-based approach see Refs. [99, 166].

7.1 Parity-violating asymmetries

In the Born approximation, the weak neutral current amplitude is given by

$$\mathcal{M}_Z = -\frac{2g^2}{(4\cos\theta_W)^2} \frac{1}{M_Z^2 - q^2} j_{Z\mu} J_Z^\mu \approx -\left(\frac{G_F}{\sqrt{2}}\right) j_{Z\mu} J_Z^\mu, \quad (73)$$

where $g = e/\sin\theta_W$ is the weak coupling constant, M_Z is the Z boson mass, and the strength of the effective four-fermion interaction is given by the Fermi constant $G_F = \pi\alpha/(\sqrt{2}M_Z^2 \sin^2\theta_W \cos^2\theta_W)$. At tree level the weak mixing angle θ_W is related to the weak boson masses by $\sin^2\theta_W = 1 - M_W^2/M_Z^2$, where M_W is the W boson mass. The weak leptonic current is given by a sum of vector and axial-vector terms [167],

$$j_{Z\mu} = \bar{u}_e(k', h) \gamma_\mu (g_V^e - g_A^e \gamma_5) u_e(k, h), \quad (74)$$

where the vector (g_V^e) and axial-vector (g_A^e) couplings of the electron to the weak current are defined as

$$g_V^e = -\frac{1}{2}(1 - 4\sin^2\theta_W), \quad g_A^e = -\frac{1}{2}, \quad (75)$$

respectively. Note that some of the TPE literature [8, 83, 88, 163, 168, 169, 170, 171, 172, 173] uses definitions whereby the vector and axial charges are scaled by a factor 2 relative to those in Eq. (75), so that care should be taken when comparing formulas for amplitudes.

The matrix elements of the weak hadronic neutral current is given by

$$J_Z^\mu = \bar{u}_N(p') \Gamma_Z^\mu(q) u_N(p), \quad (76)$$

where the current operator is parametrized by three weak nucleon form factors,

$$\Gamma_Z^\mu(q) = \gamma^\mu F_1^{ZN}(Q^2) + \frac{i\sigma^{\mu\nu}q_\nu}{2M} F_2^{ZN}(Q^2) + \gamma^\mu \gamma_5 G_A^{ZN}(Q^2). \quad (77)$$

Alternatively, the current operator can be expressed in terms of the Sachs weak form factors $G_{E,M}^{ZN}$, in analogy with the electromagnetic nucleon form factors in Eq. (11),

$$G_E^{ZN}(Q^2) = F_1^{ZN}(Q^2) - \tau F_2^{ZN}(Q^2), \quad G_M^{ZN}(Q^2) = F_1^{ZN}(Q^2) + F_2^{ZN}(Q^2). \quad (78)$$

The differential cross section including γ and Z exchange is given by Eq. (8), where the amplitude is now a sum of the γ and Z Born contributions,

$$|\mathcal{M}|^2 = |\mathcal{M}_\gamma + \mathcal{M}_Z|^2 = |\mathcal{M}_\gamma|^2 + 2\mathcal{R}e(\mathcal{M}_\gamma^* \mathcal{M}_Z) + |\mathcal{M}_Z|^2. \quad (79)$$

At the kinematics of interest in this review, the purely weak contribution $|\mathcal{M}_Z|^2$ is small compared with the other terms and can be neglected. The purely electromagnetic contribution cancels in the numerator of the asymmetry in Eq. (72), so that A_{PV} is sensitive to the parity-violating part of $2\mathcal{R}e(\mathcal{M}_\gamma^* \mathcal{M}_Z)$, involving the interference of \mathcal{M}_γ with the product of vector and axial-vector currents in \mathcal{M}_Z . The vector-vector and axial-axial parts of \mathcal{M}_Z also cancel in the asymmetry. The denominator is dominated by the electromagnetic term, $|\mathcal{M}_\gamma|^2$. Evaluating the asymmetry explicitly, one has for PV asymmetry of the nucleon

$$A_{\text{PV}}^N = - \left(\frac{G_F Q^2}{4\pi\alpha\sqrt{2}} \right) \frac{1}{\sigma_R^{\gamma N}} \left\{ -2g_A^e \left(\varepsilon G_E^{\gamma N} G_E^{ZN} + \tau G_M^{\gamma N} G_M^{ZN} \right) + 2g_V^e \varepsilon' G_M^{\gamma N} G_A^{ZN} \right\}, \quad (80)$$

where $\varepsilon' = \sqrt{\tau(1+\tau)(1-\varepsilon^2)}$, and $\sigma_R^{\gamma N}$ is the reduced γN cross section defined in Eq. (10).

For a proton target, assuming isospin symmetry, the weak vector form factors $G_{E,M}^{Zp}$ can be related to the electromagnetic form factors of the proton (neutron) $G_{E,M}^{\gamma p(n)}$ by

$$G_{E,M}^{Zp} = (1 - 4\sin^2\theta_W) G_{E,M}^{\gamma p} - G_{E,M}^{\gamma n} - G_{E,M}^s, \quad (81)$$

where $G_{E,M}^s$ are the contributions from strange quarks, and

$$G_E^{Zp}(0) \equiv Q_W^p = 1 - 4\sin^2\theta_W \quad [\text{Born approximation}] \quad (82)$$

is the weak charge of the proton. Because Q_W^p is numerically small, the overall contribution to $G_{E,M}^{Zp}$ from the proton electromagnetic form factors is suppressed. The weak axial-vector form factor of the proton is given by $G_A^{Zp} = -G_A^p + G_A^s$, where $G_A^p(0) \equiv g_A = 1.267$ is the axial-vector charge, and G_A^s is the axial-vector strange quark contribution, related to the spin of the proton carried by strange quarks as measured in deep-inelastic scattering [174, 175]. In terms of the proton vector (A_V), axial-vector (A_A) and strange (A_s) contributions, the asymmetry can then be written as

$$A_{\text{PV}}^p = - \left(\frac{G_F Q^2}{4\pi\alpha\sqrt{2}} \right) (A_V + A_A + A_s), \quad (83)$$

where

$$A_V = -2g_A^e \left[(1 - 4\sin^2\theta_W) - \frac{1}{\sigma_R^{\gamma p}} (\varepsilon G_E^{\gamma p} G_E^{\gamma n} + \tau G_M^{\gamma p} G_M^{\gamma n}) \right], \quad (84)$$

$$A_A = 2g_V^e \frac{\varepsilon'}{\sigma_R^{\gamma p}} G_A^{Zp} G_M^{\gamma p}, \quad (85)$$

$$A_s = 2g_A^e \frac{1}{\sigma_R^{\gamma p}} (\varepsilon G_E^{\gamma p} G_E^s + \tau G_M^{\gamma p} G_M^s), \quad (86)$$

where $\sigma_R^{\gamma p}$ is the reduced cross section for a proton target.

7.2 Two-boson exchange corrections

Beyond the Born approximation, the PV asymmetry, Eq. (80), receives corrections from higher-order radiative effects, including both the electromagnetic two-photon exchange contributions discussed in

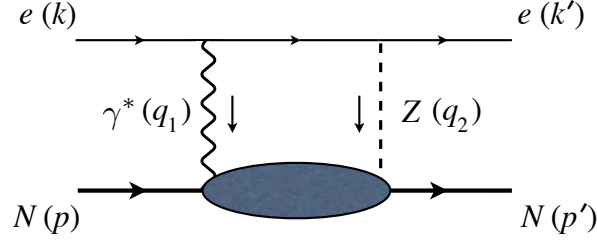


Figure 36: An example of a two-boson exchange contribution to parity-violating elastic scattering, due to γZ exchange (given by the amplitude $\mathcal{M}_{\gamma Z}$). Other contributions include the amplitude with the γ and Z interchanged (denoted by $\mathcal{M}_{Z\gamma}$), and the crossed-box diagrams.

Sec. 4 and corrections involving γ - Z boson loops. There are several ways in which the PV asymmetry can be represented in the presence of higher-order radiative corrections. The approach pioneered by Marciano and Sirlin [164, 165] parameterizes the electroweak radiative effects in terms of parameters ρ and κ , such that the weak charge of the proton in the presence of higher-order corrections becomes

$$Q_W^p \rightarrow \rho(1 - 4\kappa \sin^2 \theta_W). \quad (87)$$

Including the standard radiative corrections, such as vacuum polarization, vertex corrections, and hadron structure-independent two-boson exchange contributions, one has $\rho = 0.9877$ and $\kappa = 1.0026$ [167]. The TBE amplitudes discussed here give additional corrections to ρ and κ which are denoted in Refs. [8, 88, 169, 170] by $\Delta\rho$ and $\Delta\kappa$, respectively.

An alternative parametrization is in terms of isoscalar and isovector weak radiative corrections for the vector form factors, and a similar set of corrections for the axial-vector form factors. In this case the vector part of the PV asymmetry is written

$$A_V = -2g_A^e \left[(1 - 4\sin^2 \theta_W)(1 + R_V^p) - \frac{1}{\sigma_R^{\gamma p}} (\varepsilon G_E^{\gamma p} G_E^{\gamma n} + \tau G_M^{\gamma p} G_M^{\gamma n}) (1 + R_V^n) \right], \quad (88)$$

where the proton and neutron radiative corrections are given, to first order in $\rho - 1$ and $\kappa - 1$, by

$$R_V^p = \rho - 1 - (\kappa - 1) \frac{4\sin^2 \theta_W}{1 - 4\sin^2 \theta_W}, \quad R_V^n = \rho - 1. \quad (89)$$

The radiative corrections to the strange part of the asymmetry (86) enter via a multiplicative factor

$$A_s \rightarrow A_s(1 + R_V^{(0)}), \quad (90)$$

where the isoscalar radiative correction $R_V^{(0)} = \rho - 1$. For the axial asymmetry A_A , the generalization of the tree level axial form factor, $G_A^{Zp} \rightarrow \tilde{G}_A^{Zp}$, implicitly contains higher-order radiative corrections for the proton axial current, as well as the hadronic anapole contributions [168, 176].

More explicitly, the corrections to the cross section arising from the $\gamma\gamma$ and γZ TBE contributions can be obtained from Eq. (79) by the replacements

$$\mathcal{M}_\gamma \rightarrow \mathcal{M}_\gamma + \mathcal{M}_{\gamma\gamma}, \quad \mathcal{M}_Z \rightarrow \mathcal{M}_Z + \mathcal{M}_{\gamma Z} + \mathcal{M}_{Z\gamma}, \quad (91)$$

where $\mathcal{M}_{\gamma Z}$ and $\mathcal{M}_{Z\gamma}$ correspond to the two different orderings of the γ and Z exchanges in the box and crossed-box diagrams, Fig. 36.

Because the coupling of the Z boson to the electron and to the proton contains both vector and axial-vector components, the interference amplitude $\mathcal{M}_{\gamma Z}$ (and similarly $\mathcal{M}_{Z\gamma}$) contains (parity-conserving) vector electron–vector hadron and axial electron–axial hadron terms from the Z exchange, along with (parity-violating) vector electron–axial hadron and axial electron–vector hadron terms (the γ exchange contributions are pure of course pure vector–vector). The parity-violating asymmetry A_{PV} selects only the vector–axial vector part of the amplitude, $\mathcal{M}_{\gamma Z}^{(\text{PV})}$, which can be decomposed into the vector hadron contribution $\mathcal{M}_{\gamma Z}^{V(\text{PV})}$ and the axial–vector contribution $\mathcal{M}_{\gamma Z}^{A(\text{PV})}$. These have the crossing symmetry properties under the interchange $s \leftrightarrow u$ (or $E \leftrightarrow -E'$),

$$\mathcal{M}_{\gamma Z}^{V(\text{PV})\text{xbox}}(u, t) = - \mathcal{M}_{\gamma Z}^{V(\text{PV})\text{box}}(s, t) \Big|_{s \rightarrow u}, \quad (92)$$

$$\mathcal{M}_{\gamma Z}^{A(\text{PV})\text{xbox}}(u, t) = + \mathcal{M}_{\gamma Z}^{A(\text{PV})\text{box}}(s, t) \Big|_{s \rightarrow u}, \quad (93)$$

and similarly for $\mathcal{M}_{Z\gamma}^{(\text{PV})}$.

The relative corrections from the $Z(\gamma\gamma)$ and $\gamma(\gamma Z)$ interference terms to the PV asymmetry can then be identified as

$$\delta_{Z(\gamma\gamma)} = \frac{2\mathcal{R}e\left(\mathcal{M}_Z^{(\text{PV})*} \mathcal{M}_{\gamma\gamma}\right)}{2\mathcal{R}e\left(\mathcal{M}_Z^{(\text{PV})*} \mathcal{M}_\gamma\right)}, \quad (94)$$

$$\delta_{\gamma(Z\gamma)} = \frac{2\mathcal{R}e\left(\mathcal{M}_\gamma^* \mathcal{M}_{\gamma Z}^{(\text{PV})} + \mathcal{M}_\gamma^* \mathcal{M}_{Z\gamma}^{(\text{PV})}\right)}{2\mathcal{R}e\left(\mathcal{M}_\gamma^* \mathcal{M}_Z^{(\text{PV})}\right)}, \quad (95)$$

with the full PV asymmetry, including TBE corrections, given by

$$A_{\text{PV}} = (1 + \delta) A_{\text{PV}}^0 \equiv \left(\frac{1 + \delta_{Z(\gamma\gamma)} + \delta_{\gamma(Z\gamma)}}{1 + \delta_{\gamma(\gamma\gamma)}} \right) A_{\text{PV}}^0, \quad (96)$$

where A_{PV}^0 is the Born level asymmetry in Eq. (80). The electromagnetic TPE correction $\delta_{\gamma(\gamma\gamma)}$ from Eq. (35) is typically only a few percent [5, 6, 7], so that the full correction δ can be written approximately as

$$\delta \approx \delta_{Z(\gamma\gamma)} + \delta_{\gamma(Z\gamma)} - \delta_{\gamma(\gamma\gamma)}. \quad (97)$$

The amplitudes $\mathcal{M}_{\gamma\gamma}$, $\mathcal{M}_{\gamma Z}$ and $\mathcal{M}_{Z\gamma}$ contain contributions from both nucleon elastic and inelastic intermediate states. At forward scattering angles the contributions from the high-mass inelastic continuum can be described with the help of dispersion relations, discussed in Sec. 7.3 below. For non-forward angles, the elastic and inelastic terms must be computed directly, along the lines of the $\gamma\gamma$ corrections in Sec. 4.

7.2.1 Nucleon elastic contributions

The calculation of the γZ correction with a nucleon intermediate state to the $\vec{e}p \rightarrow ep$ cross section, where the incident electron is polarized with helicity h , mirrors that of the $\gamma\gamma$ amplitude $\mathcal{M}_{\gamma\gamma}$ in Eq. (30), with the replacement of the γNN vertex function Γ_γ^μ by Γ_Z^μ in Eq. (77) [83, 88, 169],

$$\mathcal{M}_{\gamma Z}^N = -i e^2 \left(\frac{G_F}{\sqrt{2}} \right) M_Z^2 \int \frac{d^4 q_1}{(2\pi)^4} L_{\mu\nu}^{\gamma Z} H_{(\gamma Z)N}^{\mu\nu} \Delta_F(q_1, h) \Delta_F(q_2, M_Z). \quad (98)$$

Here the leptonic tensor $L_{\mu\nu}^{\gamma Z}$ for the box diagram is given by

$$L_{\mu\nu}^{\gamma Z} = \bar{u}_e(k', h) (g_V^e \gamma_\mu - g_A^e \gamma_\mu \gamma_5) S_F(k - q_1, m_e) \gamma_\nu u_e(k, h). \quad (99)$$

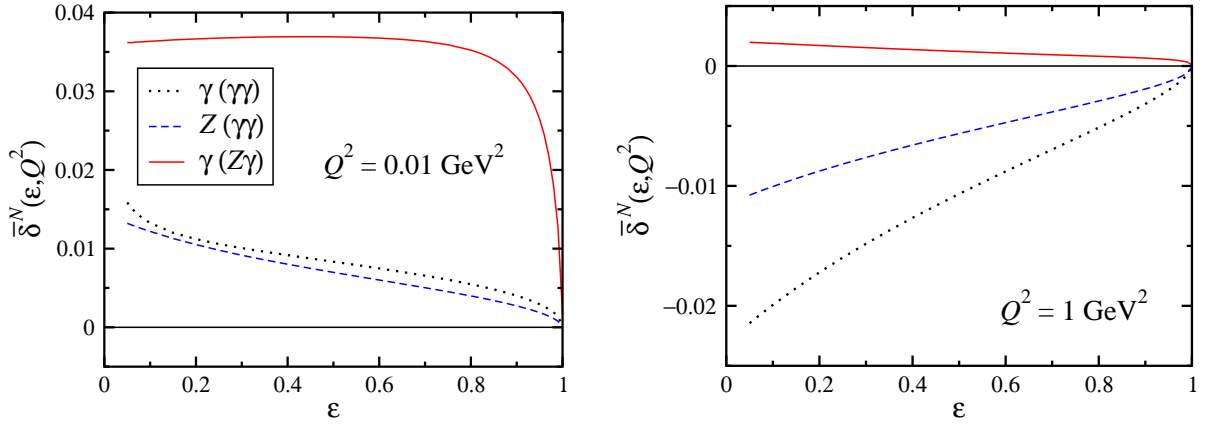


Figure 37: TBE corrections with nucleon intermediate states, for the $\gamma(\gamma\gamma)$ (dotted), $Z(\gamma\gamma)$ (dashed) and $\gamma(Z\gamma)$ (solid) contributions at $Q^2 = 0.01$ (left) and 1 GeV^2 (right). The finite part of the correction is defined with respect to the Mo-Tsai IR contribution, $\bar{\delta}^N = \delta^N - \delta_{\text{IR}}(\text{MoT})$ [37, 38]. The $\gamma(\gamma\gamma)$ correction enters with the opposite sign in the asymmetry, Eq. (97). Figure adapted from Ref. [83].

The hadronic γZ interference tensor $H_{(\gamma Z)N}^{\mu\nu}$ for the nucleon elastic intermediate state is given by

$$H_{(\gamma Z)N}^{\mu\nu} = \bar{u}_N(p') \Gamma_Z^\mu(q_2) S_F(p + q_1, M) \Gamma_\gamma^\nu(q_1) u_N(p). \quad (100)$$

Similar expressions hold for the conjugate amplitude $\mathcal{M}_{Z\gamma}^N$. Only the PV parts of the amplitudes $\mathcal{M}_{Z\gamma}^N$ and $\mathcal{M}_{\gamma Z}^N$ contribute to the PV asymmetry A_{PV} .

While the electromagnetic nucleon form factors used in the γNN vertex functions are relatively well constrained by data, for the weak ZNN vertex the form factors are generally less well determined. For the weak vector current, the form factors can be directly related to the γNN form factors through the conservation of the vector current (CVC). The axial-vector current, on the other hand, is not conserved, however, some constraints on the axial form factor have been obtained from elastic neutrino scattering data. Using a dipole fit, $G_A^{Zp}(Q^2) = -g_A/(1 + Q^2/\Lambda_{N(A)}^2)^2$, one finds that the mass parameter $\Lambda_{N(A)}^2 \approx 1 \text{ GeV}$. Since one of the main purposes of the PV experiments is to extract strange contributions to form factors by comparing the measured asymmetry with the predicted zero-strangeness asymmetry, in the computation of the TBE corrections one can set the strange form factors to zero, $F_{1,2}^s = 0 = G_A^s$.

The contributions from the nucleon intermediate states to the TBE correction δ^N are illustrated in Fig. 37 as a function of ε for $Q^2 = 0.01$ and 1 GeV^2 . At low Q^2 the $\gamma(\gamma\gamma)$ and $Z(\gamma\gamma)$ contributions are very similar, and therefore partially cancel in the asymmetry A_{PV} . Consequently the asymmetry is determined mostly by the $\gamma(Z\gamma)$ component. At larger Q^2 ($\gtrsim 1 \text{ GeV}^2$) the $\gamma(Z\gamma)$ component decreases in magnitude, while the $\gamma(\gamma\gamma)$ and $Z(\gamma\gamma)$ pieces become large and more negative [5, 6, 83]. The dependence of the total correction δ^N on the input form factors was found [6, 83] to be very weak for all ε , and only becomes appreciable at large Q^2 ($Q^2 \gtrsim 1 \text{ GeV}^2$). The correction at $Q^2 = 0.01 \text{ GeV}^2$ also appears relatively flat over the range $0.1 \lesssim \varepsilon \lesssim 0.8$, before dropping rapidly as $\varepsilon \rightarrow 1$. At large Q^2 the total TBE correction becomes more strongly ε dependent, decreasing in magnitude at forward scattering angles but increasing at backward angles ($\varepsilon \rightarrow 0$).

7.2.2 Δ intermediate states

Contributions to TBE amplitudes from the excitation of the $\Delta(1232)$ resonance were recently considered by Tjon *et al.* [83] and Nagata *et al.* [170]. Evaluation of the relevant TBE amplitudes follows that of

the electromagnetic contribution in Sec. 4.4.1, extending the formalism of Kondratyuk *et al.* [7] to the weak sector.

For the $ZN\Delta$ vertex both vector and axial-vector contributions enter. The vector transitions are required by CVC to have the same form as the $\gamma N\Delta$ in Eq. (38),

$$\begin{aligned} \Gamma_{ZN\rightarrow\Delta}^{\alpha\mu(V)}(p_\Delta, q) &= \frac{1}{2M_\Delta^2} \sqrt{\frac{2}{3}} \left\{ g_1^V(Q^2) [g^{\alpha\mu} \not{q} \not{p}_\Delta - \not{q} \gamma^\alpha p_\Delta^\mu - \gamma^\alpha \gamma^\mu q \cdot p_\Delta + \not{p}_\Delta \gamma^\mu q^\alpha] \right. \\ &\quad \left. + g_2^V(Q^2) [q^\alpha p_\Delta^\mu - g^{\alpha\mu} q \cdot p_\Delta] + \frac{g_3^V(Q^2)}{M_\Delta} [q^2 (\gamma^\alpha p_\Delta^\mu - g^{\alpha\mu} \not{p}_\Delta) + q^\mu (q^\alpha \not{p}_\Delta - \gamma^\alpha q \cdot p_\Delta)] \right\} \gamma_5, \end{aligned} \quad (101)$$

where again the factor $\sqrt{2/3}$ is associated with the $N \rightarrow \Delta$ weak isospin transition. Using CVC and isospin symmetry, the vector $ZN\Delta$ form factors can be related to the $\gamma N\Delta$ form factors by [83]

$$g_i^V(Q^2) = 2(1 - 2 \sin^2 \theta_W) g_i(Q^2), \quad i = 1, 2, 3 \quad (102)$$

where the Q^2 dependence of the electromagnetic $\gamma N\Delta$ form factor is parametrized as in Sec. 4.4.1.

For the axial-vector vertex, nonconservation of the axial-vector current implies the existence of an addition form factor. One can use the partially conserved axial current (PCAC) hypothesis to relate two of the form factors, leaving a similar expression to that in Eq. (101),

$$\begin{aligned} \Gamma_{ZN\rightarrow\Delta}^{\alpha\mu(A)}(p_\Delta, q) &= \frac{1}{2M_\Delta^2} \sqrt{\frac{2}{3}} \left\{ g_1^A(Q^2) [g^{\alpha\mu} \not{q} \not{p}_\Delta - \not{q} \gamma^\alpha p_\Delta^\mu - \gamma^\alpha \gamma^\mu q \cdot p_\Delta + \not{p}_\Delta \gamma^\mu q^\alpha] \right. \\ &\quad \left. + g_2^A(Q^2) [q^\alpha p_\Delta^\mu - g^{\alpha\mu} q \cdot p_\Delta] + \frac{g_3^A(Q^2)}{M_\Delta} [q^2 (\gamma^\alpha p_\Delta^\mu - g^{\alpha\mu} \not{p}_\Delta) + q^\mu (q^\alpha \not{p}_\Delta - \gamma^\alpha q \cdot p_\Delta)] \right\}. \end{aligned} \quad (103)$$

Note that here the weak isospin transition factor has been absorbed into the definition of the couplings [177, 178].

The axial form factors are less well determined, but some constraints have been extracted from analysis of ν scattering data. In a recent analysis, Lalakulich *et al.* [177, 178] parametrized the $\nu N \rightarrow \mu \Delta$ cross sections from bubble chamber experiments at low Q^2 in terms of phenomenological form factors. The available data can be described by the form factors [83, 178, 179] $g_1^A(Q^2) = 0$, $g_2^A(Q^2) = (Q^2/4M^2) g_3^A(Q^2)$, with the couplings at $Q^2 = 0$ determined in Ref. [178], and the Q^2 dependence given by a dipole form having a cut-off mass of $\Lambda_{\Delta(A)} = 1.0$ GeV. Note that Ref. [170] uses a different basis of form factors than in Eqs. (101) and (103); for the relation between these see [83]. As for the electromagnetic case, the vertex with an incoming Δ can be obtained from Eq. (39).

The γZ interference amplitude for the box diagram with a Δ intermediate state can then be written [83, 170]

$$\mathcal{M}_{\gamma Z}^\Delta = -i e^2 \left(\frac{G_F}{\sqrt{2}} \right) M_Z^2 \int \frac{d^4 q_1}{(2\pi)^4} L_{\mu\nu}^{\gamma Z} H_{(\gamma Z)\Delta}^{\mu\nu} \Delta_F(q_1, 0) \Delta_F(q_2, M_Z), \quad (104)$$

where the leptonic tensor $L_{\mu\nu}^{\gamma Z}$ is the same as in Eq. (99). The hadronic interference tensor $H_{(\gamma Z)\Delta}^{\mu\nu}$ for the Δ intermediate state is now

$$H_{(\gamma Z)\Delta}^{\mu\nu} = \bar{u}_N(p') \Gamma_{\Delta\rightarrow ZN}^{\mu\alpha} (p + q_1, -q_2) S_{\alpha\beta} (p + q_1, M_\Delta) \Gamma_{\gamma N\rightarrow\Delta}^{\beta\nu} (p + q_1, q_1) u_N(p), \quad (105)$$

where $\Gamma_{\Delta\rightarrow ZN}^{\mu\alpha}$ is the sum of the vector and axial-vector vertices. The corresponding amplitude $\mathcal{M}_{\gamma Z}^\Delta$ can be derived in a similar manner.

The total TBE contribution from Δ intermediate states, relative to the Mo-Tsai IR result [37, 38], is shown in Fig. 38 as a function of ε for $Q^2 = 0.01$ and 0.1 GeV². At low Q^2 values the Δ contribution is dominated by the $\gamma(Z\gamma)$ term. The negligible $\gamma\gamma$ interference with the Born γ or Z exchange reflects

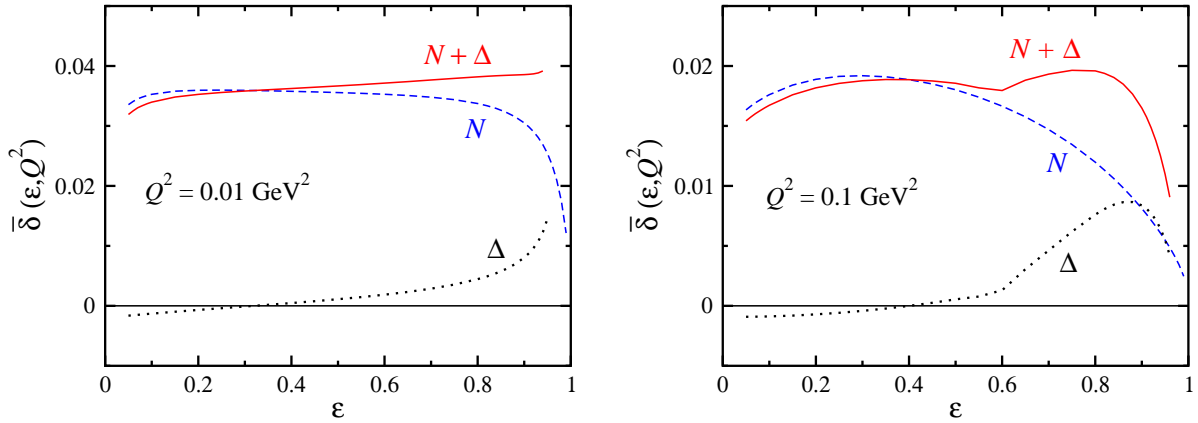


Figure 38: Total finite parts of the TBE corrections $\bar{\delta}$, relative to the Mo-Tsai contribution [37, 38], with nucleon (dashed) and Δ (dotted) intermediate states, as well as the sum (solid), at $Q^2 = 0.01 \text{ GeV}^2$ (left) and 0.1 GeV^2 (right). Figure adapted from Ref. [83].

the vanishing of the two-photon exchange correction in the $Q^2 \rightarrow 0$ limit. For comparison we also show in Fig. 38 the nucleon elastic contribution, and the sum of the nucleon and Δ terms. The Δ correction is strongly suppressed at low ε , but grows with increasing ε , becoming as important as the nucleon elastic part near the forward limit, $\varepsilon \rightarrow 1$. It is interesting to contrast this with the role of the Δ in TPE corrections to electromagnetic scattering discussed in Sec. 4.4.1, where the Δ contribution was negligible at forward angles but becomes important at backward angles, where it magnetic scattering is dominant.

The increased magnitude of the Δ contribution to PVES at forward angles reflects the growth of the invariant center of mass energy for fixed Q^2 as $\varepsilon \rightarrow 1$ [83, 170] — since the Δ intermediate state amplitudes $\mathcal{M}_{\gamma\gamma}^\Delta$ and $\mathcal{M}_{\gamma Z}^\Delta$ have numerators with higher powers of loop momenta than the corresponding nucleon amplitudes, δ^Δ will grow faster with invariant energy than δ^N . One method to ensure consistency with the physical bounds at asymptotically high energy requires is to use so-called “sideways” form factors, which depend on the center of mass energy as well as on the mass of the virtual boson. Alternatively, a dispersive approach, where the intermediate states are on-shell, may be adopted, such as that at forward angles discussed in Sec. 7.3. In the absence of a detailed analysis of the high-energy behavior of the higher-mass contributions, the predictions of the Δ calculation should not be taken too literally at very large $\varepsilon \sim 1$.

7.2.3 Effects on the strange form factors

While the TBE contributions to the parity-violating asymmetry in elastic ep scattering are relatively small, there are two ways in which the impact on the measurements can be enhanced. Although the asymmetry does not have large corrections, these measurements are typically looking for contributions from strange quarks which are seen through very small deviations from the asymmetry expected in the absence of strange quarks. A few-percent correction to A_{PV} will therefore be significant if the contribution from strange quarks is at the level of 5 – 10%. In addition, the corrections discussed in the previous section show the difference between the Born prediction for A_{PV} and the value including TBE contributions, assuming that one is starting from the correct electromagnetic form factors. There is an additional effect for measurements which used proton form factors extracted without accounting for TPE corrections in determining the value of A_{PV} for the case with no strange quark contributions.

In Ref. [119], the impact of TPE on the electromagnetic form factors and the TPE corrections to the parity-violating asymmetry were examined, but γZ box contributions were not included. The

direct TPE contributions to the asymmetry were found to be $\lesssim 1\%$ for $Q^2 \leq 3 \text{ GeV}^2$, and smallest at large ε , where the highest precision measurements were planned. However, the impact of using proton form factors that did not have TPE corrections applied was found to be much larger, well over 5% at 3 GeV^2 , with the largest corrections in high- ε region where high precision measurements were planned. A prescription was given that allowed for approximate corrections to be applied, without explicit inclusion of the TPE corrections. But because this estimate did not include the γZ contributions and the TPE-corrected form factors can now be reliably extracted, this procedure is now relevant mainly if looking at previous extractions of the strangeness contribution based on TPE-uncorrected form factors.

The full effects of the TBE corrections (two-photon and γZ exchange) on the A_{PV} asymmetry at kinematics corresponding to experiments [152, 153, 154, 155, 156, 157, 158, 159, 160, 161] designed to measure the strange quark form factors of the nucleon were considered in Refs. [83, 88, 169, 170]. For the forward angle HAPPEX [152] and G0 [156] measurements, the nucleon correction δ^N was found to be in the vicinity of $\sim 0.1 - 0.2\%$, increasing to $\sim 1.0 - 1.5\%$ for the backward angle G0 [157] and the earlier SAMPLE [158] measurements. In contrast, the Δ contribution δ^Δ is almost negligible at backward angles, but becomes more important at forward angles, where as discussed above its evaluation is more questionable.

The impact of these corrections on the strange form factors is difficult to gauge without performing a full reanalysis of the data, since in general different electroweak parameters and form factors are used in the various experiments. Nevertheless, following Zhou *et al.* [169] attempts have been made [8, 88, 170] to quantify the effect from the TBE corrections on the combination $G_E^s + \beta G_M^s$ measured in the PV experiments, where β depends on the kinematics of a particular experiment. Zhou *et al.* assume the experimental asymmetry $A_{\text{PV}}^{\text{exp}}$ can be written as [169]

$$A_{\text{PV}}^{\text{exp}}(\rho, \kappa) = A_{\text{PV}}^0(\rho', \kappa')(1 + \delta^N + \delta^\Delta), \quad (106)$$

where A_{PV}^0 is the Born asymmetry (80), and $\rho' = \rho - \Delta\rho$ and $\kappa' = \kappa - \Delta\kappa$ remove the existing (hadron structure-independent) two-boson exchange corrections contained in ρ and κ [164, 165]. From the calculated TBE corrections one can then determine A_{PV}^0 and extract the strange asymmetry A_s (86). Defining the relative correction δ_G to the strange form factors by $\overline{G}_E^s + \beta \overline{G}_M^s = (G_E^s + \beta G_M^s)(1 + \delta_G)$, where $\overline{G}_{E,M}^s$ is extracted from the experimental asymmetry and $G_{E,M}^s$ is obtained from the Born asymmetry, one has [169]

$$\delta_G = \frac{1}{A_{\text{PV}}^{\text{exp}} - A_V - A_A} \left\{ A_{\text{PV}}^{\text{exp}} \left(\frac{\Delta\rho}{\rho} - \delta \right) + \frac{G_F Q^2}{2\sqrt{2}\pi\alpha} \rho \sin^2 \theta_W \Delta\kappa - A_A \frac{\Delta\rho}{\rho} \right\}. \quad (107)$$

Because the magnitude of the strange form factors is generally rather small [176, 180], dividing by the strange asymmetry in Eq. (107) can give a quite large relative correction δ_G . The size of the correction was found to be typically within 10–20% for most PV experiments [88].

The model dependence of these corrections was explored in Ref. [8], where an estimate was made of the induced difference in the strange asymmetry extracted using various input electroweak form factors. Comparing results with empirical [118] and monopole form factors (as used in Ref. [169]), the effects ranged from around 15% for the HAPPEX kinematics [152, 155] to over 30% for the PVA4 kinematics [159]. One should caution, however, that these values are indicative only, and a more detailed reanalysis of the strange form factor data including TBE effects *a priori* would be needed to reach more robust conclusions.

In addition, the fractional contributions may not reflect the importance of the corrections because the strange quark contributions are related to the difference between the measured asymmetry and the expected asymmetry in the absence of strange quark contributions. Thus, a large fractional correction could simply indicate that the strangeness contribution is extremely small. It may therefore be more useful to compare the size of the TBE corrections to the uncertainty in the A_{PV} measurements.

A preliminary attempt at incorporating TBE corrections in a global strange form factors analysis was made recently by Young [181]. Using PV scattering data below $Q^2 = 0.3 \text{ GeV}^2$ the TBE corrections in the proton were found to modify the strange electric and magnetic form factors by

$$G_E^s = 0.0025(182) \longrightarrow 0.0023(182), \quad G_M^s = -0.011(254) \longrightarrow -0.020(254), \quad (108)$$

at a scale $Q^2 = 0.1 \text{ GeV}^2$. The effect on the strange magnetic form factor is an almost factor two increase in the magnitude; while significant, this is still well within the current experimental uncertainty. The shift in the strange electric form factor is somewhat smaller. This is mostly because the G_E^s form factor is determined largely by the ^4He data, and the TBE effects here have not yet been computed. Overall, though, the conclusion appears to be that TBE effects provide relatively mild corrections to strange quark form factors. On the other hand, a significantly larger effect from TBE has been found in nearly forward PV electron scattering at very low Q^2 , which we discuss next.

7.3 γZ corrections to the proton weak charge

In parallel with the discussion of Sec. 4.7, we consider the forward scattering limit, where $k' = k - q$, with $t = q^2$ kept small but finite. The parity-violating proton asymmetry in Eq. (83) is related to the weak charge of the proton Q_W^p [168],

$$A_{\text{PV}} \rightarrow \frac{G_F}{4\pi\alpha\sqrt{2}} t Q_W^p. \quad (109)$$

Including electroweak radiative corrections, the proton weak charge is defined at zero energy and momentum transfer as [182]

$$Q_W^p = (1 + \Delta\rho + \Delta_e)(1 - 4\sin^2\theta_W(0) + \Delta'_e) + \square_{WW} + \square_{ZZ} + \square_{\gamma Z}(0), \quad (110)$$

where $\sin^2\theta_W(0) = 0.23867(16)$ is the weak mixing angle at zero momentum, and the corrections $\Delta\rho$, Δ_e and Δ'_e are given in Ref. [182]. The contributions \square_{WW} and \square_{ZZ} from the WW and ZZ box and crossed-box diagrams can be computed perturbatively, while the γZ interference correction $\square_{\gamma Z}(E)$ in addition depends on physics at long distance scales [168, 164, 165, 182, 183]. The current best theoretical estimate from Ref. [183] is $Q_W^p = 0.0713(8)$. An explicit energy-dependence is shown for $\square_{\gamma Z}(E)$ in Eq. (110), in anticipation of a significant variation of this quantity for electron scattering in the GeV range. The other radiative corrections in Eq. (110) are not expected to show such a dependence.

Note that the absolute correction $\square_{\gamma Z}$ to the proton weak charge is related to the relative correction $\delta_{\gamma Z}$ in Eq. (95) by

$$\square_{\gamma Z}(0) \equiv Q_W^p \delta_{\gamma Z} = Q_W^p \frac{\text{Re} \left(\mathcal{M}_\gamma^* \left[\mathcal{M}_{\gamma Z}^{(\text{PV})} + \mathcal{M}_{Z\gamma}^{(\text{PV})} \right] \right)}{\text{Re} \left(\mathcal{M}_\gamma^* \mathcal{M}_Z^{(\text{PV})} \right)}. \quad (111)$$

Corrections from the interference of $\mathcal{M}_Z^{(\text{PV})}$ with the TPE amplitude under the replacement $\mathcal{M}_\gamma \rightarrow \mathcal{M}_\gamma + \mathcal{M}_{\gamma\gamma}$ (namely, $\delta_{Z(\gamma\gamma)}$ in Eq. (95)) vanish in the forward limit, and therefore do not affect the asymmetry.

A precise determination of the proton weak charge Q_W^p can provide an important test of the Standard Model through verification of the predicted running of the weak mixing angle from the Z boson pole to low energies [183]. The Q_{weak} experiment at Jefferson Lab [162], which will complete data taking in 2012, was designed to measure Q_W^p to a higher level of precision than previously possible. In combination with constraints from atomic parity violation [184], the Q_{weak} measurement aims to either discover evidence

for new physics beyond the Standard Model that leads to parity violation in electron scattering, or raise the limit on its mass scale to above 2 TeV, complementing direct searches at the LHC [183, 185].

As discussed above, the γZ correction in general has contributions from the vector electron–axial vector hadron coupling of the Z boson ($\square_{\gamma Z}^A$) and from the axial electron–vector hadron coupling of the Z ($\square_{\gamma Z}^V$), $\square_{\gamma Z} = \square_{\gamma Z}^A + \square_{\gamma Z}^V$. The vector hadron contribution $\square_{\gamma Z}^V$ vanishes in the limit of zero energy, but is finite at $E > 0$. The axial hadron correction $\square_{\gamma Z}^A$, which is dominant at very low electron energies relevant to atomic parity-violation experiments, was estimated some time ago by Marciano and Sirlin [164, 165] in terms of a free quark model-inspired loop calculation.

At forward angles, the correction $\square_{\gamma Z}$ can be computed from its imaginary part using standard forward dispersion relations analogous to Eq. (53) [171],

$$\mathcal{R}e \square_{\gamma Z}(E) = \frac{1}{\pi} \mathcal{P} \int_{-\infty}^{\infty} dE' \frac{\mathcal{I}m \square_{\gamma Z}(E')}{E' - E}. \quad (112)$$

The imaginary part of $\square_{\gamma Z}$ depends on the PV $ep \rightarrow eX$ cross section, which can be expressed in terms of interference electroweak structure functions. The integration over negative energies in Eq. (112) corresponds to the crossed γZ box diagram, and can be related to the box diagram using the crossing symmetry properties of the γZ amplitudes in Eq. (92) and (93). For the vector hadron and axial hadron loop corrections one has, in analogy with Eq. (54),

$$\mathcal{R}e \square_{\gamma Z}^V(E) = \frac{2E}{\pi} \mathcal{P} \int_0^{\infty} dE' \frac{1}{E'^2 - E^2} \mathcal{I}m \square_{\gamma Z}^V(E'), \quad (113)$$

$$\mathcal{R}e \square_{\gamma Z}^A(E) = \frac{2}{\pi} \mathcal{P} \int_0^{\infty} dE' \frac{E'}{E'^2 - E^2} \mathcal{I}m \square_{\gamma Z}^A(E'). \quad (114)$$

It is evident from Eq. (113) that at zero energy the vector hadron correction vanishes, $\mathcal{R}e \square_{\gamma Z}^V(0) = 0$.

From the optical theorem, the imaginary part of PV γZ exchange amplitude can be written in terms of the cross section for all possible final hadronic states,

$$2 \mathcal{I}m \left(\mathcal{M}_{\gamma Z}^{(\text{PV})} + \mathcal{M}_{Z\gamma}^{(\text{PV})} \right) = 4\pi M e^2 \left(\frac{-2G_F}{\sqrt{2}} \right) \int \frac{d^3l}{(2\pi)^3 2E_l} \left(\frac{1}{Q_1^2} \right) \frac{1}{1 + Q_1^2/M_Z^2} L_{\mu\nu}^{\gamma Z} W_{\gamma Z}^{\mu\nu}, \quad (115)$$

where $l = k - q_1$, $E_l = \sqrt{(\mathbf{k} - \mathbf{q}_1)^2 + m_e^2}$, and $Q_1^2 = -q_1^2$. The γZ interference hadronic tensor can be parametrized in terms of three interference electroweak structure functions,

$$MW_{\gamma Z}^{\mu\nu} = -g^{\mu\nu} F_1^{\gamma Z} + \frac{p^\mu p^\nu}{p \cdot q_1} F_2^{\gamma Z} - i\varepsilon^{\mu\nu\lambda\rho} \frac{p_\lambda q_{1\rho}}{2p \cdot q_1} F_3^{\gamma Z}. \quad (116)$$

The structure functions $F_{1,2}^{\gamma Z}$ are analogous to the electromagnetic structure functions in Eq. (51) and contribute to the vector hadron correction $\square_{\gamma Z}^V$, while the $F_3^{\gamma Z}$ structure function contributes to the axial hadron correction $\square_{\gamma Z}^A$. They are in general functions of the exchanged boson virtuality Q_1^2 and of the invariant mass W of the exchanged boson and proton, or alternatively of the Bjorken variable $x = Q_1^2/(W^2 - M^2 + Q_1^2)$.

In analogy with Eq. (52), the imaginary parts of the vector hadron and axial hadron contributions to the γZ box diagrams can be written [171, 173, 186, 187, 188]

$$\mathcal{I}m \square_{\gamma Z}^V(E) = \frac{\alpha}{(2ME)^2} \int_{M^2}^s dW^2 \int_0^{Q_{1,\text{max}}^2} \frac{dQ_1^2}{1 + Q_1^2/M_Z^2} \left[F_1^{\gamma Z} + \frac{s(Q_{1,\text{max}}^2 - Q_1^2)}{Q_1^2(W^2 - M^2 + Q_1^2)} F_2^{\gamma Z} \right], \quad (117)$$

$$\mathcal{I}m \square_{\gamma Z}^A(E) = \hat{v}_e \frac{\alpha}{(2ME)^2} \int_{M^2}^s dW^2 \int_0^{Q_{1,\text{max}}^2} \frac{dQ_1^2}{1 + Q_1^2/M_Z^2} \left[\frac{2ME}{W^2 - M^2 + Q_1^2} - \frac{1}{2} \right] F_3^{\gamma Z}, \quad (118)$$

where $\hat{v}_e \equiv (1 - 4\hat{s}^2)$, with $\hat{s}^2 \equiv \sin^2 \theta_W(M_Z^2) = 0.23116(13)$ in the $\overline{\text{MS}}$ scheme [167]. Note that the corresponding expressions for $\square_{\gamma Z}^V$ in Refs. [171, 172] are a factor 2 smaller than that in Eq. (117); the correct expression is used in Ref. [173]. The expression for $W_{\gamma Z}^{\mu\nu}$ in Refs. [171, 173] also differs by a factor 2 for the $F_3^{\gamma Z}$ term from that in Eq. (116), although the results for $\square_{\gamma Z}^A$ agree with that in Eq. (118).

In evaluating the imaginary parts of $\square_{\gamma Z}^{V,A}$ it is convenient to split the integration into three regions: (i) elastic with $W^2 = M^2$; (ii) resonance with $(M + m_\pi)^2 \leq W^2 \lesssim 4 \text{ GeV}^2$; and (iii) deep inelastic scattering (DIS) region, with $W^2 > 4 \text{ GeV}^2$. The elastic contributions, including both the γZ and $Z\gamma$ orderings, can be written in terms of the elastic electroweak form factors defined in Sec. 7.1,

$$F_1^{\gamma Z(\text{el})}(W^2, Q_1^2) = 2M^2\tau G_M^{\gamma p} \delta(W^2 - M^2), \quad (119)$$

$$F_2^{\gamma Z(\text{el})}(W^2, Q_1^2) = \frac{4M^2\tau}{1+\tau} \left(G_E^{\gamma p} G_E^{Zp} + \tau G_M^{\gamma p} G_M^{Zp} \right) \delta(W^2 - M^2), \quad (120)$$

$$F_3^{\gamma Z(\text{el})}(W^2, Q_1^2) = -4M^2\tau G_M^p G_A^Z \delta(W^2 - M^2), \quad (121)$$

where here $\tau = Q_1^2/4M^2$. Note that with dipole parameterizations of form factors the integrals (113), (114), (117) and (118) can be performed analytically, providing a useful cross-check of the numerical calculations. One can verify that the results in fact coincide exactly with the direct loop calculations [8, 169] of the γZ corrections in Sec. 7.2.1, which do not use dispersion relations, and in which the intermediate nucleon is off-shell. The result for $\mathcal{R}e \square_{\gamma Z}^A(E)$ also agrees at $E = 0$ with the classic calculation of Marciano and Sirlin [164], if the parameters are adjusted to correspond to those of Ref. [164]. At zero energy one has $\mathcal{R}e \square_{\gamma Z}^{A(\text{el})}(0) = 0.0126 \hat{v}_e$, and at the Q_{weak} energy $\mathcal{R}e \square_{\gamma Z}^{A(\text{el})}(1.165 \text{ GeV}) = 0.0009 \hat{v}_e$ [188].³

In the nucleon resonance region, while there is an abundance of electroproduction data, there are no direct measurements of the interference structure functions $F_{1,2,3}^{\gamma Z}$. For vector transitions to isospin $I = 3/2$ states, such as the $\Delta(1232)$ resonance, conservation of the vector current and isospin symmetry require the weak isovector transition form factors to be equal to the electromagnetic ones multiplied by $(1 + Q_W^p)$. For isospin $I = 1/2$ resonances, which contain contributions from isovector and isoscalar currents, using SU(6) quark model wave functions one can verify that for the most prominent $I = 1/2$ states the magnitudes of the Z -boson transition couplings are equal to the respective photon couplings to within a few percent [173, 186]. Estimates of the resonance region contribution to the box diagram, $\square_{\gamma Z}^{V(\text{res})}$, have been made recently [171, 173, 186, 187] by parameterizing resonance region structure function data from SLAC, Jefferson Lab and elsewhere in terms of resonant and nonresonant background components [186, 189]. The model dependence of relating the vector γZ resonance structure functions to the electromagnetic structure functions has been studied in Ref. [173].

For the axial-vector resonance contributions, $\square_{\gamma Z}^{A(\text{res})}$, one can use parameterizations of the transition form factors in neutrino scattering from Lalakulich *et al.* [177, 178], with modified isospin factors appropriate to γZ . These form factors have been fit to the Jefferson Lab pion electroproduction data (vector part) and pion production data in ν and $\bar{\nu}$ scattering at ANL, BNL and Serpukhov (axial-vector part) up to $Q_1^2 = 3.5 \text{ GeV}^2$. At larger Q_1^2 the resonance contributions are suppressed by the Q_1^2 dependence of the transition form factors, which is stronger for the dominant $\Delta(1232)$ resonance than for the higher-mass resonances [178]. The resulting resonance contribution $\square_{\gamma Z}^{A(\text{res})}(0) = 0.0044 \hat{v}_e$ is smaller than the elastic term at $E = 0$, but decreases less rapidly with increasing energy. At the Q_{weak} energy, Blunden *et al.* find [188] $\square_{\gamma Z}^{A(\text{res})}(1.165 \text{ GeV}) = 0.0022 \hat{v}_e$.

The contributions from high W can be computed by analyzing the high- Q_1^2 ($Q_1^2 > Q_0^2$) and low- Q_1^2 ($Q_1^2 < Q_0^2$) regions separately, with Q_0^2 taken to be $\approx 1 \text{ GeV}^2$. Structure functions in the high- W , high- Q_1^2 region of deep-inelastic scattering can be related to leading twist parton distribution functions

³To simplify notation, in the following we denote $\mathcal{R}e \square_{\gamma Z}^{V,A}$ by $\square_{\gamma Z}^{V,A}$, since these are the quantities of interest for the observables.

(PDFs), and at leading order in α_s are given by

$$F_2^{\gamma Z(\text{DIS})} = x \sum_q 2 e_q g_V^q (q + \bar{q}) = 2x F_1^{\gamma Z(\text{DIS})}, \quad (122)$$

$$x F_3^{\gamma Z(\text{DIS})} = x \sum_q 2 e_q g_A^q (q - \bar{q}), \quad (123)$$

where q and \bar{q} are the quark and antiquark PDFs, and $g_V^u = 1/2 - (4/3)\sin^2\theta_W$ and $g_V^d = -1/2 + (2/3)\sin^2\theta_W$ are the weak vector charges for u and d quarks, respectively. Note that in the limit $2g_V^q \rightarrow e_q$ the interference structure functions $F_2^{\gamma Z(\text{DIS})} \rightarrow F_2^{\gamma(\text{DIS})}$, where

$$F_2^{\gamma(\text{DIS})} = x \sum_q e_q^2 (q + \bar{q}). \quad (124)$$

In the case of a free quark target one has $F_3^{\gamma Z} = (5/3)x\delta(1-x)$, which gives a contribution to the axial hadron γZ correction

$$\square_{\gamma Z}^{A(\text{free quark})} = \hat{v}_e \frac{5\alpha}{2\pi} \left(\ln \frac{M_Z^2}{m^2} + \frac{3}{2} \right), \quad (125)$$

where m is a hadronic mass scale. This reproduces the perturbative result in the free quark model of Ref. [164] at $E = 0$.

As observed in Ref. [171], for instance, for three quark flavors the sum over electroweak charges $\sum_q 2 e_q g_V^q = \frac{2}{3}(1 + Q_W^p) \approx \sum_q e_q^2$, so that in the high- W region dominated by sea quarks, the quark distributions are approximately flavor independent, in which case $F_{1,2}^{\gamma Z} \approx F_{1,2}^{\gamma}$. In addition, while the Callan-Gross relation between the F_1 and F_2 structure functions is assumed in Eq. (122) at high Q_1^2 , at finite Q_1^2 the contribution from F_1 is obtained from F_2 and the ratio $R_{LT} \equiv \sigma_L/\sigma_T = (1 + 4M^2x^2/Q_1^2)F_2/(2xF_1) - 1$ of the longitudinal and transverse cross sections [190].

One can simplify the expressions for $\square_{\gamma Z}^{V,A}$ in the DIS region by firstly interchanging the order of the integrations in Eqs. (113), (114) and (117), (118) to perform the integrals over the energy analytically [187, 188]. The resulting integrands can be expanded at high Q_1^2 and low E in powers of x^2/Q_1^2 , yielding a series whose coefficients are moments of structure functions [188],

$$\square_{\gamma Z}^{V(\text{DIS})}(E) = \frac{\alpha}{\pi} 2ME \int_{Q_0^2}^{\infty} \frac{dQ_1^2}{Q_1^4(1 + Q_1^2/M_Z^2)} \left[M_2^{(2)} + \frac{2}{3}M_1^{(2)} + \frac{2M^2}{3Q_1^4}(E^2 - Q_1^2)M_2^{(4)} + \frac{2M^2}{5Q_1^4}(4E^2 - 5Q_1^2)M_1^{(4)} + \dots \right], \quad (126)$$

$$\square_{\gamma Z}^{A(\text{DIS})}(E) = \hat{v}_e \frac{3\alpha}{2\pi} \int_{Q_0^2}^{\infty} \frac{dQ_1^2}{Q_1^2(1 + Q_1^2/M_Z^2)} \left[M_3^{(1)} + \frac{2M^2}{9Q_1^4}(5E^2 - 3Q_1^2)M_3^{(3)} + \dots \right]. \quad (127)$$

Here the moments of the structure functions are defined as

$$M_i^{(n)}(Q_1^2) \equiv \int_0^1 dx x^{n-2} \mathcal{F}_i^{\gamma Z}(x, Q_1^2), \quad i = 1, 2, 3, \quad (128)$$

where $\mathcal{F}_i^{\gamma Z} = \{x F_1^{\gamma Z}, F_2^{\gamma Z}, x F_3^{\gamma Z}\}$. Note that the upper limit x_{max} on the x -integrals in Eqs. (126) and (127) has been approximated by 1; the resulting error was found to be less than 10^{-4} for $Q_1^2 > 1 \text{ GeV}^2$ [188]. The large- x contributions to $M_i^{(n)}(Q_1^2)$ become more important for large n ; however, the higher moments are suppressed by increasing powers of $1/Q_1^2$. In practice, the integrals in Eqs. (126) and (127) are dominated by the lowest moments, with the $1/Q_1^2$ corrections being relatively small in DIS

kinematics. For the axial-vector hadron part, the lowest moment, $M_3^{(1)}(Q_1^2)$, is the γZ analog of the Gross–Llewellyn Smith (GLS) sum rule [191] for νN DIS, which at leading order counts the number of valence quarks in the nucleon. The corresponding quantity for γZ is $\sum_q 2e_q g_A^q = 5/3$, so that at next-to-leading order in the $\overline{\text{MS}}$ scheme

$$M_3^{(1)}(Q_1^2) = \frac{5}{3} \left(1 - \frac{\alpha_s(Q_1^2)}{\pi} \right). \quad (129)$$

The lowest moment contribution to Eq. (127) is therefore

$$\square_{\gamma Z}^{A(\overline{\text{MS}})}(0) \approx \hat{v}_e \frac{3\alpha}{2\pi} \int_{Q_0^2}^{\infty} dQ_1^2 \frac{M_3^{(1)}(Q_1^2)}{Q_1^2(1 + Q_1^2/M_Z^2)}, \quad (130)$$

which is identical to the Marciano-Sirlin result [164] for the high energy contribution to the box diagram.

For $Q_1^2 < Q_0^2$ a partonic description of the structure functions is not valid. In particular, since the integrals over Q_1^2 in Eqs. (117) and (118) extend down to $Q_1^2 = 0$, and the upper limit on the x -integral, x_{max} , is also limited by Q_1^2 , one requires the behavior of the structure functions in the limit of both low x and low Q_1^2 . In the case of the vector $F_2^{\gamma Z}$ structure function, conservation of the two vector currents requires $F_2^{\gamma Z} \sim Q_1^2$ as $Q_1^2 \rightarrow 0$. In computing the high- W contributions to $\square_{\gamma Z}^V$ several authors have used Regge inspired parameterizations [110, 192, 193] of the electromagnetic structure functions, and approximating $F_2^{\gamma Z} \approx F_2^\gamma$ at small x .

By contrast, $F_3^{\gamma Z}$ depends on both vector and axial-vector currents, so that no analogous current conservation constraint exists. In the absence of data on $F_3^{\gamma Z}$ in the low- x , low- Q_1^2 region, Blunden *et al.* considered models for its possible x and Q_1^2 dependence such that $F_3^{\gamma Z}$ at x_{max} should not diverge as $Q_1^2 \rightarrow 0$, and should match the partonic structure function at $Q_1^2 = Q_0^2$.

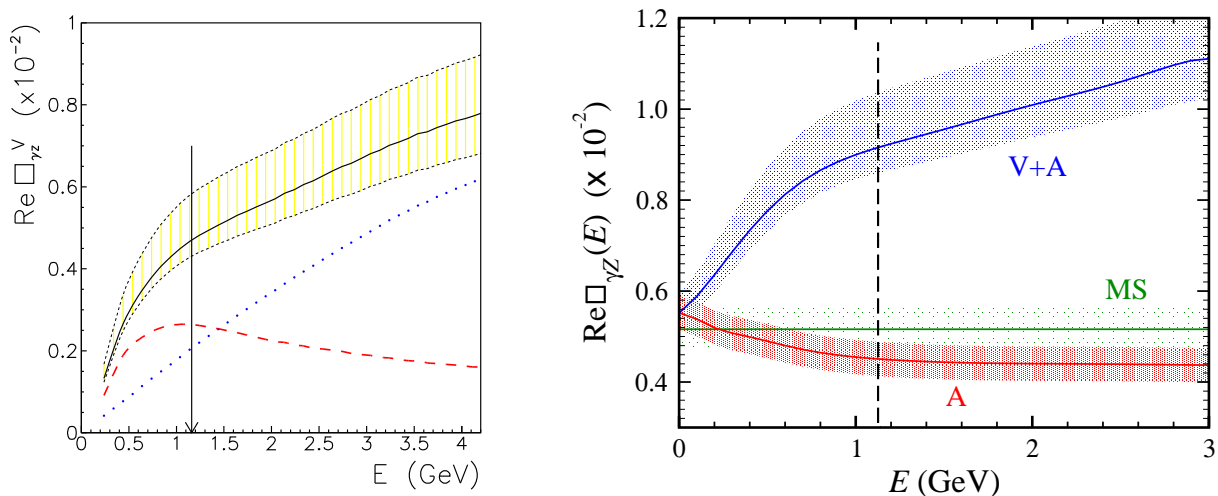


Figure 39: γZ box corrections to Q_W^p for the **(left)** vector hadron $\square_{\gamma Z}^V$ contribution showing the resonant (dashed) and nonresonant (dotted) components, and the sum (solid, and shaded); **(right)** axial hadron $\square_{\gamma Z}^A$ contribution (labeled “A”) together with the sum of axial and vector hadron corrections (“V+A”), and the $E = 0$ result from Ref. [164] (“MS”, extended to finite E). The vertical lines at $E = 1.165$ GeV indicate the energy of the Q_{weak} experiment. Figures taken from Refs. [186, 188].

The total vector and axial hadron corrections $\square_{\gamma Z}^{V,A}$ are shown in Fig. 39 as a function of the incident electron energy E . For the vector hadron correction $\square_{\gamma Z}^V$, Fig. 39 (left), most of the strength ($\sim 80\%$)

comes from relatively low energies, below 4 GeV, where the Q_1^2 range extends to $\sim 6 \text{ GeV}^2$, and W to $\sim 3 \text{ GeV}$. This coincides precisely with the region that a wealth of very accurate electroproduction data exists from Jefferson Lab [129, 194, 195, 196]. The nonresonant contribution to $\square_{\gamma Z}^V$ is small at low energies, but rises logarithmically with increasing E . The resonant part increases steeply to a maximum at $E \sim 1 \text{ GeV}$, before falling off like $1/E$ [171, 186]. Sibirtsev *et al.* find the resonant and nonresonant contributions to $\square_{\gamma Z}^V$ to be 0.0026 and 0.0021, respectively, at the energy relevant for the Q_{weak} experiment, $E = 1.165 \text{ GeV}$ (although one should note that this separation is somewhat arbitrary, as only the total cross section is physically meaningful). The correction to Q_W^p at the Q_{weak} energy is then $0.0047_{-0.0004}^{+0.0011}$, or $6.6_{-0.6}^{+1.5} \%$ of the Standard Model value $0.0713(8)$ for Q_W^p , with the error band obtained from the uncertainty in the fit parameters using a variational method [186].

Using different structure function inputs, Rislow and Carlson [187] find $\square_{\gamma Z}^V(1.165 \text{ GeV}) = 0.0057 \pm 0.0009$, which is slightly higher than but consistent with the value from Sibirtsev *et al.* [186]. Gorchtein *et al.* [173], on the other hand, find $\square_{\gamma Z}^V(1.165 \text{ GeV}) = 0.0054 \pm 0.0020$, which is again consistent with the other estimates but has a larger uncertainty due to the larger range of input structure functions considered there.

The axial hadron correction $\square_{\gamma Z}^A$ in Fig. 39 (right) is dominated by the DIS contribution, which has negligible E dependence. On the other hand, the resonance and low- Q^2 DIS contributions dominate the uncertainties. The total contribution to $\square_{\gamma Z}^A$ is $(0.073 \pm 0.005) \hat{v}_e$ at $E = 0$ and $(0.060 \pm 0.005) \hat{v}_e$ at $E = 1.165 \text{ GeV}$ [188]. This should be compared to the value $(0.068 \pm 0.006) \hat{v}_e$ used in Ref. [182], which is assumed to be energy-independent. Also shown in Fig. 39 is the total $\square_{\gamma Z}^V + \square_{\gamma Z}^A$ from Refs. [186, 188]. The combined result raises the theoretical estimate for Q_W^p to $0.0717(8)$, with a correction $\square_{\gamma Z}(E) - \square_{\gamma Z}(0)$ of $0.0037_{-0.0004}^{+0.0011}$ at the Q_{weak} kinematics.

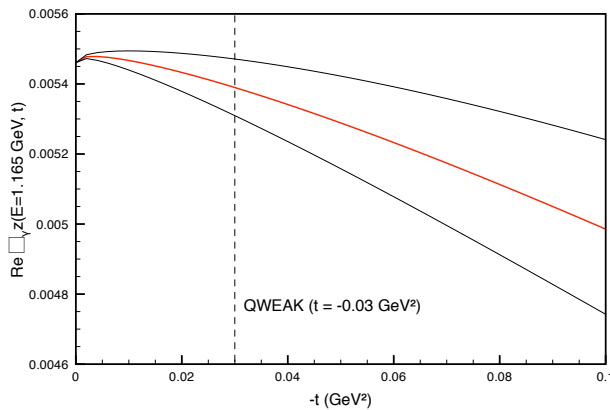


Figure 40: Dependence of the vector hadron correction $\square_{\gamma Z}^V$ on the momentum transfer squared t at the Q_{weak} energy $E = 1.165 \text{ GeV}$. The outer curves indicate the uncertainty. Figure taken from Ref. [173].

The t dependence of the γZ corrections, from the forward limit $-t \equiv Q^2 = 0$ to the Q_{weak} value of $-t = 0.03 \text{ GeV}^2$, was considered by Gorchtein *et al.* [171, 173] using the phenomenological *ansatz*

$$\square_{\gamma Z}(E, t) = \square_{\gamma Z}(E, 0) \frac{\exp(-B|t|/2)}{F_1^{\gamma p}(t)}, \quad (131)$$

where $F_1^{\gamma p}(t)$ is the Dirac proton form factor, and $B = (7 \pm 1) \text{ GeV}^{-2}$ is extracted from analysis of data forward Compton scattering data on ^4He nuclei [197]. Although the estimate is considered by the authors to be exploratory, it suggests that the dispersion correction decreases by only about 2% from its $t = 0$ value [173].

The corrections $\square_{\gamma Z}^{V,A}$ are important for the interpretation of the Q_{weak} experiment, given its projected uncertainty of ± 0.003 [162]. It is also critical to the physical interpretation of the experiment which is expected to constrain possible sources of parity violation from beyond the Standard Model at a mass scale of $\gtrsim 2$ TeV [185]. The uncertainties in the corrections can be reduced with future parity-violating structure function measurements at low Q^2 , such as those planned at Jefferson Lab [198, 199]. The high precision determination of Q_W^p would then allow more robust extraction of signals for new physics beyond the Standard Model.

8 Conclusions and outlook

The renewed interest in the role of two-photon exchange in electron–hadron scattering sprouted from the challenge to resolve a major discrepancy between new polarization transfer measurements of the proton’s electric to magnetic form factor ratio and earlier results using Rosenbluth separations of elastic cross sections, which has been confirmed now by several independent experiments. In the intervening decade since the first polarization transfer experiments were performed at Jefferson Lab, the study of TPE has flourished into an area rich in phenomenology, with many developments in experiment and theory which have significantly altered how we think about the basic process of electromagnetic scattering from hadrons. The most likely candidate that has emerged to explain the form factor discrepancy is two-photon exchange, in particular the hadron structure dependent parts of the $\gamma\gamma$ box and crossed-box diagrams neglected in the standard treatments of radiative corrections.

In this article we have reviewed the developments in the study of TPE over the past decade, focusing on the hadronic framework for radiative corrections applicable for most measurements extending into the $Q^2 \sim \text{few GeV}^2$ range. This period has witnessed major advances in theoretical calculations of TPE amplitudes, which we have outlined in this review, together with their implications for observables. We have surveyed the effects of TPE corrections on various elastic ep scattering observables, including Rosenbluth separations of cross sections, polarization measurements, and e^+p/e^-p ratios, as well as the Born-forbidden normal beam and target asymmetries. Two-photon effects also find their way into other observables, such as neutron form factors, resonance electroproduction, the pion form factor, and elastic electron–nucleus (deuteron and ^3He) cross sections, which we have summarized here. The theoretical advances in TPE computations have furthermore allowed for the first time the inclusion of TPE corrections *a priori* in a global fit of form factor data, which has recently been performed.

Extending the discussion into the weak sector, we reviewed the calculation of corrections to parity-violating elastic scattering cross sections and asymmetries from γZ interference diagrams. These turn out to have relatively minor impact on the extraction of the strange nucleon electromagnetic form factors, but play an important role in measurements of the weak charge of the proton at forward angles, which gives direct access to the weak mixing angle, $\sin^2 \theta_W$.

At present the main experimental constraints on the size of the TPE contributions come from comparisons of positron and electron scattering from the proton at large ε , and the limit on nonlinear contributions in ε to polarization observables, as well as the beam normal single spin asymmetries which are sensitive to the imaginary parts of TPE amplitudes. In future an important goal will be to obtain *direct* experimental verification that the form factor discrepancy is indeed explained by TPE effects. This will involve an experimental program consisting of several efforts, including measurement of the e^+p/e^-p cross section ratio and detailed examination of the ε dependence of polarization observables, particularly since in some cases theoretical predictions for these vary considerably. An important opportunity may be presented by the development of *positron* beams at a future 12 GeV upgraded Jefferson Lab [200]. In addition, measurement of various beam and target normal asymmetries will provide direct evidence for Born-forbidden effects and constrain input for dispersion relation analyses.

Further theoretical work will seek better control of higher-mass intermediate state contributions to

the box diagrams, especially at higher Q^2 values. Along this direction, it will be important to go beyond the resonance approximation to include the nonresonant background in the intermediate state spectrum. This naturally becomes difficult to do within any specific model, and a more effective approach may be to utilize dispersion relation to obtain TPE amplitudes from the imaginary parts of the Compton scattering *data*. This is particularly appealing at forward angles, where the amplitudes can be related to inclusive structure functions.

This approach is proving to be especially relevant for estimating γZ interference corrections to the proton weak charge at low Q^2 , currently being measured in the Q_{weak} experiment at Jefferson Lab. Extending this program into the non-forward region will be an important challenge, but one which will allow for a reliable global analysis of the parity-violating elastic scattering data to extract strange nucleon form factors correcting for the effects of two-boson exchange.

Finally, we should note that TPE corrections are indeed small in general, and for a large range of experiments are at the $\mathcal{O}(\alpha)$ (or $\sim 1\%$) level that has historically been assumed. It is only certain cases, typically at backward angles for two-photon exchange or forward angles for γZ corrections, where they tend to be larger, at the $\sim \text{few } \%$ level; G_E^p is a very special case where even a few percent effect in the cross section has a large impact on the Rosenbluth G_E/G_M extraction. Two-photon exchange corrections therefore do not necessarily require revising methodologies for electron scattering in general, so much as reminding us of the need to take greater care in estimating their possible impact on observables that may be particularly susceptible to their effects.

Acknowledgments

We are grateful to our collaborator, the late John A. Tjon, for his many fundamental contributions to the study of radiative corrections — his footprint runs throughout this review. We also thank A. Afanasev, S. Kondratyuk, A. Sibirtsev, I. Sick, R. E. Segel, E. Tomasi-Gustafsson, A. W. Thomas and S. N. Yang for helpful discussions and collaborations that contributed to this article. This work was supported by NSERC (Canada) and the U.S. Department of Energy, Office of Nuclear Physics under contract DE-AC02-06CH11357, and contract DE-AC05-06OR23177, under which Jefferson Science Associates, LLC operates Jefferson Lab.

References

- [1] C. E. Perdrisat, V. Punjabi and M. Vanderhaeghen, *Prog. Part. Nucl. Phys.* 59 (2007) 694.
- [2] J. Arrington, C. D. Roberts and J. M. Zaontti, *J. Phys. G* 34 (2007) S23.
- [3] J. Arrington, C. W. de Jager and C. E. Perdrisat, arXiv:1102.2463 [nucl-ex].
- [4] M. E. Peskin and D. V. Schroeder, *An Introduction to Quantum Field Theory*, Addison-Wesley (1995).
- [5] P. G. Blunden, W. Melnitchouk and J. A. Tjon, *Phys. Rev. Lett.* 91 (2003) 142304.
- [6] P. G. Blunden, W. Melnitchouk and J. A. Tjon, *Phys. Rev. C* 72 (2005) 034612.
- [7] S. Kondratyuk, P. G. Blunden, W. Melnitchouk and J. A. Tjon, *Phys. Rev. Lett.* 95 (2005) 172503.
- [8] J. A. Tjon and W. Melnitchouk, *Phys. Rev. Lett.* 100 (2008) 082003.
- [9] J. A. Tjon, P. G. Blunden and W. Melnitchouk, *Phys. Rev. C* 81 (2010) 018202.
- [10] M. N. Rosenbluth, *Phys. Rev.* 79 (1950) 615.
- [11] R. C. Walker *et al.*, *Phys. Rev. D* 49 (1994) 5671.
- [12] J. Arrington, *Phys. Rev. C* 68 (2003) 034325.

- [13] M. E. Christy *et al.*, *Phys. Rev. C* 70 (2004) 015206.
- [14] I. A. Qattan *et al.*, *Phys. Rev. Lett.* 94 (2005) 142301.
- [15] L. C. Maximom and W. C. Parke, *Phys. Rev. C* 61 (2000) 045502.
- [16] M. K. Jones *et al.*, *Phys. Rev. Lett.* 84 (2000) 1398.
- [17] O. Gayou *et al.*, *Phys. Rev. C* 64 (2001) 038202.
- [18] O. Gayou *et al.*, *Phys. Rev. Lett.* 88 (2002) 092301.
- [19] V. Punjabi *et al.*, *Phys. Rev. C* 71 (2005) 055202.
- [20] G. MacLachlan *et al.*, *Nucl. Phys. A* 764 (2006) 261.
- [21] G. Ron *et al.*, *Phys. Rev. Lett.* 99 (2007) 202002.
- [22] A. J. R. Puckett *et al.*, *Phys. Rev. Lett.* 104 (2010) 242301.
- [23] X. Zhan *et al.*, arXiv:1102.0318 [nucl-ex].
- [24] A. J. R. Puckett *et al.*, arXiv:1102.5737 [nucl-ex].
- [25] G. Ron *et al.*, arXiv:1103.5784 [nucl-ex].
- [26] C. B. Crawford *et al.*, *Phys. Rev. Lett.* 98 (2007) 052301.
- [27] M. K. Jones *et al.*, *Phys. Rev. C* 74 (2006) 035201.
- [28] P. Jain and J. P. Ralston, *Pramana* 61 (2003) 987.
- [29] A. V. Belitsky, X. Ji and F. Yuan, *Phys. Rev. Lett.* 91 (2003) 092003.
- [30] P. E. Bosted, *Phys. Rev. C* 51 (1995) 409.
- [31] J. Litt *et al.*, *Phys. Lett. B* 31 (1970) 40.
- [32] L. E. Price *et al.*, *Phys. Rev. D* 4 (1971) 45.
- [33] W. Bartel *et al.*, *Nucl. Phys. B* 58 (1973) 429.
- [34] L. Andivahis *et al.*, *Phys. Rev. D* 50 (1994) 5491.
- [35] I. A. Qattan, Ph.D. Thesis, Northwestern University, nucl-ex/0610006.
- [36] J. Arrington, *Phys. Rev. C* 69 (2004) 022201(R).
- [37] Y. S. Tsai, *Phys. Rev.* 122 (1961) 1898.
- [38] L. W. Mo and Y. S. Tsai, *Rev. Mod. Phys.* 41 (1969) 205.
- [39] R. R. Lewis *et al.*, *Phys. Rev.* 102 (1956) 537.
- [40] S. D. Drell and M. Ruderman, *Phys. Rev.* 106 (1957) 561.
- [41] S. D. Drell and S. Fubini, *Phys. Rev.* 113 (1959) 741.
- [42] N. R. Werthammer and M. A. Ruderman, *Phys. Rev.* 123 (1961) 1005.
- [43] J. A. Campbell, *Nucl. Phys. B* 1 (1967) 283.
- [44] J. A. Campbell, *Phys. Rev.* 180 (1969) 1541.
- [45] G. K. Greenhut, *Phys. Rev.* 184 (1969) 1860.
- [46] R. Ent *et al.*, *Phys. Rev. C* 64 (2001) 054610.
- [47] L. C. Maximom and J. A. Tjon, *Phys. Rev. C* 62 (2000) 054320.
- [48] R. Rosenfelder, *Phys. Lett. B* 479 (2000) 381.
- [49] J. Arrington and I. Sick, *Phys. Rev. C* 70 (2004) 028203.
- [50] P. A. M. Guichon and M. Vanderhaeghen, *Phys. Rev. Lett.* 91 (2003) 142303.
- [51] M. P. Rekalo and E. Tomasi-Gustafsson, *Nucl. Phys. A* 742 (2004) 322.
- [52] A. Afanasev, S. Brodsky and C. Carlson, presented at the Oct. 2003 meeting of the DNP.

- [53] Y. C. Chen, A. Afanasev, S. J. Brodsky, C. E. Carlson and M. Vanderhaeghen, *Phys. Rev. Lett.* 93 (2004) 122301.
- [54] D. Yount and J. Pine, *Phys. Rev.* 128 (1962) 1842.
- [55] A. Browman, F. Liu and C. Schaerf, *Phys. Rev.* 139 (1965) B1079.
- [56] R. L. Anderson *et al.*, *Phys. Rev. Lett.* 17 (1966) 407.
- [57] W. Bartel *et al.*, *Phys. Lett. B* 25 (1967) 242.
- [58] R. L. Anderson *et al.* *Phys. Rev.* 166 (1968) 1336.
- [59] B. Bouquet *et al.*, *Phys. Lett. B* 26 (1968) 178.
- [60] J. Mar *et al.*, *Phys. Rev. Lett.* 21 (1968) 482.
- [61] L. Camilleri *et al.*, *Phys. Rev. Lett.* 23 (1969) 149.
- [62] J. Arrington, *Phys. Rev. C* 69 (2004) 032201(R).
- [63] J. Arrington *et al.*, *Two-photon exchange and elastic scattering of electrons/positrons on the proton*, proposal for an experiment at VEPP-3 (2004), nucl-ex/0408020.
- [64] Jefferson Lab Experiment E07-005, *Beyond the Born approximation: A precise comparison of positron-proton and electron-proton elastic scattering in CLAS*, W. Brooks *et al.*, spokespersons.
- [65] M. Kohl, *AIP Conf. Proc.* 1160 (2009) 19.
- [66] Jefferson Lab Experiment E05-017, *A measurement of two-photon effects in unpolarized electron-proton scattering*, J. Arrington, spokesperson.
- [67] J. Bernauer *et al.*, *Phys. Rev. Lett.* 105 (2010) 242001.
- [68] V. Tvaskis *et al.*, *Phys. Rev. C* 73 (2006) 025206.
- [69] E. Tomasi-Gustafsson and G. I. Gakh, *Phys. Rev. C* 72 (2005) 015209.
- [70] M. P. Rekalo, E. Tomasi-Gustafsson and D. Prout, *Phys. Rev. C* 60 (1999) 042202.
- [71] Y.-C. Chen, C.-W. Kao and S.-N. Yang, *Phys. Lett. B* 652 (2007) 269.
- [72] Z. Abidin and C. E. Carlson, *Phys. Rev. D* 77 (2007) 037301.
- [73] A. V. Afanasev, S. J. Brodsky, C. E. Carlson, Y. C. Chen and M. Vanderhaeghen, *Phys. Rev. D* 72 (2005) 013008.
- [74] M. Meiziane *et al.*, *Phys. Rev. Lett.* 106 (2011) 132501.
- [75] G. 't Hooft and M. Veltman, *Nucl. Phys. B* 153 (1979) 365.
- [76] J. Schwinger, *Phys. Rev.* 76 (1949) 790.
- [77] G. Passarino and M. J. Veltman, *Nucl. Phys. B* 160 (1979) 151.
- [78] F. Weissbach, K. Hancken, D. Trautmann and I. Sick *Phys. Rev. C* 80 (2009) 064605.
- [79] Y. M. Bystritskiy, E. A. Kuraev and E. Tomasi-Gustafsson *Phys. Rev. C* 75 (2007) 015207.
- [80] T. Hahn and M. Perez-Victoria, *Comput. Phys. Commun.* 118 (1999) 153.
- [81] W. Beenakker and A. Denner, *Nucl. Phys. B* 338 (1990) 349.
- [82] N. T. Meister and D. R. Yennie, *Phys. Rev.* 130 (1963) 1210.
- [83] J. A. Tjon, P. G. Blunden and W. Melnitchouk, *Phys. Rev. C* 79 (2009) 055201.
- [84] P. Mergell, U.-G. Meissner and D. Drechsel, *Nucl. Phys. A* 596 (1996) 367.
- [85] E. J. Brash *et al.*, *Phys. Rev. C* 65 (2002) 051001(R).
- [86] H. F. Jones and M. D. Scadron, *Ann. Phys.* 81 (1973) 1.
- [87] S. Kondratyuk and O. Scholten, *Phys. Rev. C* 64 (2001) 024005.
- [88] H. Q. Zhou, C. W. Kao, S. N. Yang and K. Nagata, *Phys. Rev. C* 81 (2010) 035208.
- [89] V. Pascalutsa and J. A. Tjon, *Phys. Rev. C* 70 (2004) 035209.

- [90] S. Kondratyuk and P. G. Blunden, *Phys. Rev. C* 75 (2007) 038201.
- [91] A. Yu. Korchin and O. Scholten, *Phys. Rev. C* 60 (2000) 015205.
- [92] G. Penner and U. Mosel, *Phys. Rev. C* 66 (2002) 055212.
- [93] D. Borisjuk and A. Kobushkin, *Phys. Rev. C* 75 (2007) 038202.
- [94] E. A. Kuraev and E. Tomasi-Gustafsson, *Phys. Part. Nucl. Lett.* 7 (2010) 67.
- [95] R. H. Dalitz, *Proc. Roy. Soc. (London)* A206 (1951) 509.
- [96] P. G. Blunden and I. Sick, *Phys. Rev. C* 72 (2005) 057601.
- [97] I. Sick and D. Trautmann, *Nucl. Phys. A* 637 (1998) 559.
- [98] I. F. Iskhakov, *Russ. Phys. Jour.* 36 (1993) 582.
- [99] C. Carlson and M. Vanderhaeghen, *Ann. Rev. Nucl. Part. Sci.* 57 (2007) 171.
- [100] D. Borisjuk and A. Kobushkin, *Phys. Rev. D* 79 (2009) 034001.
- [101] N. Kivel and M. Vanderhaeghen, *Phys. Rev. Lett.* 103 (2009) 092004.
- [102] P. Hoodbhoy, *Phys. Rev. D* 73 (2006) 054027.
- [103] R. de L. Kronig, *Opt. Soc. Am.* 12 (1926) 547; H. A. Kramers, *Atti Cong. Intern. Fisica (Transactions of Volta Centenary Congress)*, Como 2 (1927) 545.
- [104] D. Borisjuk and A. Kobushkin, *Phys. Rev. C* 78 (2008) 025208.
- [105] D. Borisjuk and A. Kobushkin, *Phys. Rev. C* 74 (2006) 065203.
- [106] D. Borisjuk and A. Kobushkin, *Phys. Rev. C* 83 (2011) 025203.
- [107] J. A. Peñarrocha and J. Bernabéu, *Ann. Phys.* 135 (1981) 321.
- [108] J. Bordes, J. A. Peñarrocha and J. Bernabéu, *Phys. Rev. D* 35 (1987) 3310.
- [109] M. Gorchtein, *Phys. Lett. B* 644 (2007) 322.
- [110] G. Cvetič, D. Schildknecht, B. Surrow and M. Tentyukov, *Eur. Phys. J. C* 20 (2001) 77.
- [111] D. M. Nikolenko *et al.*, *Phys. Atom. Nucl* 73 (2010) 1322.
- [112] D. M. Nikolenko *et al.*, PoS ICHEP2010 (2010) 164.
- [113] D. Borisjuk and A. Kobushkin, *Phys. Rev. D* 83 (2011) 057501.
- [114] J. Guttmann, N. Kivel, M. Meziane and M. Vanderhaeghen, arXiv:1012.0564 [hep-ph].
- [115] J. Kelly, *Phys. Rev. C* 70 (2002) 068202.
- [116] D. Dutta *et al.*, *Phys. Rev. C* 68 (2003) 064603.
- [117] C. Adamuscin, L. Bimbot, S. Dubnicka, A. Z. Dubnickova and E. Tomasi-Gustafsson, *Phys. Rev. C* 78 (2008) 025202.
- [118] J. Arrington, W. Melnitchouk and J. A. Tjon, *Phys. Rev. C* 76 (2007) 035205.
- [119] J. Arrington and I. Sick, *Phys. Rev. C* 76 (2007) 035201.
- [120] J. Arrington, *Phys. Rev. C* 71 (2005) 015202.
- [121] S. Venkat, J. Arrington, G. A. Miller and X. Zhan, *Phys. Rev. C* 83 (2010) 015203.
- [122] X. Zhan and J. Arrington, to be submitted to *Phys. Rev. C*.
- [123] A. De Rújula, J. M. Kaplan and E. de Rafael, *Nucl. Phys. B* 35 (1971) 365.
- [124] Jefferson Lab Experiment E07-013, *Target normal single-spin asymmetry in inclusive DIS $n(e, e')$ with a polarized ^3He target*, T. Averett *et al.*, spokespersons.
- [125] Jefferson Lab Experiment E08-005, *Measurement of the target single-spin asymmetry A_y in the quasi-elastic $^3\text{He} \rightarrow e, e'n$ reaction*, V. A. Sulkosky contact person.
- [126] A. Lung *et al.*, *Phys. Rev. Lett.* 70 (1993) 718.

- [127] R. Madey *et al.*, *Phys. Rev. Lett.* 91 (2003) 122002.
- [128] Jefferson Lab Experiment E04-110, *The neutron electric form factor at $Q^2=4.3$ (GeV/c) 2 from the reaction $^2\text{H}(\bar{e}, e'\bar{n})^1\text{H}$ via recoil polarimetry*, R. Madey, spokesperson.
- [129] Y. Liang *et al.*, arXiv:nucl-ex/0410027.
- [130] V. Pascalutsa, C. E. Carlson and M. Vanderhaeghen, *Phys. Rev. Lett.* 96 (2006) 012301.
- [131] S. Kondratyuk and P. G. Blunden, *Nucl. Phys. A* 778 (2006) 44.
- [132] S. Kondratyuk and O. Scholten, *Nucl. Phys. A* 677 (2000) 396.
- [133] H. J. Weber and H. Arenhövel, *Phys. Rep.* 36 (1978) 277. .
- [134] A. Deltuva *et al.*, *Phys. Rev. C* 69 (2004) 034004.
- [135] V. Pascalutsa and M. Vanderhaeghen, *Phys. Rev. Lett.* 94 (2005) 102003.
- [136] D. Y. Chen, H. Q. Zhou and Y. B. Dong, *Phys. Rev. C* 78 (2008) 045208.
- [137] B. Aubert *et al.*, *Phys. Rev. D* 73 (2006) 012005.
- [138] E. Tomasi-Gustafsson, E. A. Kuraev, S. Bakmaev and S. Pacetti, *Phys. Lett. B* 659 (2008) 197.
- [139] T. Horn *et al.*, *Phys. Rev. Lett.* 97 (2006) 192001.
- [140] V. Tadevosyan *et al.*, *Phys. Rev. C* 75 (2007) 055205.
- [141] G. M. Huber *et al.*, *Phys. Rev. C* 78 (2008) 045203.
- [142] Y. -B. Dong and S. D. Wang, *Phys. Lett. B* 684 (2010) 123.
- [143] N. Kaiser, *J. Phys. G* 38 (2011) 025003.
- [144] W. Melnitchouk, *Eur. Phys. J. A* 17 (2003) 223.
- [145] Y. B. Dong, C.W. Kao, S. N. Yang and Y. C. Chen, *Phys. Rev. C* 74 (2006) 064006.
- [146] Y. B. Dong, *Phys. Rev. C* 80 (2009) 025208.
- [147] Y. B. Dong and D. Y. Chen, *Phys. Lett. B* 675 (2009) 426.
- [148] A. P. Kobushkin, Ya. D. Krivenko-Emetov and S. Dubnička, *Phys. Rev. C* 81 (2010) 054001.
- [149] Y. B. Dong, *Phys. Rev. C* 82 (2010) 068202.
- [150] A. Amroun *et al.*, *Nucl. Phys. A* 579 (1994) 596.
- [151] Jefferson Lab Experiment E04-018, *Elastic electron scattering off ^3He and ^4He at large momentum transfers*, J. Gomez, A. Katramatou and G. Petratos, spokespersons.
- [152] K. A. Aniol *et al.*, *Phys. Rev. C* 69 (2004) 065501.
- [153] K. A. Aniol *et al.*, *Phys. Lett. B* 635 (2006) 275.
- [154] K. A. Aniol *et al.*, *Phys. Rev. Lett.* 96 (2006) 022003.
- [155] A. Acha *et al.*, *Phys. Rev. Lett.* 98 (2007) 032301.
- [156] D. S. Armstrong *et al.*, *Phys. Rev. Lett.* 95 (2005) 092001.
- [157] D. Androic *et al.*, *Phys. Rev. Lett.* 104 (2010) 012001.
- [158] B. Mueller *et al.*, *Phys. Rev. Lett.* 78 (1997) 3824.
- [159] F. E. Maas *et al.*, *Phys. Rev. Lett.* 93 (2004) 022002.
- [160] F. E. Maas *et al.*, *Phys. Rev. Lett.* 94 (2005) 152001.
- [161] S. Baunack *et al.*, arXiv:0903.2733 [nucl-ex].
- [162] Jefferson Lab Experiment E05-020, *Qweak: A search for new physics at the TeV scale via a measurement of the proton's weak charge*, R. D. Carlini *et al.*, spokespersons.
- [163] E. J. Beise, M. L. Pitt and D. T. Spayde, *Prog. Part. Nucl. Phys.* 54 (2005) 289.
- [164] W. J. Marciano and A. Sirlin, *Phys. Rev. D* 27 (1983) 552.

- [165] W. J. Marciano and A. Sirlin, *Phys. Rev. D* 29 (1984) 75.
- [166] A. V. Afanasev and C. E. Carlson, *Phys. Rev. Lett.* 94 (2005) 212301.
- [167] K. Nakamura *et al.*, *J. Phys. G* 37 (2010) 075021.
- [168] M. J. Musolf *et al.*, *Phys. Rep.* 239 (1994) 1.
- [169] H. Q. Zhou, C. W. Kao and S. N. Yang, *Phys. Rev. Lett.* 99 (2007) 262001.
- [170] K. Nagata, H. Q. Zhou, C. W. Kao and S. N. Yang, *Phys. Rev. C* 79 (2009) 062501.
- [171] M. Gorchtein and C. J. Horowitz, *Phys. Rev. Lett.* 102 (2009) 091806.
- [172] M. Gorchtein, C. J. Horowitz and M. J. Ramsey-Musolf, *AIP Conf. Proc.* 1265 (2010) 328.
- [173] M. Gorchtein, C. J. Horowitz and M. J. Ramsey-Musolf, arXiv:1102.3910 [hep-ph].
- [174] D. B. Kaplan and A. Manohar, *Nucl. Phys. B* 310 (1988) 527.
- [175] S. D. Bass, R. J. Crewther, F. M. Steffens and A. W. Thomas, *Phys. Lett. B* 634 (2006) 249.
- [176] R. D. Young, J. Roche, R. D. Carlini and A. W. Thomas, *Phys. Rev. Lett.* 97 (2006) 102002.
- [177] O. Lalakulich and E. A. Paschos, *Phys. Rev. D* 71 (2005) 074003.
- [178] O. Lalakulich, E. A. Paschos and G. Piranishvili, *Phys. Rev. D* 74 (2006) 014009.
- [179] O. Lalakulich, W. Melnitchouk and E. A. Paschos, *Phys. Rev. C* 75 (2007) 015202.
- [180] J. L. Liu, R. D. McKeown and M. J. Ramsey-Musolf, *Phys. Rev. C* 76 (2007) 025202.
- [181] R. D. Young, private communication.
- [182] J. Erler, A. Kurylov and M. J. Ramsey-Musolf, *Phys. Rev. D* 68 (2003) 016006.
- [183] J. Erler and M. J. Ramsey-Musolf, *Phys. Rev. D* 72 (2005) 073003.
- [184] S. G. Porsev, K. Beloy and A. Derevianko, *Phys. Rev. Lett.* 102 (2009) 181601.
- [185] R. D. Young, R. D. Carlini, A. W. Thomas and J. Roche, *Phys. Rev. Lett.* 99 (2007) 122003.
- [186] A. Sibirtsev, P. G. Blunden, W. Melnitchouk and A. W. Thomas, *Phys. Rev. D* 82 (2010) 013011.
- [187] B. Rislow and C. E. Carlson, arXiv:1011.2397 [hep-ph].
- [188] P. G. Blunden, W. Melnitchouk and A. W. Thomas, arXiv:1102.5334 [hep-ph].
- [189] M. E. Christy and P. E. Bosted, *Phys. Rev. C* 81 (2010) 055213.
- [190] L. W. Whitlow *et al.*, *Phys. Lett. B* 250 (1990) 193.
- [191] D. J. Gross and C. H. Llewellyn Smith, *Nucl. Phys. B* 14 (1969) 337.
- [192] A. Capella, A. Kaidalov, C. Merino and J. Tran Thanh Van, *Phys. Lett. B* 337 (1994) 358.
- [193] A. B. Kaidalov and C. Merino, *Eur. Phys. J. C* 10 (1999) 153.
- [194] M. Osipenko *et al.*, *Phys. Rev. D* 67 (2003) 092001.
- [195] I. Niculescu *et al.*, *Phys. Rev. Lett.* 85 (2000) 1186.
- [196] S. P. Malace *et al.*, *Phys. Rev. C* 80 (2009) 035207.
- [197] A. S. Aleksanian *et al.*, *Sov. J. Nucl. Phys.* 45 (1987) 628.
- [198] Jefferson Lab Experiment E05-007, *PVDIS: Parity violation in deep-inelastic scattering*, R. Michaels *et al.*, spokespersons.
- [199] Jefferson Lab Experiment E12-07-102, *Precision measurement of the parity-violating asymmetry in deep-inelastic scattering off deuterium using baseline 12 GeV equipment in Hall C*, K. Paschke *et al.*, spokespersons.
- [200] J. Dumas, J. Grames and E. Voutier, *AIP Conf. Proc.* 1160 (2009) 120.